The Economic Cost of Climate Change: A Micro-based, Bottom-up Approach*

Diogo Baptista Hélia Costa Filiz Unsal †

March 26, 2026

Abstract

This paper develops a micro-based, bottom-up approach to quantify the macroeconomic costs of climate change. It combines empirically estimated local climate damages with a global spatial general equilibrium model: the Climate and Adaptation Spatial General Equilibrium Model (OECD-CASGEM). The model links location-specific climate hazards to economy-wide outcomes through trade, migration, production networks, and factor adjustments. We find that global GDP per capita declines by 3% by 2050 and 6.3% by 2100 under a current-policy scenario, and by 6% and 18%, respectively, under a high-emission scenario, with large associated uncertainty. Losses are highly heterogeneous across regions, disproportionally affecting lower-latitude and more historically exposed regions. Counterfactual simulations show that trade linkages, migration and production networks can dampen or amplify losses depending on countries' exposure, economic structure and position in global networks. Spatial mechanisms, in particular, reduce cross-regional dispersion in impacts, effectively operating as a form of implicit loss-sharing across locations.

Keywords: Climate change; spatial general equilibrium; climate damages; adaptation; trade and migration; production networks

JEL Codes: Q54, Q51, F12, R13

*We thank Eddy Casey, Jean Chateau, Francesco Filippucci, Catherine Gamper, Yvan Guillemette, Asa Johansson, Andy King, Luisa Lutz, Sherie Nicol, Mauro Pisu, Matthias Schief, Simon Touboul, and Sebastian Turban for helpful comments and discussions. We are also grateful to numerous seminar participants at the OECD and the IMF. The views expressed in this paper are those of the authors and do not necessarily reflect those of OECD. All errors are our own. The authors declare that there are no sources of research support, financial relationships, or other potential conflicts of interest to disclose related to this work.

†Organisation for Economic Co-operation and Development (OECD). Emails: diogo.baptista@oecd.org, helia.costa@oecd.org, filiz.unsal@oecd.org

1. Introduction

Climate change is increasingly shaping global welfare and macroeconomic outcomes (IPCC, 2022; Bank of England, 2025; European Central Bank, 2021). A growing body of evidence suggests that impacts on output, productivity, infrastructure and well-being are already material and are likely to intensify over the coming decades. Existing estimates of the economy-wide costs of climate change vary across studies and are surrounded by uncertainty. This reflects data limitations, ambiguity about future climate conditions and policy responses, and differences in existing empirical and modelling approaches. For economic policy, the key question is not only how large the losses will be, but also how they arise and how they spread across sectors and space. Quantifying these effects calls for analytical frameworks capable of integrating multiple, interacting sources of climate hazard and their impacts across regions, time, and sectors. Equally essential for policy design is the ability to trace the specific transmission channels through which climate shocks propagate through the economy.

In this paper, we develop a micro-based, bottom-up approach to measure the economic cost of climate change around the world. Our approach is built around three modules (see Figure 1). In Module I, we estimate the local impact of four climate hazards - heat stress, changes in agro-climatic conditions (i.e. changes in precipitation, temperature and solar radiation which affect crop growth), floods, and sea level rise - on key determinants of economic activity - productivity, capital depreciation, and land supply. In Module II, we combine these estimates with economic and climate projections from multiple climate projection models under alternative shared socioeconomic pathways (SSPs) to quantify future losses up until 2100. Finally, in module III, we develop and calibrate the Climate and Adaptation Spatial General Equilibrium Model (CASGEM) and feed the projected climate damages from Module II to estimate their macroeconomic impact and evaluate how economic adjustments such as trade reorientation and migration shape the final outcomes.

Existing estimates of the economic cost of climate change vary substantially in magnitude, making it difficult to draw robust policy conclusions. One strand of the literature consisting of macro-econometric studies (e.g. Dell et al., 2014; Burke et al., 2015; Kahn et al., 2021; Bilal and Känzig, 2024) exploits historical variation in aggregate economic variables and weather realizations to construct damage functions and project future climate impacts. Although instrumental in providing reduced-form evidence on the relationship between climate and economy, these studies follow a partial equilibrium approach that misses the inherently global nature of climate change and how spatially correlated and intensifying shocks will propagate across national boundaries. Moreover, they provide limited insight into how such shocks transmit through general equilibrium forces and spatial spillovers, or how agents adjust in response to changing climate conditions.

Another strand of the literature uses Computable General Equilibrium (CGE) models to study the economic impacts of climate change. (e.g. Nordhaus and Yang, 1996; Bosello et al., 2007; Château et al., 2014; Kompas et al., 2018). These models provide a detailed representation of production, consumption, and trade linkages that allows for rich sectoral interactions and policy counterfactuals. However, standard CGE models typically operate at a high level of spatial aggre-

gation, often at the country or multi-country level. Therefore, they abstract from within-country heterogeneity in exposure and vulnerability to climate, limiting their ability to capture how spatial frictions shape the propagation of and adaptation to climate shocks. Moreover, key adjustment mechanisms, such as migration, land use, and real estate markets, are often either absent or modeled in reduced-form, rather than estimated in a way that is consistent with observed spatial patterns of economic activity.

A more closely related literature embeds climate change in quantitative spatial and dynamic general equilibrium frameworks. Early contributions such as Desmet and Rossi-Hansberg (2015) and Costinot et al. (2016) show how climate change reshapes the economic geography of production and population through trade, migration, and local adaptation. More recent work extends this approach to forward-looking settings with endogenous spatial reallocation and capital adjustment (e.g. Rudik et al., 2022; Krusell and Smith, 2022; Kleinman et al., 2023; Cruz and Rossi-Hansberg, 2024). Within this literature, many papers focus on specific transmission channels or individual hazards, including agricultural productivity and trade (Costinot et al., 2016; Nath, 2025), agricultural productivity and migration (Conte, 2023), sea-level rise (Desmet et al., 2021; Balboni, 2025), and extreme weather events like storms and heat waves and the role of forward-looking anticipation and adaptation (Bilal and Rossi-Hansberg, 2023). Relative to this work, we develop a unified spatial general equilibrium framework that integrates multiple climate hazards and enables a comprehensive assessment of their macroeconomic and sub-national impacts, as well as the role of spatial adjustment through trade and migration. Moreover, we map hazards into distinct economic damage channels using micro-based estimates derived from high-resolution data on weather realisations, firm-level outcomes and climate projections.

We estimate micro-level impacts on productivity (from heat stress and changes in agro-climatic conditions), capital stocks (from flooding) and the supply of land (from sea level rise). We do this in module I using econometric methods applied to granular firm-level data, high-resolution climate data that capture the range of impacts across space and sectors, and state-of-the-art climatological, hydrological, and agricultural models commonly used in the climate science literature.

Using high-resolution flood maps matched with firm-level balance sheet data for 17 European and Asian economies, we find that floods mainly affect firm outcomes through persistent capital losses rather than productivity declines. The analysis also reveals sizeable spatial spillovers. Firms that are not directly flooded but are geographically close to affected firms experience declines in value added and investment likely due to disruptions in local supply chains, infrastructure and demand, or tighter financial conditions. This underscores the importance of accounting for indirect effects when assessing climate damages.

To quantify heat stress, we use and extend firm-level evidence showing how daily temperature fluctuations affect worker productivity (Costa et al., 2024). Specifically, we estimate impacts of local climatic conditions for all sectors except agriculture. We proxy the impact of climate change on agricultural productivity through changes in agro-climatic potential yields derived from climate-crop models which represent the maximum attainable crop yield under future soil and climatic

conditions. Finally, the impacts of sea level rise are estimated by combining population exposure and coastal flooding hazard maps to determine which areas of land are expected to be permanently submerged in the absence of further adaptation to coastal flooding.

For module II, we construct future impact scenarios based on projections from Shared Socioeconomic Pathways (SSP), which represent alternative emissions and global socioeconomic development paths. We draw on an ensemble of climate models that use these SSPs to generate projections of future climatic, environmental and weather conditions. This allows us to understand how much more (or less) frequent and how much more (or less) intense different climate hazards will become in the future. We combine the damage impacts estimated in module I with these projections to estimate how the size of climate damages to productivity, capital, and land will evolve in the future, ensuring they remain grounded in observed historical relationships between climate conditions and economic outcomes.

Finally, in module III, we develop and calibrate a quantitative spatial model, the Climate and Adaptation Spatial General Equilibrium Model (OECD-CASGEM), and feed the projected damages to quantify the economic cost of climate change. The model features multiple locations within and across countries that differ in exposure, vulnerability, and productive capacity, and are connected through trade, migration, and input-output linkages. A key feature of the framework is that it embeds spatial frictions in both goods and labour markets, allowing shocks in one location to transmit across space through endogenous adjustments in trade, migration, and local economic activity. As a result, climate impacts are shaped not only by local damages but also by equilibrium responses across interconnected regions and sectors.

The model incorporates general equilibrium adjustments in goods, labour, capital, and real estate markets, and allows for heterogeneous impacts and endogenous adaptation through trade and migration across locations. We calibrate the model to 927 regions and 11 sectors, using detailed information on production, employment, wages, trade flows, migration, and input-output relationships. Under this calibration, the model closely matches the observed spatial distribution of economic activity, providing a realistic representation of observed economic patterns. A key strength of the model is its ability to aggregate local, sector-level damages into macroeconomic outcomes, providing a comprehensive assessment of the economic impact of future climate conditions. It allows us to quantify not only the magnitude of economic losses, but also how they originate and propagate. The framework also enables counterfactual analysis, allowing individual transmission channels to be isolated and the role of spatial adjustment mechanisms to be evaluated.

Our quantitative results show that climate change generates sizable macroeconomic losses that grow over time. Across OECD countries, GDP per capita is projected to be about 2.6% lower by 2050 and around 9% lower by 2100 under a high-emissions scenario (SSP5-8.5), relative to a baseline where climate conditions are fixed at historic levels. Under a current-policy scenario (SSP2-4.5), losses are smaller but still material, at roughly 1.7% by 2050 and 3.1% by 2100. Losses are larger in lower-latitude and warmer countries like in Southern Europe, parts of the United States, and Australia, reflecting greater exposure to heat stress and agricultural productivity declines.

Losses also vary greatly within countries, with largest dispersion in countries like Chile, Italy, Netherlands, and Australia, where significant regional losses sometimes coexist with gains in other regions. Globally, losses to GDP per capita amount to around 6% (3%) in 2050 and 18% (6.3%) in 2100 under a high-emission (current-policy) scenario, with countries in West and Central Africa, South Asia and parts of the Middle East facing declines exceeding 20-30% (15-20%) by the end of the century. Note that climate projections are subject to a large degree of uncertainty. Considering variation across climate models yields a range of plausible projected GDP per capita losses in OECD economies of approximately 3.3% to 16.5% by 2100 (and 6.7% and 29.6%, globally) under SSP5-8.5.

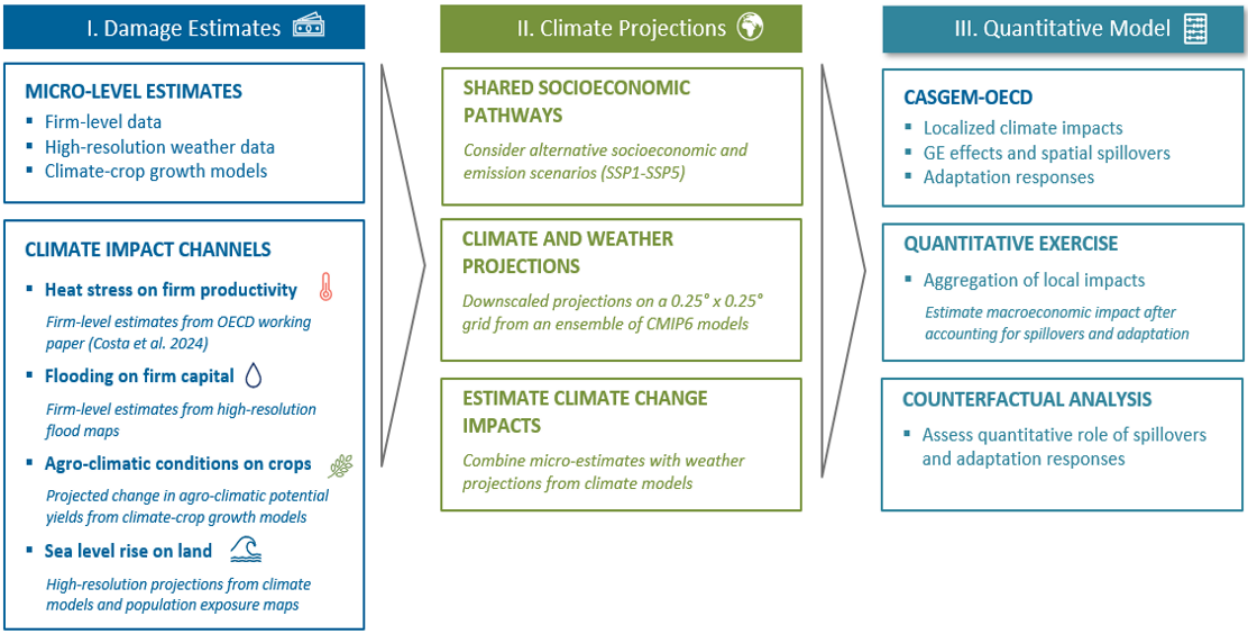
We then examine what drives these patterns. Heat stress emerges as the main source of economic losses worldwide, including in advanced economies, followed by losses due to changes in agro-climatic conditions. Flooding and sea-level rise play important roles in specific coastal and low-lying regions but contribute less to the global economic impact. Climate change also reshapes the geography of population across countries and regions. As economic conditions evolve across regions, households relocate toward less-affected areas: regions suffering the largest economic damages experience substantial population outflows, while cooler and relatively less affected regions like Northern Europe and parts of North America become net recipients of migrants. These flows occur both across and within countries and lead to sizeable changes in population distribution already by 2050.

To understand the transmission channels through which local climate shocks translate into economy-wide impacts, we conduct counterfactual simulations that restrict key mechanisms in the model. By shutting down trade, migration, or production linkages, we isolate how shocks spread across regions and sectors. We find that spatial linkages and production networks substantially shape both the size and the distribution of climate damages. Trade and migration sometimes cushion losses and sometimes transmit shocks across regions and borders, and supply chains act as a powerful amplification channel in most economies.

We next examine how the economy's ability to adjust influences the magnitude of impacts. We compare scenarios where trade and labour mobility can respond to changes in climate with cases in which they are fixed to assess how much resilience or vulnerability these adjustment margins generate. These counterfactuals reveal that at the global level these adjustment margins act as a stabilizing force, lowering world GDP per capita losses in 2100 by roughly 9% under a high-emission scenario. However, they can either mitigate or amplify local climate damages, depending on regions' exposure and their position in the global economy. These mechanisms also reduce the cross-regional dispersion in impacts, effectively acting as a form of loss-sharing.

The remainder of the paper is organized as follows. Section 2 describes the climate hazards considered and their estimation. Section 3 outlines how climate projections are translated into future damages. Section 4 presents the structure and calibration of our spatial quantitative model, OECD-CASGEM. Section 5 reports the results and, finally, section 6 concludes.

Figure 1: Quantifying the Cost of Climate Change: A Micro-based, Bottom-up Approach



Notes: This figure describes the three modules making up our micro-based, bottom-up approach.

2. Estimation of local climate damages (Module I)

We focus on four impact channels that capture salient and well-documented first order effects of climate, whose choice is guided by existing literature and insights from our micro-level analysis described below. Heat stress affects productivity, with impacts that vary across sectors and climatic conditions. Flooding is another important climate hazard and, as shown below, operates mainly through the destruction and accelerated depreciation of firms' physical capital. Changes in temperature, solar radiation, and precipitation (agro-climatic conditions) affect agri- cultural productivity through biophysical impacts on crop growth conditions. Finally, sea-level rise represents a slow-onset event that reduces the effective supply of productive land in low-lying coastal areas. Together, these channels provide a parsimonious representation of the core economic impacts of climate.

While this approach aims to provide a consistent and empirically grounded assessment of first-order climate damages, several caveats are worth noting. First, estimates based on historical variation may not fully capture the economic consequences of rare extreme events, threshold effects or potential tipping points that could become more prevalent under future climate conditions, implying that damages could be nonlinear at higher levels of warming. Second, hazards may interact in ways that are not purely additive, such that the combined effects of multiple shocks may exceed the sum of their individual impacts. Where feasible, we mitigate this risk by jointly controlling for correlated climate variables in our empirical specifications.[1] Third, historical estimates implicitly

[1]For example, the empirical analysis of flooding controls for concurrent heat stress to reduce the risk of confound-

embed past adaptation responses, while future adaptation capacities, costs and technological developments remain uncertain, possibly resulting in over- or underestimate future damages. Fourth, our analysis does not incorporate several important climate hazards like storms (i.e. tropical cyclones, hurricanes and typhoons), wildfires, and landslides, all of which are expected to become increasingly frequent and/or severe in many parts of the world. Excluding these hazards means that our estimates may understate the full spectrum of climate-related risks, particularly for countries where these hazards are a dominant source of losses. Finally, this analysis focuses on market-based channels and abstracts from broader impacts such as food security, health impacts or irreversible ecosystem losses, all of which have impacts on welfare.

2.1. Flooding and the Capital Stock

Floods are a major climate-related condition for economic activity, primarily through their effects on firms' physical capital and balance sheets. To quantify these impacts, we rely on firm-level estimates from an original empirical analysis linking balance-sheet data from Moody's Orbis (covering over 2.5 million firms across 17 European and Asian advanced economies from 2000 to 2018) with geographically detailed information on major flood events from the Global Flood Database (Tellman et al., 2021). The analysis exploits high spatial resolution in flood exposure, allowing us to distinguish between firms directly affected by flooding and nearby firms exposed only through local spillovers.

The empirical strategy relates firm value added and its determinants – including capital stock, productivity and employment – to flood exposure. It compares firms directly affected by floods with otherwise similar firms located more than 100 km away, while accounting for spillovers to nearby but unflooded firms. The specification controls for firm characteristics, local weather conditions, and firm, sector-year, and country-year fixed effects. To capture persistence, the static analysis is complemented with local projection methods tracing the dynamic response of capital stocks in the four years following a flood event.

The results indicate that floods primarily affect firms through capital destruction rather than sustained productivity losses or employment. On average, direct flood exposure reduces firms' capital stocks by 2.7% over the four years following the event. Estimated effects on multifactor productivity are modest and statistically insignificant and labour appears to be unaffected. The change in capital stock is partially reflected on a decrease in value added consistent with traditional values for capital shares. These estimates are used to calibrate flood-related increases in effective capital depreciation in the macroeconomic model.

Floods also generate economically meaningful spatial spillovers: firms located within 100 km of a flooded area experience capital losses amounting to over one third of the direct effect. Firms experiencing floods lasting longer than the sample median experience substantially larger capital

ing correlated climate shocks. Moreover, projections for future agro-climatic conditions are derived from climate-crop growth models that simultaneously account for the effect of changes in temperature, drought conditions (i.e. precipitation and evapotranspiration) and solar radiation.

losses, with average declines of 3.3%, compared to losses of 2.2% for firms affected for shorter durations. Dynamic estimates show that capital accumulation continues to deteriorate in the years following a flood, with the largest negative effect occurring approximately 3 years after the event, and only partial recovery thereafter. Smaller and less liquid firms suffer larger losses and recover more slowly in the aftermath of a firm. The data, methodology, and empirical results are described in detail in Annex B.

2.2. Heat stress and productivity

Heat stress is an increasingly important climate-related condition for economic activity, particularly through its impact on labour productivity. To quantify these effects, for all sectors apart from the agriculture sector, we rely on estimates from Costa et al. (2024), who link firm-level data from Orbis (covering over 2.7 million firms across 23 advanced economies from 2000 to 2021) with high-resolution ERA-5 reanalysis data. We follow their approach, which exploits granular daily temperature variation, measuring exposure to hot days in different temperature ranges, and allows impacts to vary by local climatic conditions.

The empirical strategy relates firm-level multi-factor productivity (MFP) to the annual number of hot days in each temperature bin while controlling for firm characteristics, other weather variables, firm and country-year fixed effects, and the interaction between heat exposure and long-run average local temperatures. This design captures both heterogeneous sectoral vulnerability and the role of baseline climate in mediating adaptation capacity.

The results show consistent losses in firm productivity on days exceeding 30°C, with impacts rising sharply at higher temperatures. Heat effects are largest in cooler regions where adaptation levels are lower. Impacts of days above 35°C are on average larger than those between 30°C and 35°C, and the difference increases for firms in colder climates. Days above 40°C have much larger impacts, with each additional day costing almost 0.2% of annual productivity, on average, compared to 0.03% for days in the 30–35°C range and 0.02% for days range in the 35°–40°C range. These elasticities are used to calibrate annual sector-level productivity shocks from heat stress across all sectors except for agriculture. The full results are available in Annex C.

2.3. Changes in agro-climatic conditions and agricultural productivity

Agricultural productivity is highly sensitive to climate, particularly temperature, precipitation, and soil moisture, and is therefore especially vulnerable to climate change. To quantify the effects of future climate on agricultural productivity, we follow Conte (2023) and draw on data from the FAO's Global Agro-Ecological Zones (GAEZ) Data Portal, which provides high-resolution estimates of agro-climatic potential yields. These yields represent the maximum attainable output under given climatic, soil and terrain conditions and are calculated under alternative assumptions regarding water management (rain-fed versus irrigated) and input intensity (low versus high input use). By focusing on potential rather than observed yields, this approach isolates the biophysical suitability of land for crop production, abstracting from differences in soil and crop management, and market

conditions.

The GAEZ framework integrates outputs from a set of five climate–crop growth models to generate projections of agro-climatic conditions over different periods (2011–2040, 2041–2070 and 2071–2100).[2] These models simulate the impact of future climate conditions on key determinants of crop growth, in particular soil moisture, temperature and solar radiation. We compute model-specific percentage changes in agro-climatic potential yields relative to the 2011–2040 period. As FAO-GAEZ does not provide model projections for a historical reference period, we use 2011–2040 as the closest available baseline. We then take the ensemble median of these relative changes across models, yielding a central estimate of the effect of future climate on agricultural potential.

The analysis covers sixteen major crops spanning cereals (barley, maize, millet, rice, sorghum and wheat), roots and tubers (cassava, sweet potato, white potato and yams), legumes (cowpeas and groundnuts), and cash crops (palm oil, sugarcane and soybeans), as well as grasslands for capturing changes in livestock productivity. All data are available at a spatial resolution of approximately 10×10 km grid cells, allowing us to capture fine-scale heterogeneity in agricultural suitability across space. We then combine these spatial projections of relative yield change with gridded information on current crop areas and production to construct crop-weighted changes in effective crop productivity at the sub-national level. In parallel, information on the geographic distribution of livestock, drawn from the Gridded Livestock of the World (GLW 4) 2020 dataset, is used to measure the spatial distribution of livestock density around the world.

These spatially detailed, crop-specific changes in agro-climatic potential yields are subsequently translated into productivity shocks to the agricultural sector in each region. Specifically, for each 10 km × 10 km grid cell, crop-level yield changes are aggregated into a single agricultural productivity shock by taking a weighted average of relative yield changes across crops and livestock, using baseline production values as weights.[3] These shocks serve as direct inputs in the model, capturing the local, first-order impact of future climate on agricultural productivity before any behavioural or general-equilibrium adjustments take place.

2.4. Sea level rise and land loss

Sea-level rise represents a structural, rather than episodic, event: in some low-lying coastal areas, the continued rise in mean sea level may result in permanent inundation, leading to structural loss of land (Nicholls and Cazenave, 2010). To capture this dimension, we combine coastal flood projections from the World Resources Institute's (WRI) Aqueduct Floods framework, in combination with information on existing coastal protection standards (Tiggeloven et al., 2020). All grid cells where future projected coastal water levels exceed protection thresholds with 50% annual probability are classified as permanently submerged, reflecting locations that are expected to be chronically under water in the long run if protection standards remain unchanged.

[2] These are GFDL-ESM2M, HADGEM2-ES, IPSL-CM5A-LR, MIROC-ESM-CHEM and NORESM1-M

[3] This aggregation abstracts from endogenous adaptation through changes in crop mix in response to evolving relative yields. In other words, crop and livestock production weights are held fixed at their baseline levels, so that productivity shocks reflect changes in agro-climatic conditions absent any endogenous reallocation within agriculture.

We treat land as a key input in the real estate sector, which produces physical structures used by households for housing and by firms as production space. Sea level rise reduces the available supply of land in affected locations, thereby constraining the inputs available to the real estate sector. This reduction in land availability raises construction costs, which are passed through to households in the form of higher rents and to firms in the form of higher production costs. In contrast to fast-onset coastal flooding events, which directly destroy capital and structures and are captured through the flooding impact channel, sea-level rise is as a slow-moving process. As a result, it does not directly lead to the destruction of existing capital stocks: real estate developers are assumed to be able to anticipate gradual inundation and relocate investment toward non-submerged areas.

Consequently, the economic costs of sea-level rise in our framework arise through changes in the production efficiency and cost structure of the real estate sector induced by land scarcity, rather than through direct physical losses. This channel is distinct from intermittent coastal flooding impacts and captures the long run structural effects of land loss on housing markets, production costs, and spatial economic activity.[4]

3. Climate projections and calibrating climate impacts (Module II)

This module combines physical climate projections with our empirically estimated damage functions to construct forward-looking, region- and sector-specific economic shocks.[5] Climate models describe how temperature, precipitation, flood risk and sea levels evolve under alternative emissions pathways, but these projections are not directly usable in an economic model. We therefore translate projected changes in climate conditions and their associated costs into calibrated shocks to the model. This calibration step ensures internal consistency across hazards and provides a transparent mapping from physical climate impacts to fundamental determinants of economic output in the general equilibrium model.

3.1. Climate projections

To project future climate impacts consistently across the four climate hazards – heat stress, flooding, agro-climatic conditions and sea-level rise – we combine historical impact estimates with geographically-disaggregated climate projections based on Shared Socioeconomic Pathways (SSP) and their associated Representative Concentration Pathways (RCP), which describe both emissions and broader socioeconomic developments. We focus on two benchmark scenarios: SSP2–4.5, commonly interpreted as a "current-policy" or intermediate stabilisation pathway, and SSP5–8.5, a high-emissions scenario. SSP2–4.5 assumes moderate population and economic growth, gradual technological progress, and the continuation of existing climate policies, leading to radiative forcing

[4]The role of land as an input into the real estate sector, and its interaction with housing supply, firm location, and production costs, is modelled explicitly within the quantitative spatial general equilibrium framework described in Section 5 and, in more detail, in Annex E.

[5]Note we estimate empirical damage functions for heat stress and flooding impacts only. The physical impacts of changes in agro-climatic conditions in sea level rise are obtained directly from existing climate projections.

of 4.5 W/m² by 2100 and an expected global mean temperature increase of roughly 2–3°C above pre-industrial levels by the end of the century. In contrast, SSP5–8.5 reflects rapid fossil-fuel-driven economic growth, energy-intensive development, and limited climate mitigation, resulting in radiative forcing of 8.5 W/m² and projected warming in the range of approximately 4°C or more by 2100.

Using these scenarios, we obtain projections of future temperature patterns, flooding events, sea-level rise, and agro-climatic conditions. This provides a coherent basis for assessing how the frequency and intensity of different climate hazards are expected to evolve over time and for translating these changes into sector- and region-specific economic damages. It is worth noting, however, that the use of climate projections to construct future impact scenarios entails important sources of uncertainty. First, climate models differ in their spatial and temporal resolution, which can affect their ability to capture highly localised climate conditions and short-lived extreme events. Coarse spatial units may fail to capture localised extreme weather events or heterogeneous weather patterns within broader regions. Second, climate projections are inherently uncertain due to a combination of emissions uncertainty, climate model uncertainty, and internal climate variability.[6]

3.1.1 Flood projections

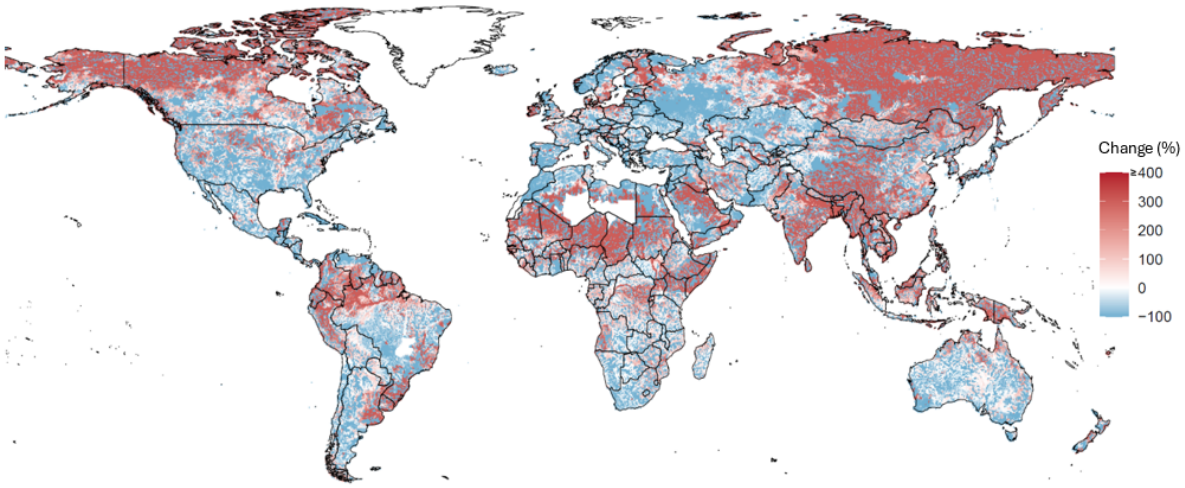
Projecting future flood risk requires linking changes in climatic conditions to existing protection standards and baseline probability of flooding. Observed flood exposure reflects not only natural hydrological processes but also the capacity of local flood protection infrastructure. We therefore combine spatially detailed information on current protection levels from the FLOPROS (Flood Protection Standards) database (Scussolini et al., 2016) with forward-looking hazard projections to assess how the effective probability of damaging floods evolves under climate change, holding protection infrastructure fixed at historical levels.

Future riverine and coastal flood hazards are derived from global climate-driven hydrological projections provided by the World Resources Institute. For each location, we evaluate whether projected flood depths exceed the historical protection threshold implied by local protection standards. An increase in exceedances implies a higher likelihood of overtopping or protection failure, and thus a rise in the frequency of damaging flood events. This framework isolates the effect of climatic shifts on flood risk, abstracting from endogenous adaptation or future upgrades in protection.

[6] Following standard practice in the literature, our analysis relies on bias-corrected, geographically disaggregated climate data and on multi-model ensembles of climate models to explore the full range of plausible climate futures.

Figure 2: Effect of climate change on flood frequency in 2080 relative to 1980

Percent change in the annual frequency of riverine flooding under RCP8.5 (ensemble mean)



Source: Scussolini et al. (2016), World Resources Institute (Aqueduct), and authors' own calculations.
Notes: The map reports values at the resolution of a 0.25° × 0.25° grid cell (approximately 25 km at the equator). Values greater than 400% are windsorized at 400%. The projections assume flood protection standards remain the same as in the baseline period (i.e. 1980).

The resulting projections reveal substantial spatial heterogeneity in changes in flood frequency (Figure 2). Under RCP8.5, some regions experience pronounced increases in riverine flood occurrence by the end of the century, while others display more moderate changes or localised reductions. Importantly, the reported changes are relative to each location's baseline probability of flooding. Regions that are historically dry may register large proportional increases despite remaining low risk in absolute terms, whereas densely populated floodplains with high baseline risk may exhibit smaller percentage changes despite substantial exposure.

To assess economic relevance, we combine the geographic extent of flood-prone areas with spatial population data provided by the Gridded Population of the World, Version 4 (GPWv4) dataset. This allows us to compute, for each location, the share of the population residing in areas subject to flooding under baseline protection standards. We do this by first identifying the pixels in which the projected flood depth exceeds zero in a 1-in-100-year flood and then computing the share of total population in each GPW grid cell residing in flood-exposed land.

3.1.2 Heat projections

We use the World Bank's Climate Change Knowledge Portal (CCKP) to obtain projections of future annual hot days and average annual temperatures. The dataset compiles climate projections from 29 general circulation models, providing annual realisations of key climate variables on a 0.25° × 0.25° grid (approximately 28 km × 28 km at the equator). From these projections, we extract the annual number of days exceeding 30°C, 35°C and 40°C, as well as average annual

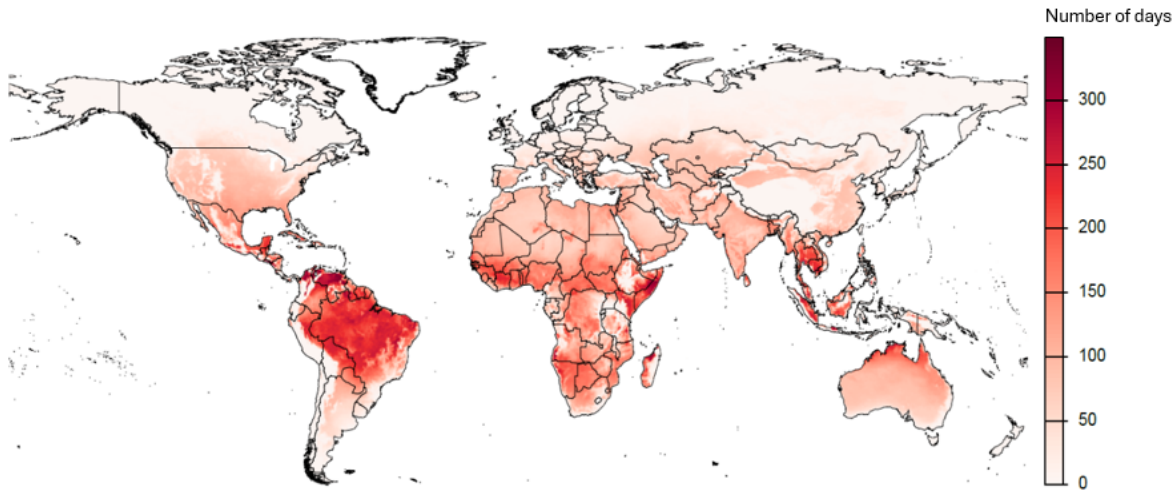
temperatures, under different emissions pathways.[7] We then combine these climate projections with our productivity impact estimates to construct a panel of annual, sector-level productivity losses from heat stress for each subnational region over the period 2025–2100. To isolate the effect of future climate conditions on heat stress - recognising that high temperatures would still occur regardless of which future climate scenario is considered - we compare projected hot days in each scenario to a no-climate-change baseline. Specifically, we use the historical period 1981–2000 as a reference and compute deviations from this baseline, thereby identifying the additional heat exposure attributable to human-induced warming.

Figure 3 shows that projected increases in the number of hot days are highly uneven across the globe, with the largest changes concentrated in low-latitude regions. Panel A indicates that days above 35°C are expected to rise sharply across much of the tropics and subtropics, with even mid-latitude regions - including the southern United States and the Mediterranean - experiencing noticeable increases. Panel B reveals an even more concentrated pattern for days above 40°C: the largest increases occur in a broad belt stretching from North Africa through the Middle East into South Asia, where many areas see more than 100 additional days per year exceeding this extreme threshold. Outside this band, and in most OECD regions, increases in 40°C days remain modest. Overall, the maps underscore the strong latitudinal gradient in exposure to extreme heat, with the most dramatic intensification occurring in regions that are already among the hottest in the world.

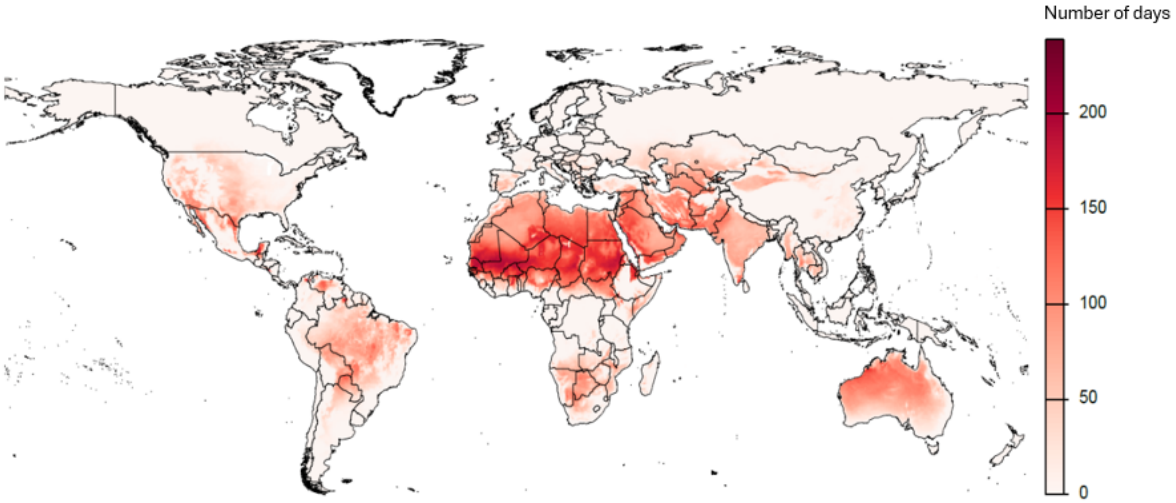
[7] We take the median value provided by the CCKP which corresponds to the median projection across all general circulation models included in the CCKP sample. We apply GIS spatial matching tools to match the administrative units in the CCKP data with the 927 regions used in the model calibration shown later.

Figure 3: Projected change in annual number of hot days (2081-2100 vs 1981-2000) under the high-emission scenario (SSP5-8.5)

(a) Change in annual number of days above 35°C



(b) Change in annual number of days above 40°C



Source: Climate Change Knowledge Portal (World Bank) and authors' own calculations.

3.1.3 Projections of agro-climatic conditions

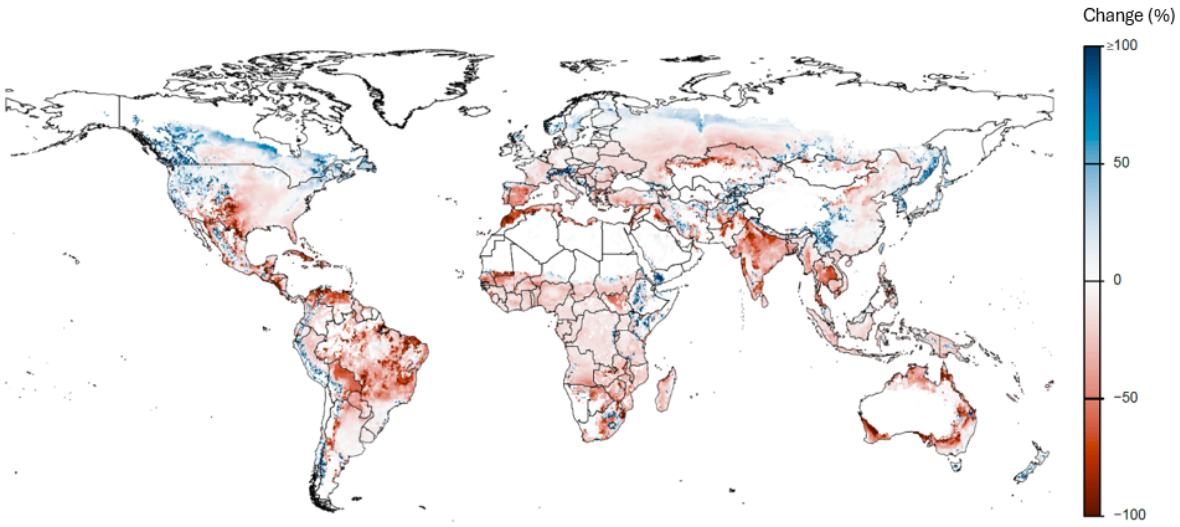
Figure 4 shows the estimated change in average agro-climatic potential yields in 2071–2100 relative to 2011–2040 under RCP8.5 across all sixteen crops, weighted by their production value in each location. The figure excludes impacts on livestock, which we capture separately through changes in grassland yields. The map reveals a predominantly negative pattern, with substantial declines in several major mid-latitude agricultural zones, including parts of the United States, southern Europe, and Australia among OECD countries, as well as much of Sub-Saharan Africa, Central and South America, and South and Southeast Asia. By contrast, some high-latitude regions - most notably Canada and the northern United States, and northern Europe - show pockets

of projected yield gains, reflecting potential benefits from longer growing seasons and improved thermal conditions. Nevertheless, these gains are relatively limited in spatial extent compared with the widespread declines observed elsewhere.

The map highlights a clear global asymmetry: agro-climatic potential yield decreases are concentrated in regions that are already warm and agriculturally vulnerable, while potential gains are restricted to a narrow set of cooler areas. Taken together, these projections suggest a systematic redistribution of agricultural potential away from many of today's major crop-producing regions in the Global South towards regions in the Global North, with important implications for global food production, trade patterns, and food security. Figure A.2 in Annex A shows the projected change in agro-climatic potential yields for the four crops that account for the largest share of global human and animal calorie consumption - maize, wheat, rice and soybeans. The figure reveals substantial spatial heterogeneity in the projected impacts of future climate on agro-climatic potential yields, with clear differences both across crops and across regions. These estimates underscore that future climate will likely alter the geographic distribution of comparative advantage in crop production.

Figure 4: Projected change in crop yields in 2071-2100 relative to 2011-2040 under the high-emission scenario (SSP5-8.5)

Percentage change in average yield (weighted by crop production value, excludes livestock)



Source: FAO-GAEZ and authors' own calculations.
Notes: The map reports values at the resolution of a 0.25° × 0.25° grid cell (approximately 25 km at the equator). Values greater than 100% are windsorized at 100%. All values correspond to the multi-model ensemble mean across five climate-crop models.

3.1.4 Sea-level rise

In line with our treatment of flood exposure, we construct a measure of population potentially affected by sea level rise. To do so, we overlay high resolution (30 arc-seconds) historical coastal flood hazard maps for a 1-in-1000-year event from the WRI with gridded population data. This very high return-period threshold allows us to capture the full extent of low-lying coastal areas that,

while rarely flooded under historical conditions, may be increasingly exposed as sea levels rise in the future. As before, we use population data from GPWv4 as a proxy for the underlying distribution of capital and economic activity. Then, to identify which of these areas will be permanently inundated, we rely on future coastal flood hazard maps from WRI to estimate the annual probability of coastal flooding in each grid cell, assuming coastal protection standards remain at their historical levels. Grid cells that at any moment in time have an estimated annual flooding probability exceeding 50% are assumed to become effectively uninhabitable.

We combine these two layers - the areas classified as permanently flooded and the population in flood-prone coastal zones - to estimate the share of land that effectively becomes uninhabitable. This population-weighted measure serves as a proxy for the reduction in the effective supply of productive land due to sea level rise and provides a direct input into the model as a negative shock to local land availability.

Figure 5 illustrates the share of the population living in areas projected to be permanently submerged by 2100 under RCP8.5. Exposure in OECD countries is highly concentrated in a limited number of low-lying coastal regions, particularly in sections of the Gulf Coast of the United States and in Northern Europe. In contrast, most of the world's interior regions and higher-elevation coastlines show negligible exposure. Importantly, this map reflects areas expected to be permanently inundated, rather than subject to episodic flooding, and therefore highlights zones where continued human settlement would require substantial protective infrastructure or relocation. These estimates represent potential physical exposure and do not account for future adaptation measures, such as building or reinforcing coastal defences, that could mitigate realized impacts.

Figure 5: Population affected by sea level rise in 2100 under the high-emission scenario (SSP5-8.5)

Percentage of population living in land that will be permanently submerged (ensemble median)



Source: World Resources Institute (Aqueduct), Gridded Population of the World (GPW v4.11), and authors' own calculations.
Notes: The map reports values at the resolution of a 0.25° × 0.25° grid cell (approximately 25 km at the equator). Values greater than 60% are windsorized at 60%.

3.2. Calibration of climate impacts

The final step of Module II consists of calibrating the projected climate impacts into a set of local economic shocks that can be fed into the spatial general equilibrium model. This calibration translates projected changes in climate impacts into time-varying, location- and sector-specific shocks to three key determinants of output: productivity, the depreciation rate of capital, and the supply of land. These impacts are estimated for the 927 regions included in the model calibration (for details, see Section 4 and Annex E).

For heat stress and flooding, we combine projected changes in frequency and intensity with the corresponding damage elasticities estimated in Module I. Heat stress projections are mapped into total factor productivity shocks using estimated elasticities linking extreme temperature exposure to firm-level multifactor productivity. Flood projections are translated into increases in effective capital depreciation rates, proportional to the projected change in flood frequency and local exposure. Changes in agro-climatic conditions are converted into total factor productivity shocks to the agricultural sector, based on projected changes in potential yields. Finally, sea-level rise is treated as a permanent reduction in the effective supply of land for housing and productive activity in affected coastal regions.

Panel A in Figure 6 shows the projected percentage change in non-agricultural sector productivity attributable to heat stress in 2100 under a high-emission scenario (SSP5-8.5). The results reveal a clear geographic gradient: productivity losses are most severe in OECD regions already characterised by high baseline temperatures, including parts of northern Australia and of Latin America. In these areas, rising temperatures push working conditions further beyond physiological and operational thresholds, leading to declines in firm productivity of more than 10% in several cases. In contrast, cooler regions at higher latitudes experience much smaller impacts, with many areas showing only marginal reductions in productivity. Overall, the map highlights that the direct impacts of heat stress constitute a predominantly tropical and subtropical challenge, with important implications for global production patterns and the capacity of exposed economies to sustain growth under a warming climate.

In panel B we see a heterogeneous global pattern of changes in agriculture sector productivity, with sizeable productivity gains concentrated in higher-latitude regions such as Canada and northern Europe, where warming temperatures and longer growing seasons improve the biophysical conditions for crop cultivation. In contrast, some OECD regions, including parts of Australia, South Europe, and Central America, experience substantial declines in suitability, in some cases exceeding 50%. Many of these areas already operate close to climatic thresholds for many staple crops and further increases in heat and water stress sharply reduce expected yields.

Panel C shows the projected increase in the annual capital depreciation rate attributable to flooding. Compared with the heat and agricultural suitability channels, the extent of flood-induced capital losses is much more geographically concentrated. The largest increases occur in regions with high baseline flood risk and growing exposure. In several of these regions, the annual depreciation rate rises by more than one percentage point, reflecting the effect of more frequent flooding

episodes. By contrast, most higher-latitude and arid regions see little or no change in depreciation rates, consistent with their low baseline flood hazard. Although more spatially limited than other damage channels, flood-driven capital losses can have substantial local economic impacts, given the concentration of people and assets in vulnerable floodplains.

Finally, Panel D reports the projected percentage of land lost due to sea level rise, i.e. areas that are expected to become chronically flooded as coastal water levels rise. The impacts are highly concentrated in East Asia, particularly Bangladesh, Vietnam, parts of China, the state of Louisiana in the US, and the Netherlands, with smaller but notable losses visible in parts of South America and select island and archipelagos. Although the absolute share of land lost may be small for most countries, the affected areas often contain large populations and critical economic infrastructure, so that that even modest reductions in land availability can generate substantial local economic pressures.

4. The climate and adaptation spatial general equilibrium model: OECD-CASGEM (Module III)

4.1. Overview

CASGEM belongs to the class of quantitative spatial models that provide a structural model for analysing the spatial distribution of economic activity and the effects of localized shocks, such as those related to climate. These models build on the foundational work of Krugman (1991) on economic geography and the quantitative model of Ricardian trade of Eaton and Kortum (2002), among others. A key feature of quantitative spatial models is their ability to capture general equilibrium interactions across locations through trade linkages, migration responses, and factor market adjustments using a network of spatial frictions that is based on realistic geography at a high level of spatial granularity.[8]

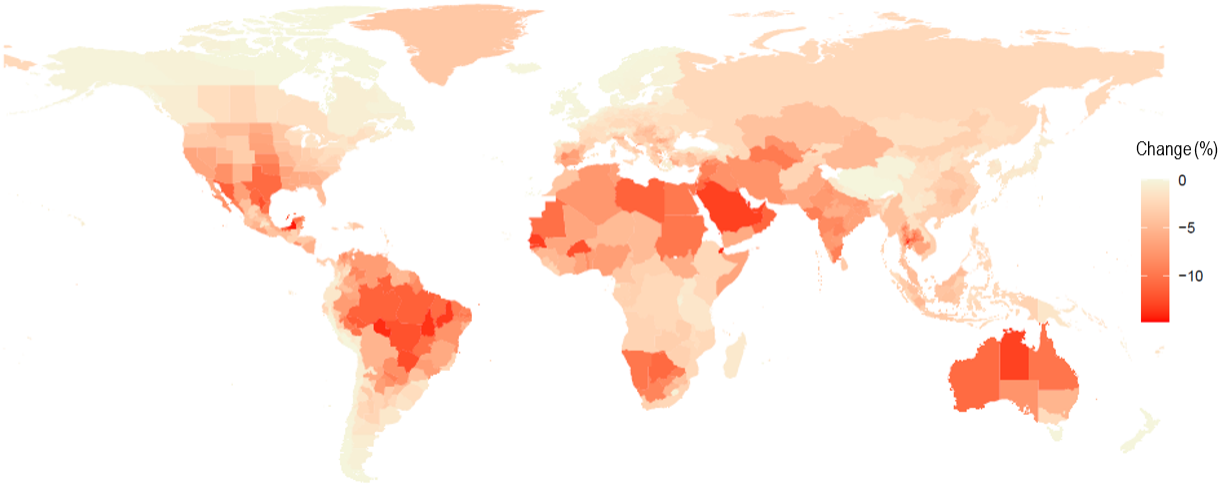
By incorporating spatial heterogeneity and movement costs for goods and people, quantitative spatial models provide a micro-founded yet tractable approach to estimating the aggregate economic consequences of localized shocks. A growing set of studies, reviewed in Desmet and Rossi-Hansberg (2024), employ these models to assess climate impacts and the role of spatial adaptation through shifts in labour and production across space and sectors (e.g. Desmet and Rossi-Hansberg, 2015; Costinot et al., 2016; Conte, 2023; Bilal and Rossi-Hansberg, 2023). These models offer some important advantages relative to other existing methods. They have the necessary spatial resolution to accommodate large heterogeneity in damages, they incorporate agents' ability to adapt to a changing climate through spatial adaptation, and they appropriately account for how spatial frictions shape interactions between locations based on realistic geography.

Our model describes a dynamic spatial economy composed of multiple sub-national locations across different countries, where households and firms interact through production, trade, and

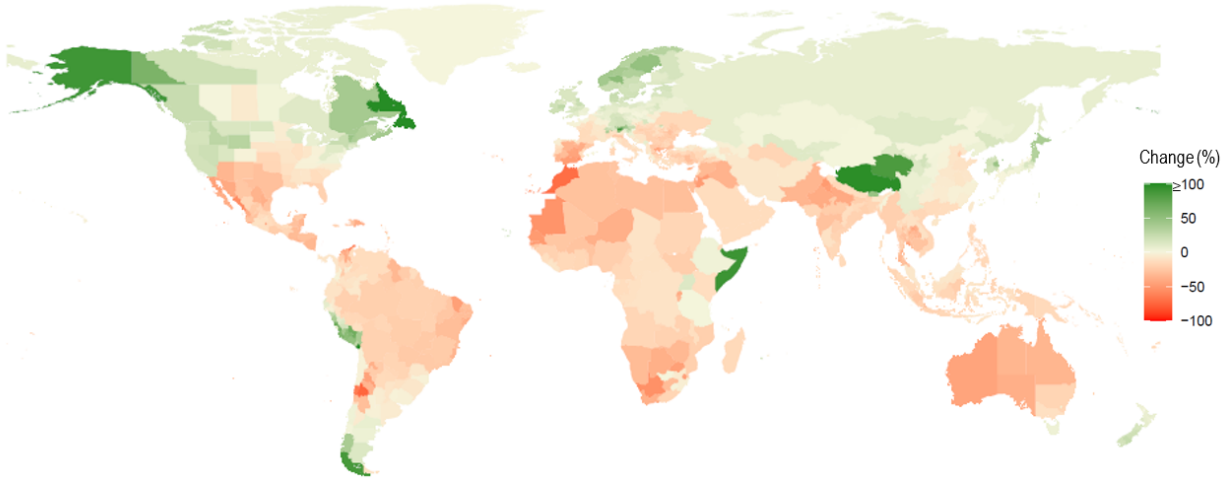
[8]See Redding and Rossi-Hansberg (2017) for a review of the quantitative spatial economics literature and Desmet and Rossi-Hansberg (2024) for a review of how these models have been used to tackle questions related to climate.

Figure 6: Damages from climate change by impact channel in 2100 under the high-emission scenario (SSP5-8.5)

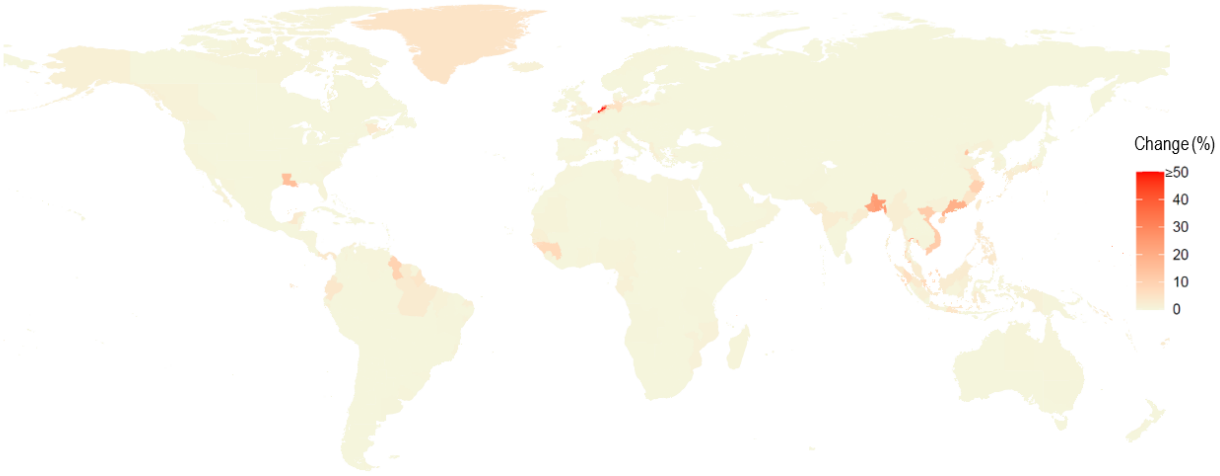
(a) Percent change in non-agricultural sector productivity due to heat stress



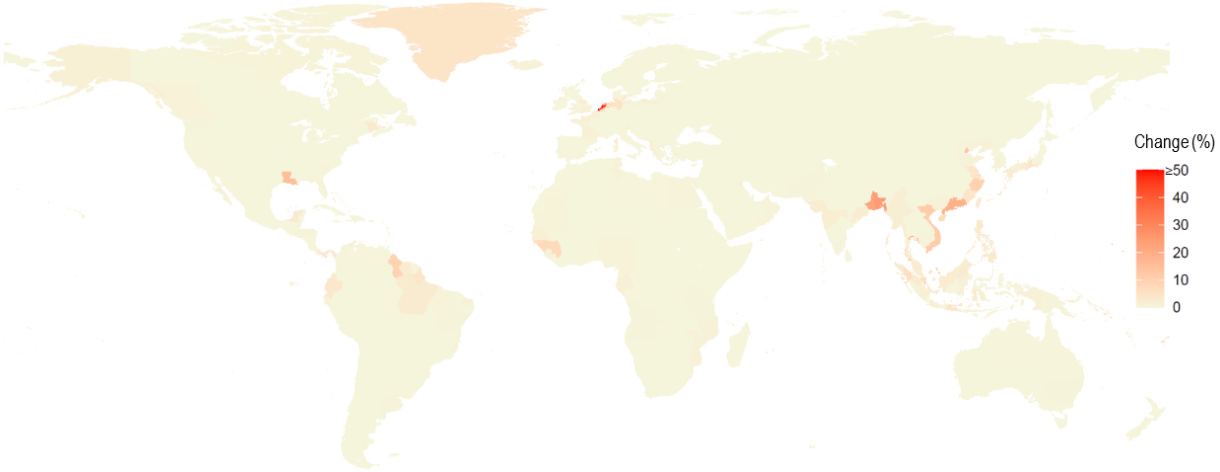
(b) Percent change in agricultural sector productivity due to changes in agro-climatic conditions



(c) Percentage point increase in annual capital depreciation rate due to flooding



(d) Percentage of land lost due to sea level rise

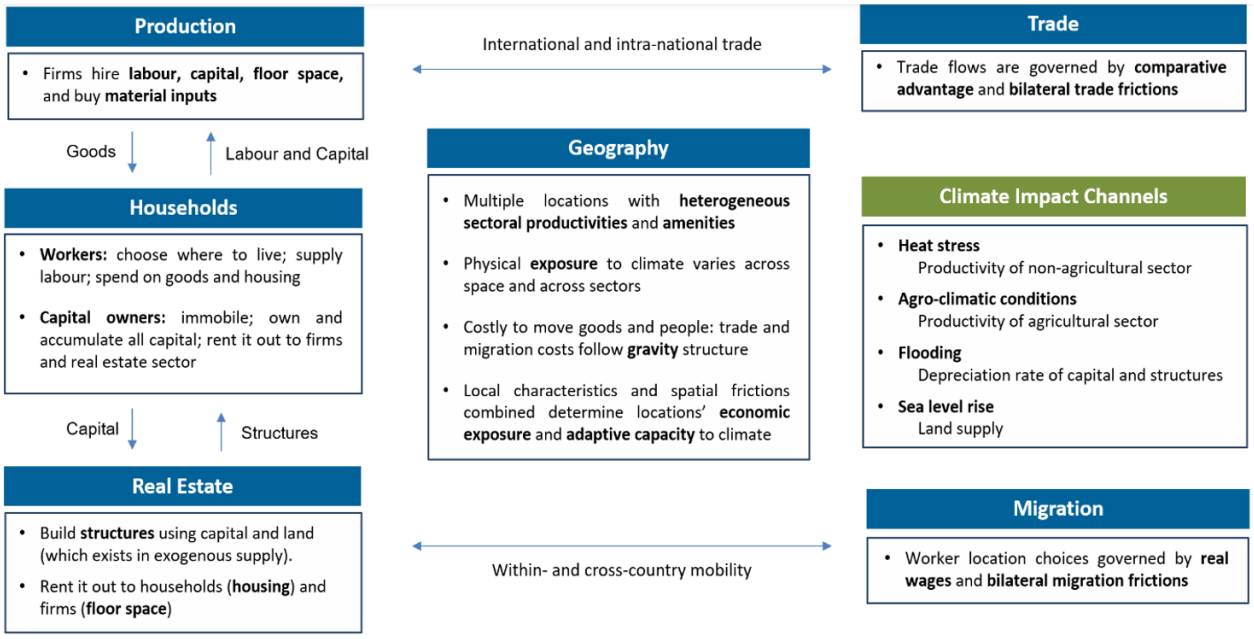


Source: Costa et al. (2024), Climate Change Knowledge Portal (World Bank), World Resources Institute (Aqueduct), Global Population Density (GPWv4), FAO-GAEZ and authors' own calculations.
Notes: The maps report values at the resolution of a 0.25° × 0.25° grid cell (approximately 25 km at the equator).

migration. It captures how local advantages, trade linkages, and mobility costs jointly determine economic outcomes across regions. Trade and migration frictions play a central role in shaping economic geography, by influencing the distribution of workers and production across space, as well as the degree of vulnerability to local and external shocks.

The model is made up of several building blocks, summarised in Figure 7. In the model, there are two types of households: workers and capitalists. Workers choose where to live and allocate their income across goods from multiple sectors and housing services. Their location choices depend on local amenities, real wages, cost of living, and migration frictions. Capital owners, on the other hand, are immobile. They own all capital in the economy and use capital income - their only source of income - to consume goods and invest in capital. On the production side, there are two types of firms: intermediate and final goods producers. Intermediate firms with heterogeneous productivity use labour, capital, floor space and material inputs to produce differentiated goods. Final goods producers then source these varieties from the suppliers offering the lowest price net of trade costs and assemble them into final goods for consumption or for use as material inputs in intermediate goods production both domestically and abroad. Housing (for households to live) and floor space (for firms to produce) are supplied by a real estate sector that produces structures by combining land, supplied exogenously, and capital, whose services are rented from capitalists. The model is described in Annex E.

Figure 7: The Climate and Adaptation Spatial General Equilibrium Model (OECD-CASGEM)



Notes: The figure provides an overview of the main building blocks of the quantitative spatial model OECD-CASGEM.

4.2. Model Description

We now lay out in more detail the main building blocks that make up the quantitative spatial general equilibrium model (OECD-CASGEM).

4.2.1 Setup

There are $n = 1, \ldots, N$ locations, each belonging to one of $l = 1, \ldots, L$ countries, with the function $\sigma : \{1, \ldots, N\} \to \{1, \ldots, L\}$ mapping each location n to a country l. A continuum $\omega \in \Omega$ of households populate the N locations. There are $j = 1, \ldots, J$ production sectors in the economy. Each location n is endowed with an amenity value $B_n > 0$, common to all households and entering positively in utility. The supply of land T_n for all $n = 1, \ldots, N$ is fixed. There is a continuum of firms producing varieties $\iota^j \in \mathcal{I}^j$, with average productivity A_n^j varying across locations. Goods can be traded across any pair of locations (i, n), incurring iceberg trade cost $\tau_{in}^j \geq 1$, with $\tau_{nn}^j = 1$. Similarly, people can migrate from any origin n to any destination i at cost $\kappa_{in} \geq 1$, with $\kappa_{nn} = 1$.

4.2.2 Workers

Workers earn income by supplying labour and have preferences over consumption, housing, and location. The indirect utility of a household $\omega \in \Omega$ residing in location n is:

$$V_n(\omega) = \max_{i \in \{1,\ldots,N\}} \frac{b_{in}(\omega)}{\kappa_{in}} \cdot \frac{B_i w_i}{P_i^{\alpha} Q_i^{1-\alpha}} \tag{1}$$

where:

- $b_{in}(\omega)$ denotes idiosyncratic preferences for locations $i = 1, \ldots, N$, which follow a Fréchet distribution $F(b) = e^{-b^{-\varepsilon}}$ with dispersion parameter $\varepsilon > 0$, independently and identically distributed across all workers and location-pairs.
- B_i is the average value of local amenities common to all workers
- P_i is the price of the final good which is itself a price index that combines the price of local final sectoral goods through the Cobb-Douglas function

$$P_i = \sum_{j=1}^{J} (P_i^j)^{\alpha^j}, \quad \text{where} \quad \sum_{j=1}^{J} \alpha^j = 1 \tag{2}$$

where $j = 1, \ldots, J$ denotes production sectors of the economy.

- Q_i is the price of housing services
- κ_{in} is the utility cost of migrating to $i = 1, 2, \ldots, N$ for a household currently residing in n

4.2.3 Capital owners

Capital owners are immobile and own all capital stock in the economy. They rent this capital to firms, where it is used as an input in goods production, and to the real estate sector, where it is used in the production of structures. Their income in each location n is equal to the rental rate of capital, r_n, multiplied by the local capital stock, K_n, which constitutes their sole source of income. Capital owners derive utility from a stream of consumption and allocate all non-consumed income to investment, which is transformed into new capital. Once installed, capital becomes geographically immobile. Formally, a capitalist in location n chooses consumption and investment to solve:

$$V_{nt}^K = E_t \sum_{s=0}^{\infty} \beta^s \frac{(C_{nt+s}^K)^{1-1/\psi}}{1-1/\psi} \tag{3}$$

subject to the intertemporal budget constraint:

$$r_{nt} K_{nt} = P_{nt} \left(C_{n,t}^K + K_{nt+1} - (1-\delta_{nt}) K_{nt} \right) \tag{4}$$

where ψ denotes the intertemporal elasticity of substitution and δ_t is the rate of capital depreciation, which may vary over time. As shown in Kleinman et al. (2023), in the special case of log-utility ($\psi = 1$), which we assume in our calibration, capital owners follow a constant savings rule with optimal investment given by the simple law of motion

$$K_{nt+1} = \beta r_{nt} K_{nt} \ . \tag{5}$$

4.2.4 Intermediate goods producers

There are two types of producers in the economy: intermediate and final goods producers. Intermediate goods producers generate all value-added in the economy by hiring labour from households, capital from capitalists and floor space from the real estate sector and purchasing material inputs from other sectors (including itself). The production function of an intermediate goods firm of type $\iota^j \in I^j$ producing goods of sector j in location n is given by:

$$q_n^j(\iota^j) = A_n^j z(\iota^j) \left[(L_n^j(\iota^j))^{\lambda} (K_n^j(\iota^j))^{\eta} (H_n^j(\iota^j))^{1-\lambda-\eta} \right]^{\beta_n^j} \prod_{k=1}^{J} (M_n^{jk}(\iota^j))^{\gamma_n^{jk}} \tag{6}$$

with $\sum_{j=1}^{J} \gamma_n^{jk} = 1 - \beta_n^j$ and where: $z(\iota^j)$ denotes firm idiosyncratic productivity which follows a Fréchet distribution $F(b) = e^{-b^{-\theta}}$ with dispersion parameter $\theta > 0$, independently and identically distributed across all firms and locations; $L_n^j(\iota^j)$ denotes employed labour; $K_n^j(\iota^j)$ denotes employed capital; $H_n^j(\iota^j)$ denotes employed structures; and $M_n^{jk}(\iota^j)$ denotes purchases of material inputs from sector k.

Profit maximization implies that intermediate goods firms will produce at a unit cost of

$$x_n^j = \mu_n^j (w_n^\lambda r_n^\eta Q_n^{1-\lambda-\eta})^{\beta^j} \prod_{k=1}^{J} (P_n^k)^{\gamma^{jk}}, \quad \text{with} \quad \beta^j + \sum_{k=1}^{J} \gamma^{jk} = 1 \ . \tag{7}$$

Due to perfect competition the factory-gate price is equal to

$$p_n^j(\iota^j) = \frac{x_n^j}{A_n^j z(\iota^j)} \ . \tag{8}$$

4.2.5 Final goods producers

In each sector $j = 1, 2, \ldots, J$ final goods producers buy varieties of intermediate goods and combine them to produce final sectoral goods according to function

$$(\tilde{Q}_i^j) = \left(\int_0^1 (\tilde{q}_i^j(\iota^j))^{\frac{\eta-1}{\eta}} d\iota^j \right)^{\frac{\eta}{\eta-1}}, \quad \text{with} \quad \eta > 0 \tag{9}$$

and source each variety from the lowest-cost supplier across all locations at price

$$\tilde{p}_i^j(\iota^j) = \min_{n=\{1,\ldots,N\}} \{\tau_{in}^j p_1^j(\iota^j), \ldots, \tau_{iN}^j p_N^j(\iota^j)\} \ , \tag{10}$$

where the optimal destination will depend on the combination of factory-gate prices $p_n^j(\iota^j)$ and bilateral trade costs τ_{in}^j.

4.2.6 Real Estate Sector

A real estate sector in each location $n = 1, \ldots, N$ uses a Cobb-Douglas production technology to transform capital K_n and land T_n into structures H_n according to the function

$$H_n = K_n^\mu T_n^{1-\mu} \ , \tag{11}$$

where land T_n is in fixed exogenous supply. The real estate sector maximizes profits and takes the rental rate of capital r_n as given which yields the following structures supply curve:

$$H_n(q_n^\star) = T_n \left(\frac{\mu}{r_n} \right)^{\frac{\mu}{1-\mu}} Q_n^{\frac{\mu}{1-\mu}} \ , \tag{12}$$

where Q_n is the price of structures in location $n = 1, \ldots, N$.

4.2.7 Trade

Iceberg trade costs between a location pair $(i.n)$ are assumed to depend on their bilateral distance dist_{in} and on country-pair specific characteristics $\phi_{\sigma(i),\sigma(n)}$ according to the expression

$$\tau_{in}^j = (\text{dist}_{in})^{\rho^j} \phi_{\sigma(i),\sigma(n)} \ , \tag{13}$$

where ρ^j is the distance-decay rate, i.e. the rate at which trade costs increase with distance, which may vary across sectors $j = 1, 2, \ldots, J$.

These iceberg trade costs, combined with profit maximization by intermediate and final goods producers and the assumed distribution of idiosyncratic firm productivity (Fréchet), imply that a location n's share of expenditure on sector $j = 1, 2, \ldots, J$ originating from location $i = 1, \ldots, N$, given by π^j_{nit}, is equal to

$$\pi^j_{ni} = \frac{A_i^{\theta^j}(x_i \tau^j_{ni})^{-\theta^j}}{\sum_{l=1}^{N} A_m^{\theta j}(x_m \tau^j_{nm})^{-\theta^j}} \ . \tag{14}$$

4.2.8 Migration

Similarly, iceberg migration costs between a location pair $(i.n)$ are also assumed to depend on their bilateral distance dist_{in} on country-pair characteristics $\psi_{\sigma(i),\sigma(n)}$ and on a move-out cost term $\eta_n > 0$ according to the expression

$$\kappa_{in} = e^{-\eta_n \mathbf{1}\{i=n\}} (\text{dist}_{in})^{\phi} \psi_{\sigma(i),\sigma(n)} \ , \tag{15}$$

where δ is the distance-decay rate, i.e. the rate at which trade costs increase with distance. The term $e^{-\eta_n \mathbf{1}\{i=n\}}$ is only different from 1 in the case where $i = n$ so that remaining in origin location n entails an extra cost reduction over and above the effect of distance.

These iceberg migration costs, combined with household utility maximization and the assumed distribution of idiosyncratic location preferences (Fréchet) imply that the share of workers living in location i who decide to move to location $n = 1, \ldots, N$ (which includes location i itself), given by λ_{ni}, is equal

$$\lambda_{ni} = \frac{B_n(\kappa_{ni} P_n^{\alpha} Q_n^{1-\alpha})^{-\varepsilon} w_n^{-\varepsilon}}{\sum_{m=1}^{N} B_m(\kappa_{mi} P_m^{\alpha} Q_m^{1-\alpha})^{-\varepsilon} w_m^{-\varepsilon}} \ . \tag{16}$$

This implies local population evolves according to

$$L_{nt} = \sum_{i=1}^{N} \lambda_{nit} L_{i,t-1} \tag{17}$$

for all $n = 1, \ldots, N$.

4.2.9 Equilibrium

We assume trade is balanced across all pairs of locations. Trade balance and the zero-profit condition imply that sales must equal to expenditure X_n^j by final goods firm, which must in turn equal the sum of firms' spending on material inputs and households' final consumption in equilibrium. In other words, for each location $n = 1, \ldots, N$ and sector $j = 1, 2, \ldots, J$, goods market clearing implies that

$$X_{nt}^{j} = \sum_{k=1}^{J} \gamma_{n}^{kj} \sum_{i=1}^{N} \pi_{int}^{j} X_{it}^{k} + \alpha^{j} w_{it} L_{it} \ . \tag{18}$$

Since wages payments are equal to a fixed share $\lambda\beta^{j}$ of firm sales (and expenditures), the goods market clearing condition may also be written as

$$w_{nt} L_{nt}^{j} = (\lambda\beta^{j}) \sum_{k=1}^{J} \gamma_{n}^{kj} \sum_{i=1}^{N} \pi_{int}^{j} ((\lambda\beta^{k})^{-1} \frac{L_{nt}^{k}}{L_{it}} + \alpha^{j}) w_{it} L_{it} \ , \tag{19}$$

which, together with the trade balance condition

$$\sum_{j=1}^{J} X_{n}^{j} = \sum_{j=1}^{J} \sum_{k=1}^{J} \sum_{i=1}^{N} \gamma_{n}^{kj} \pi_{int}^{j} X_{n}^{k} + \alpha^{j} w_{it} L_{it} \tag{20}$$

pins down equilibrium wages w_{nt} and sectoral employment shares L_{nt}^{j}/L_{nt}. Since there is a unique wage w_n, labor will therefore implicitly reallocate across sectors until all sector wages are equalized in each location.

Finally, market clearing in the real estate market implies that the supply of structures by the real estate sector equals the sum of the demand for housing by workers and of the demand for floor space by intermediate goods firms. Therefore, in equilibrium, we must have that the equilibrium price of structures Q_n (and of housing and floor space) is equal to

$$Q_{n} = T_{n}^{-(1-\mu)} \left(\left(\frac{r_{n}}{\mu} \right)^{\mu} \left((1-\alpha) w_{n} L_{n} + \sum_{j=1}^{J} \frac{w_{n} L_{n}^{j}}{\beta^{j} (1-\lambda-\eta)} \right) \right)^{1-\mu} \ . \tag{21}$$

4.2.10 Definition of equilibrium

An equilibrium is defined as a sequence of prices $\{P_{nt}^{j}, P_{nt}, x_{nt}^{j}, w_{nt}, Q_{nt}, r_{nt}\}_{t=1}^{T}$ and allocations $\{\pi_{nit}^{j}, \lambda_{nit}, L_{nt}^{j}, L_{nt}, H_{nt}, K_{nt}\}_{t=1}^{T}$ that, given parameters $\{\beta^{j}, \gamma^{jk}, \lambda, \eta, \alpha, \alpha^{j}, \theta_{j}, \varepsilon, \zeta, \tau_{ni}^{j}, \kappa_{ni}\}$, initial conditions $\{L_{n0}, K_{n0}\}$, and a sequence of exogenous variables $\{A_{nt}^{j}, B_{n}, T_{nt}, \delta_{nt}\}_{t=1}^{T}$ for all $j = 1, \ldots, J$, $n = 1, \ldots, N$ and $i = 1, \ldots, N$, satisfies equations (24)–(34) in Annex E for every $t = 1, \ldots, T$.

4.3. Model Calibration

4.3.1 Regions and sectors

The model is calibrated for 927 regions across 186 countries, covering 11 sectors of production[9] in OECD member countries and 3 aggregate sectors (agriculture, manufacturing, and services) in all other countries. We divide countries into smaller administrative units depending on their relationship to the OECD. Figure A.3 shows a map of the calibrated administrative units. For OECD member states[10], we employ the Territorial Level 2 (TL2) classification, which is the OECD's system for defining large subnational regions such as provinces or states. For OECD accession candidate countries and OECD key partners[11], denoted OECD+ in Figure A.3, we use Admin-1 sub-national units from the GADM (Global Administrative Areas) database, which provide a consistent first-level administrative division for countries outside the OECD TL2 framework. For all remaining countries, the model is calibrated at the national level, treating each country's entire territory as a single regional unit.

4.3.2 Data sources

The model calibration combines multiple international datasets to construct a harmonized panel of regional production, trade, and mobility flows, described in more detail in Annex E. For OECD member countries, we rely on regional accounts that provide gross value added, employment, and population at the sector-region level. For OECD accession countries and key partners, we use sub-national output and employment data harmonized at the first administrative level. All remaining countries are incorporated using nationally representative sectoral accounts, ensuring consistent coverage across the global economy. Across data sources, economic activity is harmonized into a common sectoral structure to preserve comparability.

To characterize production linkages and expenditure patterns, we use country-level input–output tables to compute sectoral value-added shares, intermediate input coefficients, and final demand shares. International trade flows are obtained from a global bilateral trade database and aggregated to match the sectoral structure of the model. Finally, labour mobility is measured using bilateral migration flows across countries and internal residential mobility within countries, allowing us to

[9]The sectors included are 1. Agriculture, forestry, and fishing; 2. Industry (except manufacturing and construction); 3. Manufacturing; 4. Construction; 5. Wholesale and retail trade; repair of motor vehicles and motorcycles; transportation and storage; accommodation and food service activities; 6. Information and communication; 7. Financial and insurance activities; 8. Real estate activities; 9. Professional, scientific and technical activities; administrative and support service activities; 10. Public administration, defence, education, human health and social work activities; 11. Arts, entertainment and recreation; other service activities; activities of household and extra-territorial organizations and bodies.

[10]The 38 OECD member countries are: Australia, Austria, Belgium, Canada, Chile, Colombia, Costa Rica, Czechia, Denmark, Estonia, Finland, France, Germany, Greece, Hungary, Iceland, Ireland, Israel, Italy, Japan, Korea, Latvia, Lithuania, Luxembourg, Mexico, Netherlands, New Zealand, Norway, Poland, Portugal, Slovakia, Slovenia, Spain, Sweden, Switzerland, Türkiye, the United Kingdom, and the United States.

[11]These reflect the current OECD categories as of 2025. Accession candidate countries include Argentina, Brazil, Bulgaria, Croatia, Indonesia, Peru, Romania, and Thailand. Key partners include Brazil, China, India, Indonesia, and South Africa.

calibrate both international and domestic reallocation mechanisms. Together, these datasets provide a representation of population distribution, sectoral composition, production structure, trade flows, and population movements across regions.

4.3.3 Model parameters

We combine information from these data sources with parameter values taken from the literature to calibrate the model parameters and unobserved exogenous variables, as summarized in Table E.3 in Annex E. Local sectoral TFPs, local amenities, and trade and migration cost functions are estimated through 'model inversion', as is common in the quantitative spatial literature. This involves using observed economic data – such as wages, trade flows, and migration patterns – and the model's equilibrium equations to infer unobserved structural parameters, such as local productivities, amenities, or trade and migration frictions. This approach ensures that the estimated parameters are consistent with the equilibrium conditions of the model, effectively retrieving the value of the underlying economic fundamentals that best explain the observed spatial distribution of economic activity. The calibration proceeds sequentially, as outlined below and detailed in Annex E. Figure A.13 in Annex A shows the model provides a good fit in describing the cross-country distribution of GDP per capita.

Step 1 begins with the trade-share equation (14). Following Head and Ries (2001), we rearrange the gravity equation to express bilateral iceberg trade costs as a function of bilateral trade shares and domestic absorption shares. Using bilateral trade shares from the ITPD-E dataset, we directly back out a full matrix of country-pair-specific trade costs. This step provides a data-driven measure of trade frictions that does not require solving the general equilibrium model. In Step 2, we use these inferred trade costs to recover sectoral price indices. We apply the method developed by Anderson and van Wincoop (2003), which links multilateral resistance terms to observed expenditures, sales, wages and population. Given the bilateral trade costs from Step 1 and information on sectoral spending and production patterns, we solve the system of equations implied by their framework (see equations (42) and (44) in Annex E) to obtain sectoral prices consistent with equilibrium trade behavior. Step 3 recovers implied sectoral productivities. Conditional on trade costs and prices, the goods market clearing condition (19) requires that production equals total demand in each sector and location. We use this condition to invert for the productivity levels that rationalise observed output patterns. As with the previous steps, this part of the calibration does not require iterating the full model.

The next set of parameters – bilateral migration costs (both internal and international) and local amenities – cannot be recovered without solving the model. Step 4 therefore combines inversion with a simulated method of moments procedure. We implement an iterative algorithm that jointly targets (i) observed flows of migrants across borders, (ii) the observed level of within-country mobility, and (iii) the spatial distribution of population. For any trial vector of migration costs and amenities, the model is solved to compute the implied flows and population levels. The parameters are then updated until the simulated moments match their empirical counterparts. Finally, step

5 recovers the initial distribution of capital across locations. Starting from an initial guess for the capital stock in each location, we iteratively solve the model using the parameter values estimated above and update capital in each location after every iteration. This procedure is repeated until the capital distribution converges to a steady state across all locations.

We define the calibrated model incorporating all features described above as the baseline model. Due to the presence of bilateral migration frictions, the model features transition dynamics through population movements across locations. In general, the calibrated model is not in steady state, meaning that even in the absence of shocks, population shares will continue to evolve as the economy converges toward its long-run equilibrium. Moreover, we feed country-level population projections to capture population growth dynamics consistent with each SSP scenario. We refer to the baseline path as the implied model equilibrium sequence when run forward in 2025-2100 if climate conditions remain fixed at their historical levels.

5. Quantitative results

This section presents the macroeconomic implications of climate change generated by CASGEM. We begin by reporting the country-level impact of climate change on GDP per capita and other aggregate outcomes, capturing direct, local impacts, within-region propagation through supply chains, and cross-region and international spillovers through trade and mobility, as well as the ability of economies to adjust over time. This is computed by feeding projected damages from productivity losses, capital destruction, and loss of land, derived from the local, micro-level damages and climate projections, into the calibrated model. We solve for the economy's future equilibrium path in 2025-2100 and compare it to that of an economy in which losses from climate change are absent, i.e. the baseline path. This allows countries to interact through trade and migration and to adjust both patterns of specialization and population distribution as climate conditions evolve. This benchmark simulation provides us with a comprehensive estimate of climate damages.

We then use a sequence of counterfactual exercises to disentangle the mechanisms that shape these outcomes and to identify the channels through which economies adapt. Understanding the economic costs of future climate conditions requires quantifying direct, local impacts within each economy and assessing how these shocks propagate through global linkages and how economies adjust over time. To illustrate these mechanisms, we present a set of model-based counterfactual simulations designed to highlight two questions:

- How much do economic linkages, both within and across regions, shape the transmission of climate shocks?
- How important is the ability of economies to adjust trade and migration patterns in response to climate change?

The first set of counterfactuals examines how climate damages would unfold if key economic linkages were disabled. We begin by shutting down cross-region spatial linkages, preventing trade

and migration flows across sub-national regions – including across those in the same country. This "local-only world" attributes all economic losses solely to local exposure and internal (i.e. within-region) adjustments. Comparing this to the full model highlights the role of cross-region spillovers in amplifying or mitigating climate impacts. We then perform an additional experiment in which input–output linkages are removed. This allows us to isolate the importance of production networks and supply chains, i.e. firms' purchases of intermediate inputs from other firms, both domestic and foreign. Together, these two exercises show that both within- and cross-regional linkages shape the magnitude and distribution of climate damages.

The second set of counterfactuals examines the importance of adjustment mechanisms, namely the ability of economies to marginally reorient trade and migration flows in response to climate change. In these simulations, economies remain open, but we impose that either trade or migration flows remain fixed at the levels that would have prevailed if climate conditions remained fixed at historical levels. We first freeze trade shares while allowing migration to adjust, then freeze migration shares while allowing trade to adjust, and finally freeze both. These "no-adjustment" scenarios quantify how much resilience is lost when economies are unable to redirect imports toward less-affected suppliers, shift export markets, or adjust population across sub-national regions (including within countries). Comparing each restricted scenario to the full model isolates how much each adjustment margin - trade, migration, or the combination of both - contributes to reducing or, potentially, amplifying climate damages.

These exercises provide a model-consistent decomposition of the mechanisms driving climate damages. The first set isolates how climate shocks propagate through economic linkages; the second highlights how much is gained by allowing economies to adjust along trade and migration margins. Because all simulations rely on the same climate projections and model parameters, differences in outcomes reflect differences in interaction and adjustment possibilities alone.

5.1. The macroeconomic impact of climate change

Figures 8, 9, and A.4-A.11 show the baseline results of the model under a current-policy scenario (SSP2-4.5) and a high-emission scenario (SSP5-8.5). They depict how GDP per capita across regions and countries will change in 2050 and 2100 due to changes in climate under each scenario. Figures 8 and 9 present the impacts in 2050 and 2100 for all 927 region in the calibrated model. Figures A.6 and A.7 in Annex A show the economic cost for OECD countries by impact channel and Figures A.4 and A.5 show the same for OECD+ countries.[12] Figures A.8 and A.9 offer a regional aggregation. Finally, Figures A.10 and A.11 report impacts across OECD countries under the ensemble median climate projection together with a band reflecting the range of impacts implied by alternative climate models. This interval illustrates the uncertainty arising from differences in climate projections. Together, these figures highlight the substantial and uneven global burden of alternative climate paths and illustrate how different impact channels dominate losses across different parts of the world.

[12]This includes OECD accession countries and key partners, in addition to OECD member countries.

The results show that a high-emission scenario (SSP5-8.5) is associated with widespread reductions in GDP per capita across almost all regions by mid-century, with average GDP per capita among OECD countries falling by 2.5% in 2050 and 9% in 2100 (Figure A.7). Under a current-policy scenario (SSP2-4.5), projected losses fall to around 1.7% by 2050 and 3.1% by 2100 across OECD countries (Figure A.6). Important differences emerge across OECD members with, for example, Southern European countries displaying noticeably higher losses than the OECD average. Parts of the United States, Australia, and Chile also display above-average losses due to the combination of higher heat stress and worsening crop growth conditions. By contrast, Northern Europe, Korea, and Japan experience some of the lowest impacts globally in 2050. By 2100, Southern Europe and parts of the United States and Australia face losses above 10–15 percent under SSP5-8.5. Globally, losses to GDP per capita are higher, amounting to 5.9 percent in 2050 and 18.3 percent in 2100 under SSP5-8.5 (Figure A.9), and 3% and 6.3%, respectively, under SSP2-4.5 (Figure A.8). These estimates fall within the range reported in the recent climate-macroeconomics literature. For scenarios comparable to SSP5-8.5, recent integrated assessment modelling suggests global output losses of around 7% (Barrage and Nordhaus, 2024), while temperature-growth estimates project global losses of about 23% (Burke et al., 2015), and empirical climate-economy studies find losses of about 7% or 7-14% by 2100 (Kahn et al., 2021; Kalkuhl and Wenz, 2020), respectively.

Beyond cross-country differences, the spatial distribution of damages within countries is also highly heterogeneous. The regional maps (Figures 8-9) show that neighbouring regions within the same national borders often experience markedly different projected impacts, reflecting fine-scale variation in exposure to heat stress, agricultural suitability, flooding and coastal risk, and local economic structure. For example, southern and inland regions of the United States, Mexico, Spain and Italy experience considerably larger projected losses than northern or coastal temperate areas, while in Australia damages are concentrated in hotter interior and northern regions relative to more temperate southern coastal zones. Often the largest losses are observed in regions that are already poorer, leading to increases in within-country inequality.[13] Even in countries with modest national-average effects, such as France, Germany and Japan, warmer or more agricultural regions face higher productivity and land-related damages. As a result, national averages mask important local pressures, suggesting that climate change may increasingly operate as a regional shock within advanced economies.

Globally, heat stress is the main driver of damages in most regions (Figure A.8-A.9). In 2050 (Panels A), heat stress already accounts for a substantial share of the projected losses in many regions, including in what are historically relatively cold areas in Central Asia, Northern Europe, Western Europe, and North America, with reductions in productivity driving losses that exceed 20 percent in some regions by 2100 under SSP5-8.5 (Figure A.9b). The deterioration of crop-growing conditions contributes significantly to GDP per capita losses in regions such as Northern Africa, Southern Asia, and parts of Sub-Saharan Africa, which rely heavily on the agriculture sector and

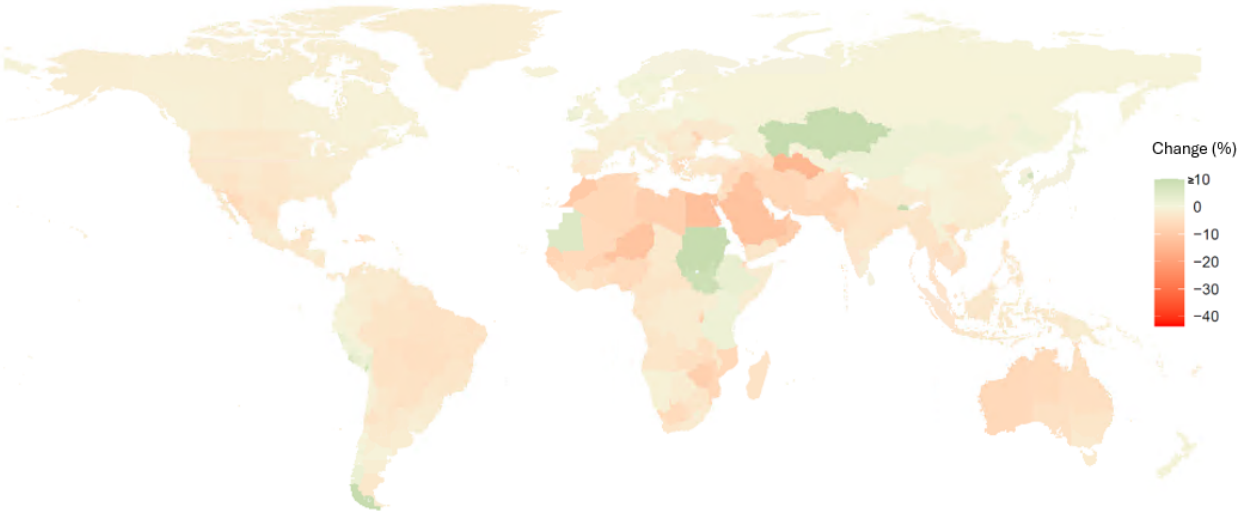
[13]For example in Italy, by 2050 and under SSP5-8.5, the largest losses are observed in Sicily and Molise, while positive impacts are estimated for South Tirole and Trento.

exhibit a larger crop sensitivity to a changing climate, but also in specific OECD members, such as those in Southern Europe, the United States, Australia, and Chile. Flood damages and sea-level rise tend to play smaller but still notable roles, especially in coastal and low-lying regions such as south and southeast Asia and Oceania. Importantly, by 2100 few regions escape negative effects entirely.

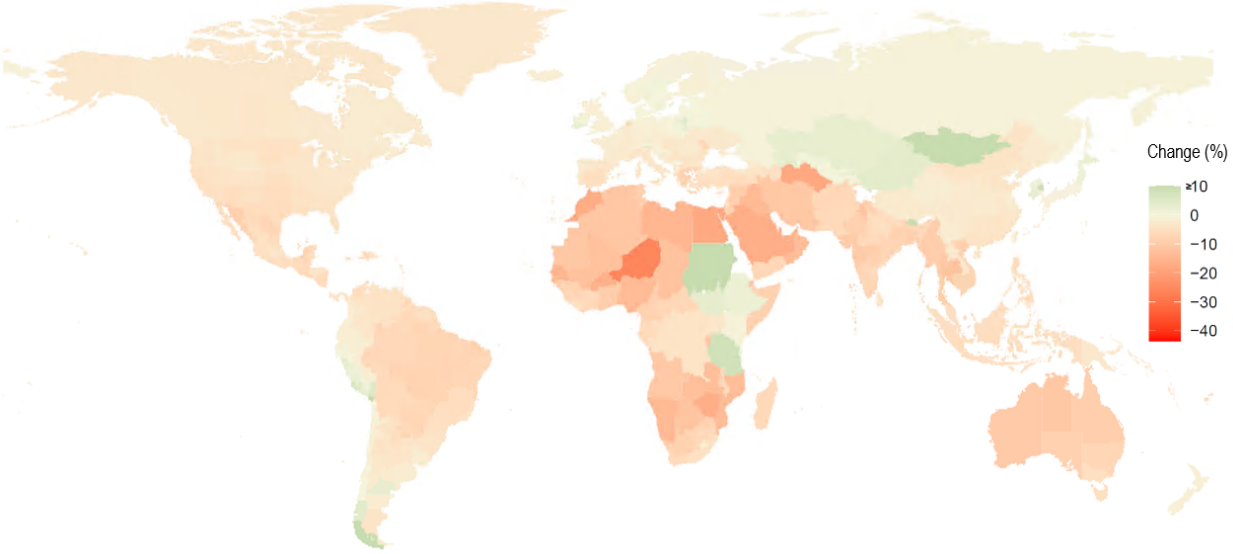
The model also predicts large endogenous reallocations of population across and within countries as households respond to spatially heterogeneous climate damages. For OECD economies, this implies a growing divergence between cooler and warmer members. Under a high-emissions scenario (SSP5-8.5), by 2050 countries in Northern Europe and North America already experience net migration inflows, while Southern European and other warmer OECD countries see modest gains or mild outflows. This pattern reflects spatial differences in future climate damages and the resulting changes in real wages across locations. By 2100, these contrasts become much more pronounced. Internal migration is an important part of this adjustment, with populations shifting within countries toward cooler, higher-latitude regions, such as in Spain, Portugal, Mexico, and the United States. These population movements, documented in detail in Annex F, arise endogenously from households' location choices in response to climate-induced changes in productivity, capital depreciation rates and land supply.

Figure 8: Economic impact of climate change under the current-policy scenario (SSP2-4.5)

(a) Percentage change in GDP per capita in 2050



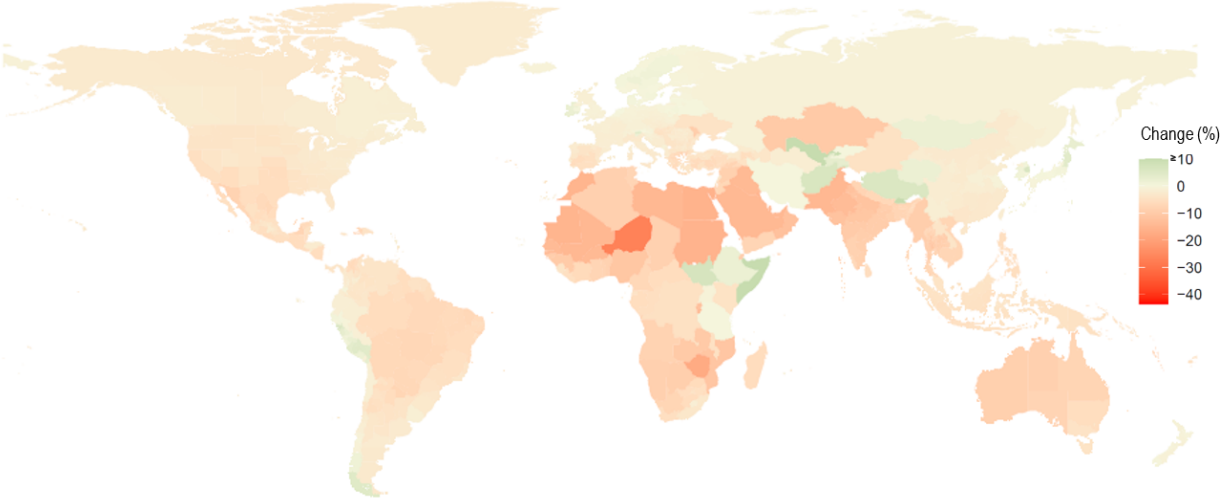
(b) Percentage change in GDP per capita in 2100



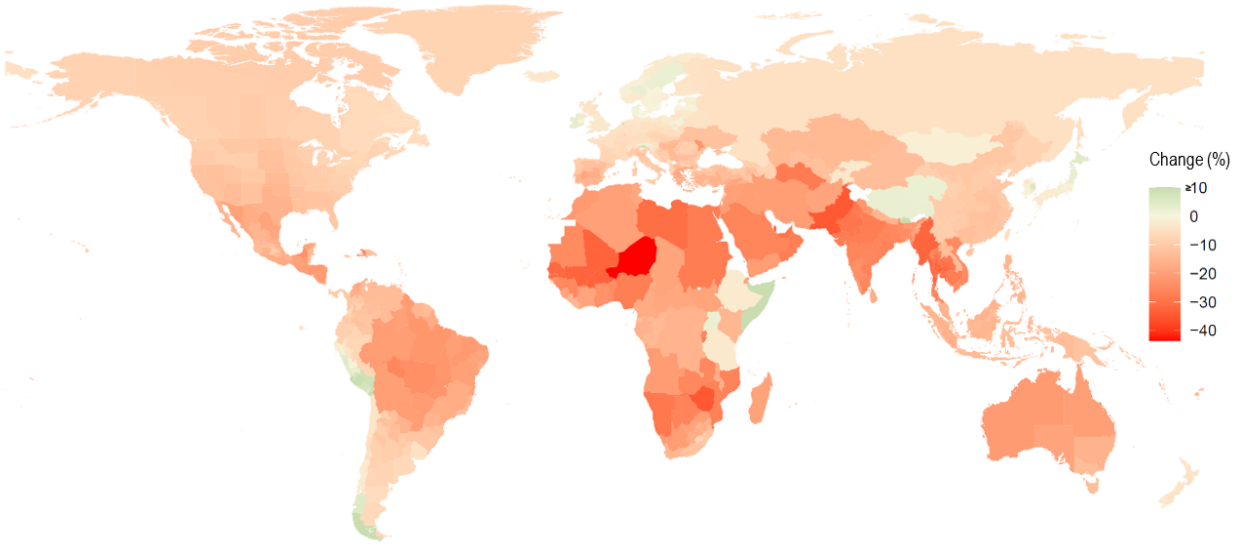
Source: Authors' calculations.
Notes: The figure shows the model-implied loss in annual GDP per capita relative to a no-climate change scenario. GDP is expressed in real terms by accounting for the price of goods. GDP loss is computed as the loss in sector-level GDP averaged across sectors using sectoral value-added weights, which we then divide by change in population to obtain GDP per capita loss. Changes larger than 10 percent and windsorized at 10 percent.

Figure 9: Economic impact of climate change under the high-emission scenario (SSP5-8.5)

(a) Percentage change in GDP per capita in 2050



(b) Percentage change in GDP per capita in 2100



Source: Authors' calculations.
Notes: The figure shows the model-implied loss in annual GDP per capita relative to a no-climate change scenario. GDP is expressed in real terms by accounting for the price of goods. GDP loss is computed as the loss in sector-level GDP averaged across sectors using sectoral value-added weights, which we then divide by change in population to obtain GDP per capita loss. Changes larger than 10 percent and windsorized at 10 percent.

5.2. The role of economic linkages in transmitting climate shocks

Having quantified the macroeconomic cost of climate change, we now examine how the model's transmission mechanisms (i.e. linkages) shape these outcomes. In general, there would only be a one-to-one relationship between local shocks and local economic outcomes if all locations operated in

autarky and shared identical characteristics. To assess the role of specific transmission mechanisms in the model, we conduct counterfactual analyses. We do this by simulating the same climate shocks under a different model calibration where we shut down model transmission mechanisms to isolate their effect. We focus on two broad types of linkages:

- **Cross-regional spatial linkages:** because locations are interconnected through trade and labour mobility, shocks will spill over beyond their location of origin. If a shock lowers TFP in one location, its trade partners will experience higher import costs and shifts in demand, so that even countries not directly affected by heat stress will be impacted by the shock. Trade linkages have an ambiguous impact on GDP losses because they can both soften and amplify the effects of shocks. On one hand, trade allows regions to diversify their sources of goods and inputs, reducing dependence on any single location. On the other hand, trade can also amplify losses by transmitting shocks through cross-country contagion. Additionally, migration flows represent another key spatial linkage through which climate impacts spread. As climate conditions worsen in one region, people may move to other areas with more favourable conditions, either within or across borders. Migration can cushion the economic impacts of climate change by redistributing labour and mitigating labour shortages in more heavily affected areas. However, migration can also exacerbate challenges in receiving regions by increasing competition for jobs (putting downward pressure on wages) and putting upward pressure on the local price of goods and housing. In our counterfactual simulations, we isolate the role of trade and migration flows by preventing movement of goods and people across borders or between regions within countries. This allows us to measure the importance of spatial linkages in determining the distribution of local economic impacts around the world.

- **Within- and cross-regional input-output linkages:** when a shock hits a sector, it propagates through the economy via the buying and selling of goods across sectors. Since firms rely on intermediate inputs from other sectors, shocks in one sector increases costs in others, creating ripple effects across the supply chain, both within regions and across them. All else equal, these linkages modify the initial shock, as firms adjust prices and reduce output, further dampening economic activity. This amplification effect will tend to be most pronounced in economies with strong upstream and downstream dependencies.

Figure 10 shows how each type of transmission channel affects the cross-country distribution of GDP per capita losses in 2100, under a high-emission scenario (SSP5-8.5). Each panel shows the difference between GDP per capita losses in the baseline model compared to losses in the counterfactual model. In other words, it shows by how much GDP per capita losses change by introducing a given transmission mechanism (compared to an economy where it is absent). Therefore, positive values (in red) imply the mechanism amplifies the shock, while negative values (in green) imply the mechanism lowers reduces its impact.

Panel A shows the difference in losses between the baseline model and a counterfactual model in which all cross-region spatial linkages – trade and migration – are shut down. The map reveals

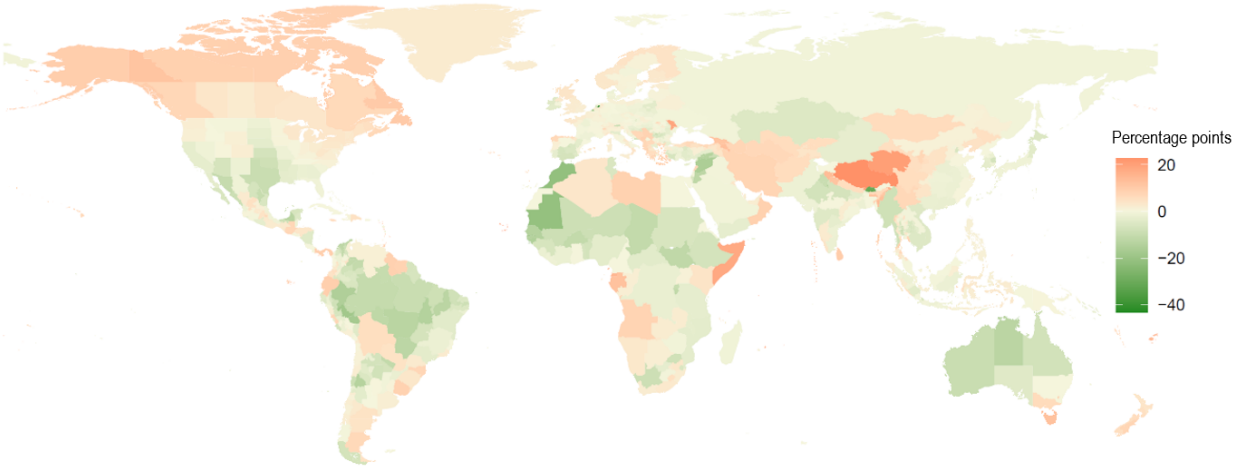
that spatial linkages tend to attenuate climate impacts in many OECD regions, including in many countries in Latin America, and parts of the United States and Australia, which appear in green. For these regions, access to trade and migration channels allows them to buy goods and services from locations less exposed to climate or rely on labour mobility to cushion the blow of climate shocks. In other regions, such as parts of Eastern Europe and Canada, spatial linkages instead amplify climate impacts, which reflects a combination of reliance on climate-exposed trading partners, the transmission of shocks through global value chains and the arrival of migrants putting upward pressure on the price of local goods and inputs. Overall, even though global damages are altered relatively little – they are only about 2.5 percent lower in 2100 with spatial linkages – Panel A highlights that openness to the global economy can sizeably affect the measured cost of climate for individual countries. For example, in 36 out of 176 countries in our calibration, GDP per capita loses are more than 25 percent larger in the absence of spatial linkages and more than 50 percent in 13 of them. Conversely, GDP per capita losses are more than 25 percent lower in 64 countries and more than 50 percent lower in 43 of them.

Panel B isolates the contribution of within- and cross-regional trade in intermediate output (input–output linkages): how sectors transmit climate shocks to one another. Here again, positive values (in red) mean that introducing input–output linkages increases GDP per capita losses, while negative values (in green) mean that these linkages reduce them. The map is predominantly red, indicating that in most countries within- and cross-regional production networks amplify climate damages. Shocks hitting climate-exposed sectors propagate downstream and upstream through their suppliers and clients, raising aggregate losses relative to a world without such linkages. Only a limited set of economies, shown in green, experience lower losses once input–output linkages are switched on. These are mainly, although not exclusively, regions that experience an increase in GDP per capita in the baseline model and so input-output linkages will tend to work in the opposite direction by further boosting the gains associated with future climate change.[14] For the world, GDP per capita impacts are about 78 percent higher with the presence of domestic input-output linkages than without, implying production networks act as a key magnification channel globally.

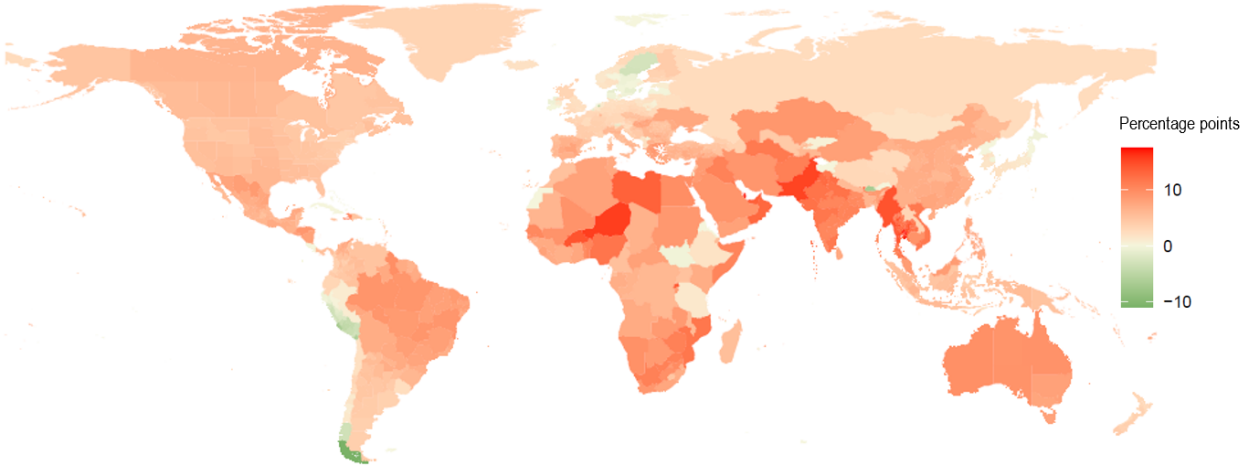
[14]Some locations, like South Sudan, have losses reduced due to the presence of input-output linkages even though they experience net losses in the baseline model. This is still consistent with the general equilibrium features of the model which can, in principle, either amplify losses in regions experiencing net gains in the baseline model or mitigate losses in regions experiencing net losses in the baseline model.

Figure 10: Model mechanisms play a key role in shaping the size of losses around the world

(a) Additional percentage point loss in GDP per capita in 2100 due to spatial linkages under SSP5-8.5



(b) Additional percentage point loss in GDP per capita in 2100 due to input-output linkages under SSP5-8.5



Source: Authors' own calculations.
Notes: The figures show additional losses in GDP per capita in 2100 in the baseline model compared to the model where the adjustment mechanism in question is shut down. Negative values (in green) imply the mechanism contributes to a decrease in the cost of climate change, while positive values (in red) imply the mechanism contributes to an increase. Climate projections are based on an SSP5-8.5 scenario.

5.3. The role of adjustment: how trade and labour mobility shape the distribution of global losses

We now quantify the role of forward-looking adjustment mechanisms. These mechanisms represent adjustments, or adaptive behaviours, that arise from agents' optimizing decisions in response to shocks. It is important to note that the ability of countries to adjust to a changing climate will not necessarily be welfare-improving on a country-by-country basis. While unilateral adjustment by a given location – holding the choices of other locations constant – will always necessarily help

mitigate losses, these benefits need not carry over once all locations are allowed to adjust simultaneously. When every region responds to climate shocks, their adjustments interact in general equilibrium and will in general generate spillovers that may either enhance or offset local gains. For example, international labour mobility allows households to move away from highly climate-exposed countries, easing pressure on local land and resources, but it may increase congestion, competition, or resource scarcity at the destination. The results that follow should therefore be interpreted as the net effect of each adjustment mechanism, combining both the direct local benefits of adaptation and the spillover effects generated by adaptation elsewhere. To quantify these mechanisms, we retain the baseline calibration and re-simulate the climate shock series while restricting agents' behaviour along one adjustment margin at a time, by holding their choices fixed at baseline levels. We divide the model's adjustment mechanisms into:

- **Labour mobility (sector- or location-based):** Climate impacts differ across sectors and across locations, prompting two forms of labour reallocation.

    1. Sector-based mobility: As hazards affect sectors unevenly, workers reallocate across industries (within and between regions) in response to shifting comparative advantages. We shut down this channel by fixing sectoral labour shares at their baseline-path values, effectively preventing any reallocation across sectors.
    2. Location-based mobility: Households also change their location choices when local conditions worsen, relocating either to other regions within countries (internal migration) or across borders (international migration). To isolate the role of spatial mobility, we fix population shares in each location at their baseline-path levels, thus preventing changes in internal or cross-region migration flows.

- **Adjustments in trade shares:** firms and households adjust how they source their intermediate and final goods, respectively, by reallocating trade shares among their trading partners, both within region and between regions. To quantify the role of trade, we consider a counterfactual economy where we do not allow agents to optimally adjust where they source their goods from in response to TFP shocks by imposing the same trade shares as in the baseline path.

The maps in Figure 11 illustrate how different adjustment mechanisms – labour mobility and trade – shape the economic costs of climate change by 2100 under a high-emission scenario (SSP5-8.5). Similarly to how we analyse transmission channels in the previous section 5.2, each panel reports the change in GDP per capita loss that arises when an adjustment margin is introduced. In other words, it shows by how much GDP per capita losses change when economies are allowed to adjust through the mechanism in question (compared to an economy where they cannot). Therefore, again, positive values (in red) imply the mechanism amplifies the economic impact of climate change, while negative values (in green) imply the mechanism reduces it. Figure A.12 in Annex A shows country-level impacts for OECD+ countries.

Panel A shows the incremental effect of labour mobility – both sectoral and location-based – on climate losses. Most of Northern Europe and North America appear in red, indicating that labour mobility increases climate-induced GDP losses in these regions. In these cases, the reallocation of workers across sectors and locations generates general-equilibrium spillovers (for example, wage and rent pressures in receiving regions) that ultimately amplify the economic impact of climate shocks. In contrast, southern regions of Europe, United States and regions in Latin America appear in green, meaning that labour mobility reduces their climate damages. For these economies, the ability of workers to shift out of highly exposed sectors or migrate toward more resilient locations provides an important buffer against local productivity losses. Labour mobility therefore acts as an adaptation mechanism that lowers damages in these regions. Globally, the ability to change sectors or migrate has a small but positive attenuating impact on world GDP per capita, reducing losses by approximately 5%.

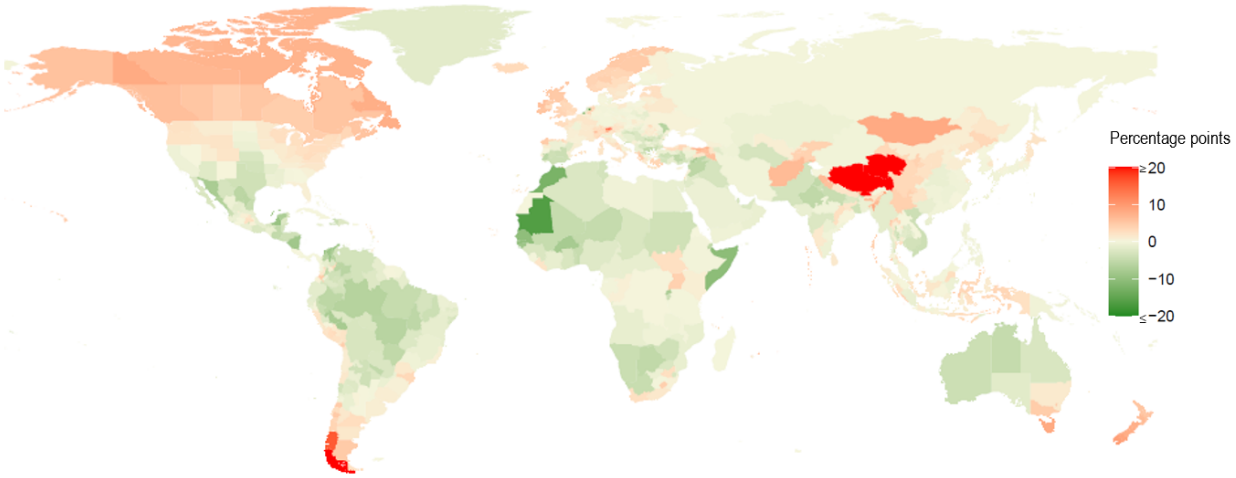
Panel B shows the additional loss attributable to adjustments in trade, meaning the reallocation in where firms and households source their goods in response to climate-induced damages. In contrast to Panel A, the pattern largely flips: countries most affected by climate change – those that tend to benefit from labour mobility adjustments – are now generally harmed when economies are allowed to alter their trade patterns. The mechanism works as follows: when trade can adjust, global markets redirect imports away from the most climate-affected countries, reducing external demand for their goods and thereby lowering local real income. Although these more heavily affected countries also gain access to cheaper imported goods, this benefit is not strong enough to offset the decline in demand. Conversely, countries (and sub-national regions) that are relatively less exposed to climate damages experience higher global demand for their output, which raises income per capita. This dynamic explains the gains observed in much of North America and Northern and Central Europe, where, relative to their trading partners, production faces smaller climate-induced losses.

Finally, Panel C reports the combined effect of adjustments in labour mobility and adjustments in trade. Importantly, this is not obtained by simply adding Panels A and B: migration and trade interact in general equilibrium, and their joint impact differs from the sum of their isolated effects. When economies are allowed to adjust both their labour allocations and their trade patterns, the spatial distribution of climate-induced losses changes substantially. At the global level, these adjustment margins act as a stabilizing force, lowering world GDP per capita losses in 2100 by roughly 9%. Yet this aggregate improvement masks considerable heterogeneity. Some regions experience substantial gains due to the combination of labour and trade adjustments relative to no adjustment along these dimensions, while others, such as Canada, much of Northern Europe, and New Zealand, see their losses deepen. Within countries, like Australia or the United States, these adjustments help stabilize economies in some regions, while expanding losses in others.

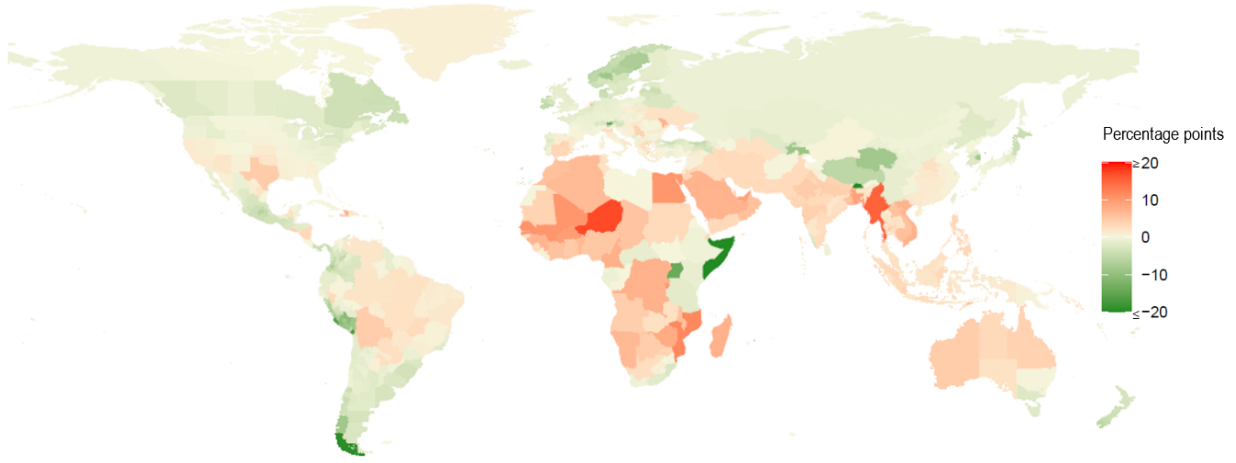
Beyond reducing global damages, allowing economies to adjust along the labour and trade margins also significantly helps to spread the burden of climate change more evenly across space. Put differently, trade and migration operate as mechanisms for sharing losses, redirecting economic ac-

Figure 11: The ability to adjust to a changing climate has a large effect on the distribution of losses

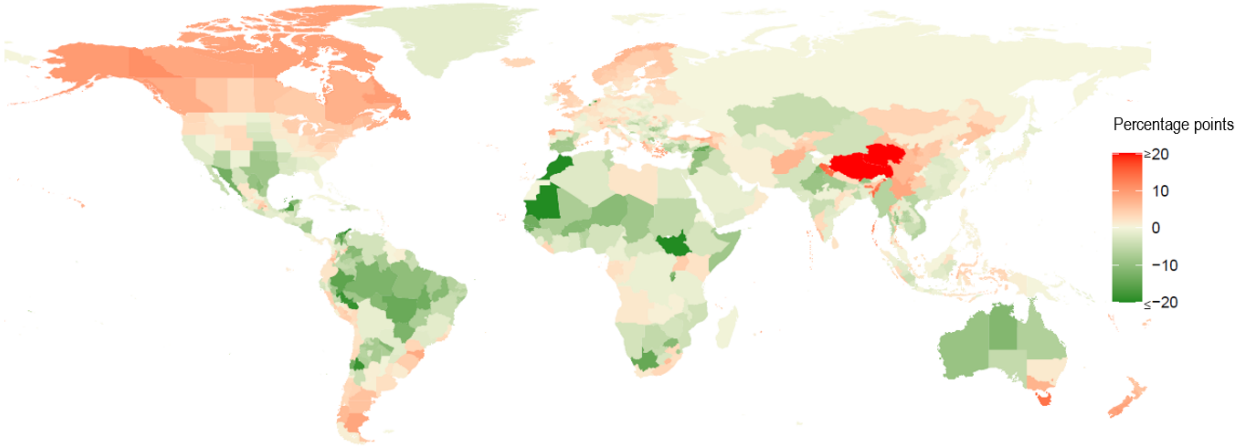
(a) Additional percentage point loss in GDP per capita in 2100 due to adjustments via labour mobility under SSP5-8.5



(b) Additional percentage point loss in GDP per capita in 2100 due to adjustments via trade adjustments under SSP5-8.5



(c) Additional percentage point loss in GDP per capita in 2100 due to adjustment via labour mobility and trade adjustments under SSP5-8.5



Source: Authors' own calculations.
Notes: The figures show the difference in GDP per capita losses in 2100 under SSP5-8.5 between the full model and one where a given adjustment mechanism is shut down. Negative values indicate that higher losses occur when the mechanism is switched off, while positive values indicate lower losses occur. All values below -20 and above 20 are windsorized at -20 and 20, respectively.

tivity and trade flows toward places less severely damaged. As a result, the cross-regional dispersion in impacts falls significantly: the coefficient of variation (standard deviation to mean ratio) of GDP per capita losses across the 927 regions declines from 0.69 to 0.58 – a reduction of roughly 20%.

6. Discussion and policy implications

This study develops a micro-based, bottom-up framework to quantify the economic costs of climate change in a way that is both empirically grounded and policy-relevant. By combining granular, and channel-specific estimates of climate damages with a spatial general equilibrium model, the analysis translates local, micro-level impacts on productivity, capital and land into aggregate macroeconomic outcomes, while explicitly accounting for linkages across regions, sectors and countries. This approach makes it possible to move beyond aggregate damage-function approaches and instead trace how different climate shocks propagate through the economy via specific transmission channels.

Our results indicate that the macroeconomic costs of climate change are substantial and increase over time under alternative climate scenarios. Losses are highly heterogeneous across countries and regions, reflecting differences in exposure, economic structure, and adjustment opportunities. A central finding is that spatial and general equilibrium mechanisms play a key role in shaping both the magnitude and the distribution of impacts. Local shocks generate spillovers through trade, migration, and input-output linkages, redistributing losses across regions and, in some cases, amplifying aggregate effects.

The paper's novel empirical analysis of flooding further provides new insights into one of the

key channels through which climate change affects economic activity. Using firm-level data across multiple advanced economies, the results show that floods primarily affect firms through persistent reductions in capital stocks, with more limited direct effects on measured productivity. Capital losses accumulate over time as severe flood events raise effective depreciation rates, and recovery is slow, often taking several years. Importantly, the pace of recovery depends on firms' financial conditions, with more constrained firms facing greater difficulty rebuilding damaged capital. The analysis also reveals sizeable spatial spillovers: firms that are not directly flooded experience declines in value added and investment likely due to disruptions in local supply chains, infrastructure and demand, or tighter financial conditions, underscoring the importance of accounting for indirect effects when assessing climate damages.

More broadly, the results highlight the value of a bottom-up modelling approach. By grounding macroeconomic projections in micro-estimated damage functions for productivity, capital and land, this approach makes it possible to trace how climate affect the economy through specific channels and how these effects interact across space. This is particularly important given the strong role of spatial spillovers identified in the analysis and in the literature (Costa and Hooley, 2025; Zappalà, 2023). At the same time, because the estimates are based on historical relationships, they are likely to be conservative with respect to unobserved non-linearities and potential tipping points.

The findings underscore that climate change is not only a local phenomenon but also a systemic one, with impacts shaped by economic interconnections and spatial adjustment. Understanding these interactions is essential for assessing the aggregate costs of climate change and for interpreting the distribution of impacts across regions and sectors.

References

Abel, G. and Cohen, J. (2019). Bilateral international migration flow estimates for 200 countries. *Scientific Data*, 6(1).

Anderson, J. and van Wincoop, E. (2003). Gravity with gravitas: A solution to the border puzzle. *American Economic Review*, 93(1):170–192.

Balboni, C. (2025). In harm's way? infrastructure investments and the persistence of coastal cities. *American Economic Review*, 115(1):77–116.

Bank of England (2025). The heat is on: why monetary policy makers are increasingly focusing on the impact of climate risks. Speech by James Talbot.

Barrage, L. and Nordhaus, W. (2024). Policies, projections, and the social cost of carbon: Results from the DICE-2023 model. *Proceedings of the National Academy of Sciences*, 121(13):e2312030121.

Barrot, J.-N. and Sauvagnat, J. (2016). Input specificity and the propagation of idiosyncratic shocks in production networks. *Quarterly Journal of Economics*, 131(3):1543–1592.

Belasen, A. and Polachek, S. (2008). How hurricanes affect wages and employment in local labor markets. *American Economic Review*, 98(2):49–53.

Bilal, A. and Känzig, D. R. (2024). The macroeconomic impact of climate change: Global vs. local temperature. NBER Working Papers 32450, National Bureau of Economic Research, Inc.

Bilal, A. and Rossi-Hansberg, E. (2023). Anticipating climate change across the united states. Working paper.

Bosello, F., Roson, R., and Tol, R. (2007). Economy-wide estimates of the implications of climate change: Sea level rise. *Environmental & Resource Economics*, 37(3):549–571.

Botzen, W., Deschenes, O., and Sanders, M. (2019). The economic impacts of natural disasters: A review of models and empirical studies. *Review of Environmental Economics and Policy*, 13(2).

Burke, M., Hsiang, S., and Miguel, E. (2015). Global non-linear effect of temperature on economic production. *Nature*, 527:235–239.

Château, J., Dellink, R., and Lanzi, E. (2014). An overview of the oecd env-linkages model: Version 3. Technical Report 65, OECD.

Conte, B. (2023). Climate change and migration: the case of africa. Technical report, Barcelona School of Economics.

Costa, H. et al. (2024). The heat is on: heat stress, productivity and adaptation among firms. Technical Report 1828, OECD.

Costa, H. and Hooley, J. (2025). The macroeconomic implications of extreme weather events. Technical Report 1837, OECD.

Costinot, A., Donaldson, D., and Smith, C. (2016). Evolving comparative advantage and the impact of climate change in agricultural markets. *Journal of Political Economy*, 124(1):205–248.

Cruz, J.-L. and Rossi-Hansberg, E. (2024). The economic geography of global warming. *The Review of Economic Studies*, 91(2):899–939.

Dell, M., Jones, B., and Olken, B. (2014). What do we learn from the weather? *Journal of Economic Literature*, 52(3):740–798.

Desmet, K., Kopp, R. E., Kulp, S. A., Nagy, D. K., Oppenheimer, M., Rossi-Hansberg, E., and Strauss, B. H. (2021). Evaluating the economic cost of coastal flooding. *American Economic Journal: Macroeconomics*, 13(2):444–86.

Desmet, K. and Rossi-Hansberg, E. (2015). On the spatial economic impact of global warming. *Journal of Urban Economics*, 88:16–37.

Desmet, K. and Rossi-Hansberg, E. (2024). Climate change economics. *Annual Review of Economics*, 16:271–304.

Eaton, J. and Kortum, S. (2002). Technology, geography, and trade. *Econometrica*, 70(5):1741–1779.

European Central Bank (2021). Climate change and central banking. Technical report. Keynote speech by Christine Lagarde.

Felbermayr, G. and Gröschl, J. (2014). Naturally negative: the growth effects of natural disasters. *Journal of Development Economics*, 111:92–106.

Gal, P. (2013). Measuring total factor productivity at the firm level using oecd-orbis. Technical Report 1049, OECD.

Guiso, L., Sapienza, P., and Zingales, L. (2004). Does local financial development matter? *Quarterly Journal of Economics*, 119(3):929–969.

Head, K. and Ries, J. (2001). Increasing returns versus national product differentiation as an explanation for the pattern of u.s.-canada trade. *American Economic Review*, 91(4):858–876.

Huizinga, J., De Moel, H., and Szewczyk, W. (2017). Global flood depth-damage functions: Methodology and the database with guidelines. Technical report.

IPCC, editor (2022). *Climate Change 2022: Impacts, Adaptation, and Vulnerability. Contribution of Working Group II to the Sixth Assessment Report of the Intergovernmental Panel on Climate Change, Cambridge University Press.* Cambridge University Press.

Jordà, Ò. (2005). Estimation and inference of impulse responses by local projections. *American Economic Review*, 95(1):161–182.

Kahn, M. et al. (2021). Long-term macroeconomic effects of climate change. *Energy Economics*, 104:105624.

Kalkuhl, M. and Wenz, L. (2020). The impact of climate conditions on economic production. evidence from a global panel of regions. *Journal of Environmental Economics and Management*, 103:102360.

Kellenberg, D. and Mobarak, A. (2011). The economics of natural disasters. *Annual Review of Resource Economics*, 3(1):297–312.

Kleinman, B., Liu, E., and Redding, S. J. (2023). Dynamic spatial general equilibrium. *Econometrica*, 91(2):385–424.

Kompas, T., Ha, P. V., and Che, T. (2018). The effects of climate change on gdp by country and the global economic gains from complying with the paris climate accord. *Earth's Future*. Available at SSRN: https://ssrn.com/abstract=3612471.

Krugman, P. (1991). Increasing returns and economic geography. *Journal of Political Economy*, 99:483–499.

Krusell, P. and Smith, A. A. (2022). Climate change around the world. Working paper.

Masson-Delmotte, V., editor (2021). *Climate Change 2021: The Physical Science Basis*. Cambridge University Press.

Nath, I. (2025). Climate change, the food problem, and the challenge of adaptation through sectoral reallocation. *Journal of Political Economy*, 133(6):1705–1756.

Nicholls, R. and Cazenave, A. (2010). Sea-level rise and its impact on coastal zones. *Science*, 328(5985):1517–1520.

Nordhaus, W. D. and Yang, Z. (1996). A regional dynamic general-equilibrium model of alternative climate-change strategies. *The American Economic Review*, 86(4):741–765.

Noy, I. (2009). The macroeconomic consequences of disasters. *Journal of Development Economics*, 88(2):221–231.

Özcan, Ş. et al. (2024). How to construct nationally representative firm-level data from the orbis global database. *American Economic Journal: Macroeconomics*, 16(2):353–374.

Pelli, M. et al. (2023). In the eye of the storm: Firms and capital destruction in india. *Journal of Urban Economics*, 134:103529.

Prieto, C. and Noy, I. (2025). How do floods affect firms' economic performance? Technical Report 11430, CESifo.

Redding, S. and Rossi-Hansberg, E. (2017). Quantitative spatial economics. *Annual Review of Economics*, 9:21–58.

Rudik, I., Lyn, G., and Tan, J. (2022). The economic effects of climate change in dynamic spatial equilibrium. Working paper.

Scussolini, P. et al. (2016). Flopros: an evolving global database of flood protection standards. *Natural Hazards and Earth System Sciences*, 16(5):1049–1061.

Tellman, B. et al. (2021). Satellite imaging reveals increased proportion of population exposed to floods. *Nature*, 596:80–86.

Tiggeloven, T. et al. (2020). Global-scale benefit–cost analysis of coastal flood adaptation. *Natural Hazards and Earth System Sciences*, 20(4):1025–1044.

Wooldridge, J. (2009). On estimating firm-level production functions using proxy variables. *Economics Letters*, 104(3):112–114.

Zappalà, G. (2023). Sectoral impact and propagation of weather shocks. Technical Report 2023/053, IMF.

A. Additional tables and figures

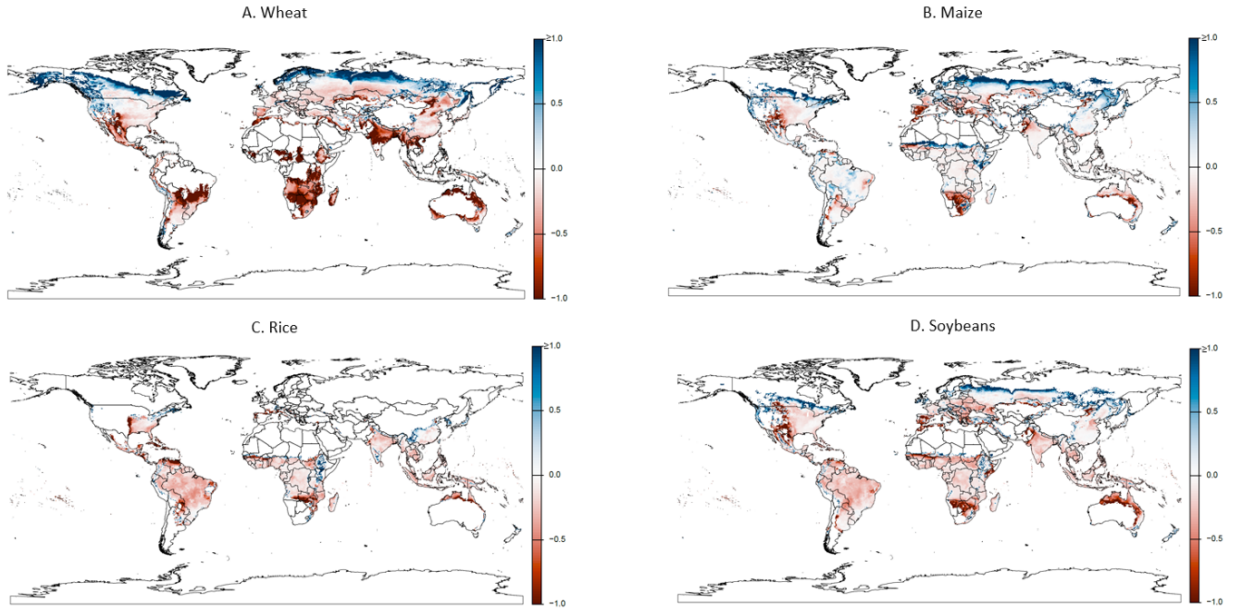
Figure A.1: Effect of climate change on coastal flood frequency in 2080 relative to 1980

Percent change in the annual frequency of coastal flooding under RCP8.5 (ensemble mean)



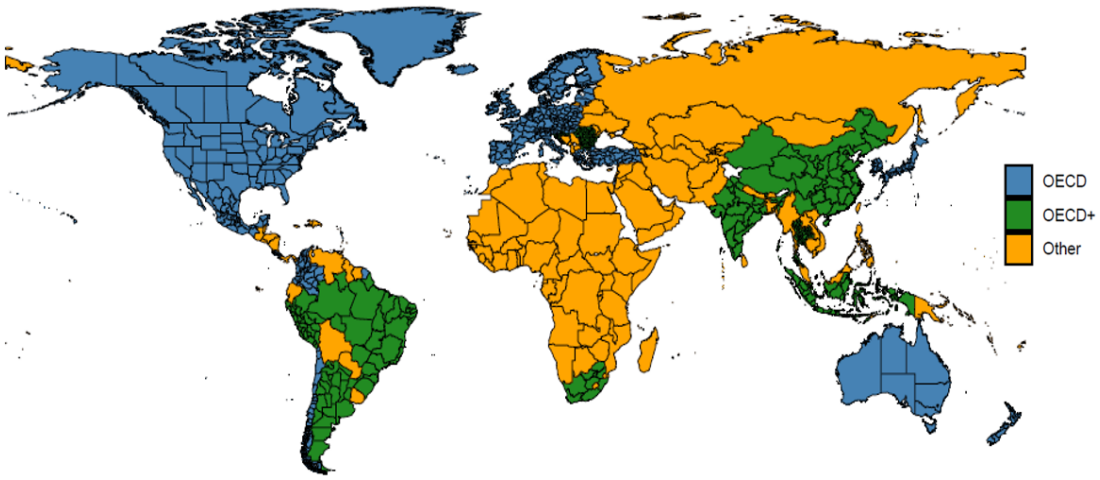
Source: Scussolini et al. (2016), World Resources Institute (Aqueduct), and authors' calculations.
Notes: The map reports values at the resolution of a 0.25° × 0.25° grid cell (approximately 25 km at the equator). Values greater than 50% and less than -50% are windsorized at 50% and -50%, respectively. The projections assume flood protection standards remain the same as in the baseline period (i.e. 1980).

Figure A.2: Change in agro-climatic potential yields of major crops in 2071–2100 relative to 2011–2040 under RCP8.5



Source: FAO-GAEZ and authors' calculations.
Notes: Potential yields estimated under rain-fed conditions and high input usage. Figures show the median relative change across climate-crop growth models. Values greater than 1 are windsorized at 1.

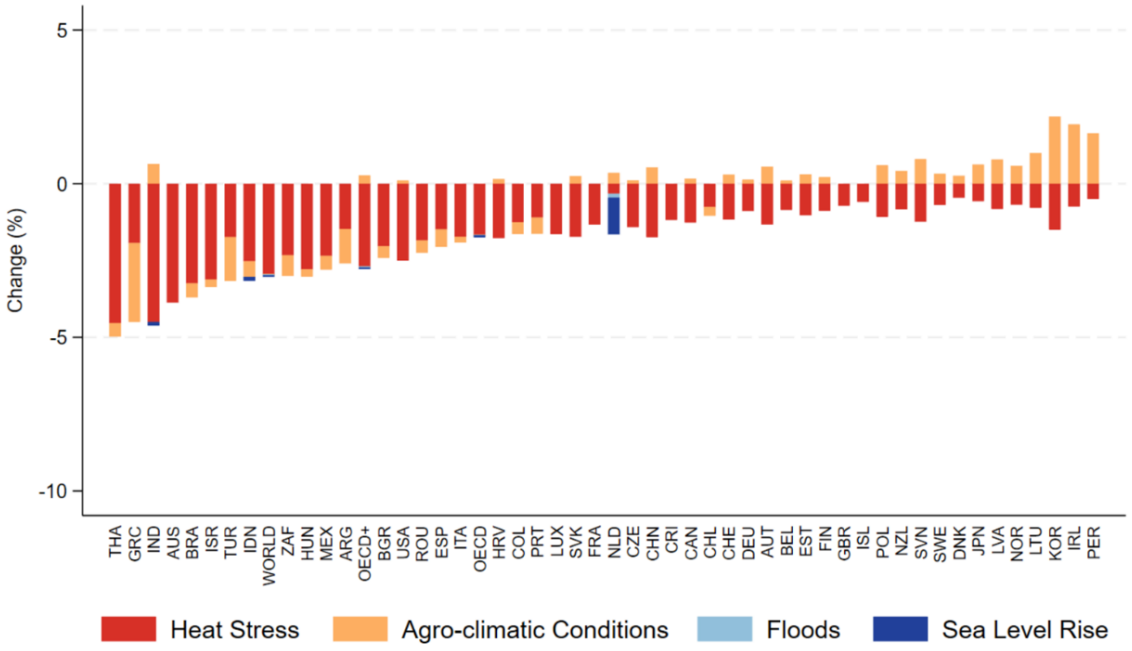
Figure A.3: Regions in calibrated model by OECD status



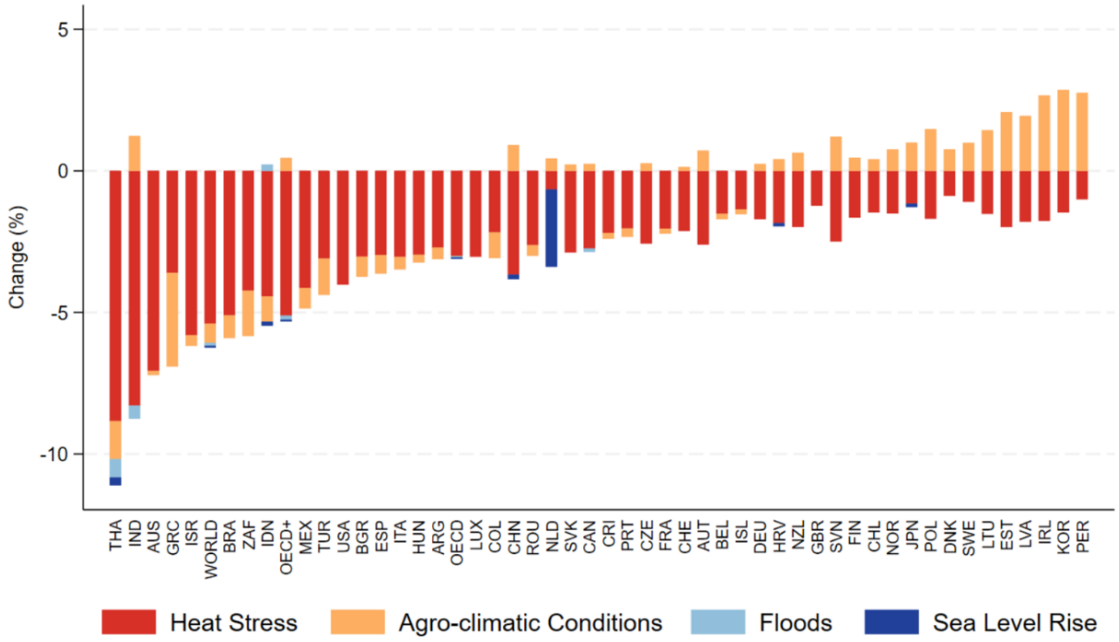
Source: Authors' calculations.
Notes: The map shows the regions included in the calibration, classified by each country's status as OECD member country, accession candidate or key partner (OECD+), or other countries. OECD member countries are subdivided into TL2 regions, the OECD's second-level territorial classification corresponding to major subnational administrative areas. OECD accession candidate countries and OECD key partners are subdivided into Admin-1 units from GADM (Global Administrative Areas). For all other countries, the model is calibrated for the entire national territory as a single entity.

Figure A.4: Impact by channel in OECD+ countries under the current-policy scenario (SSP2-4.5)

(a) Percentage change in GDP per capita in 2050



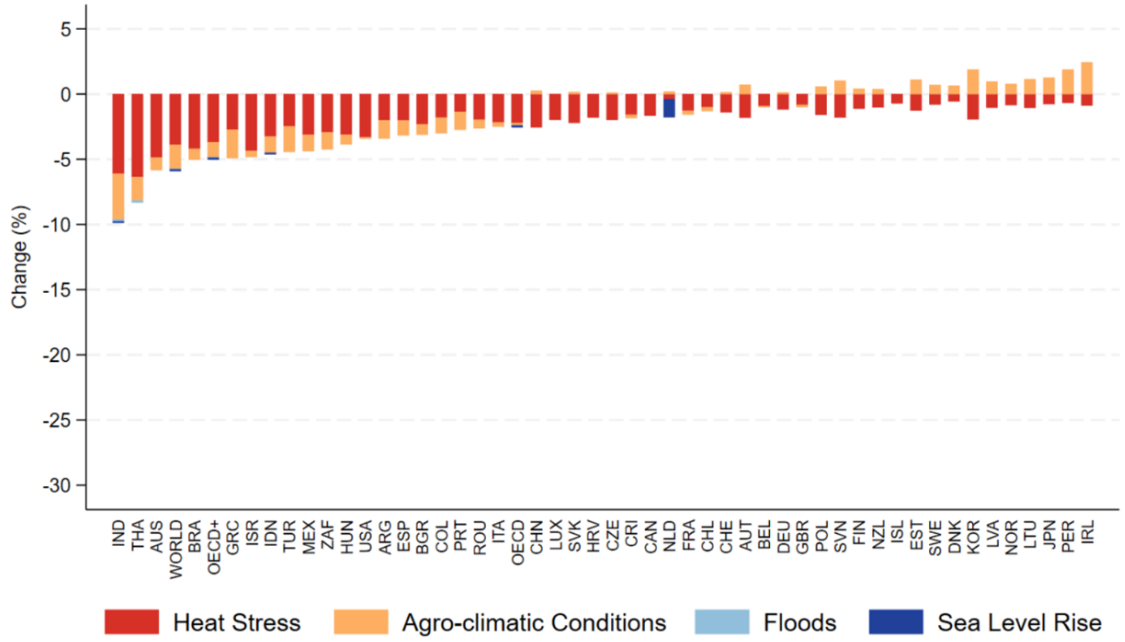
(b) Percentage change in GDP per capita in 2100



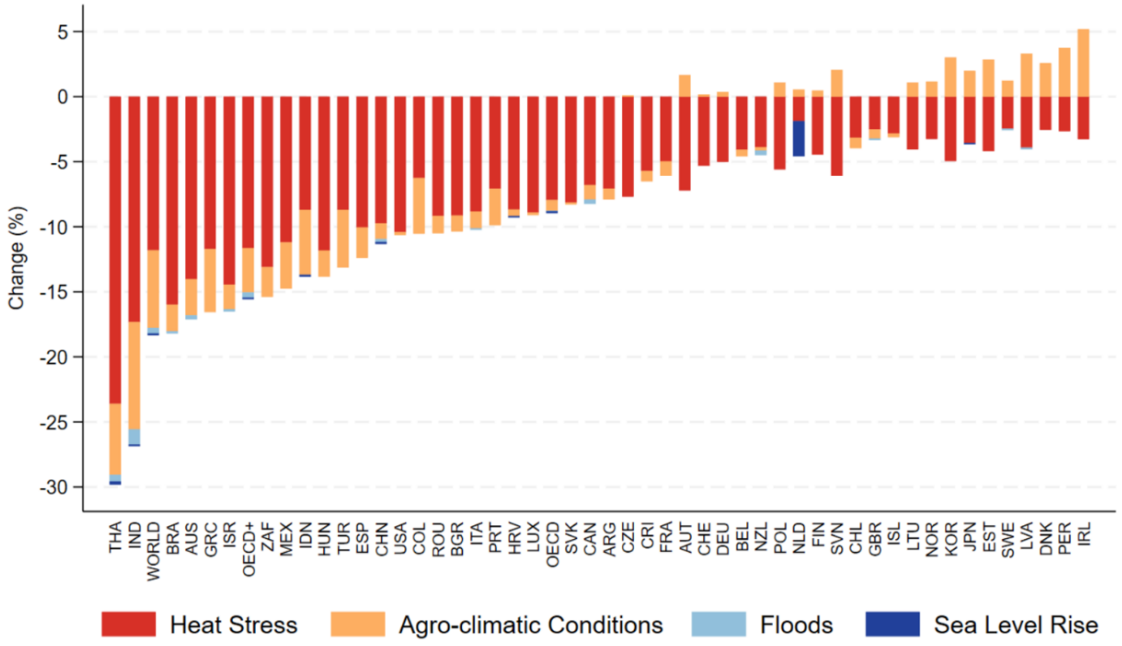
Source: Authors' calculations.
Notes: The figures show the model-implied loss in annual GDP per capita relative to a no-climate change scenario.

Figure A.5: Impact by channel in OECD+ countries under the high-emission scenario (SSP5-8.5)

(a) Percentage change in GDP per capita in 2050



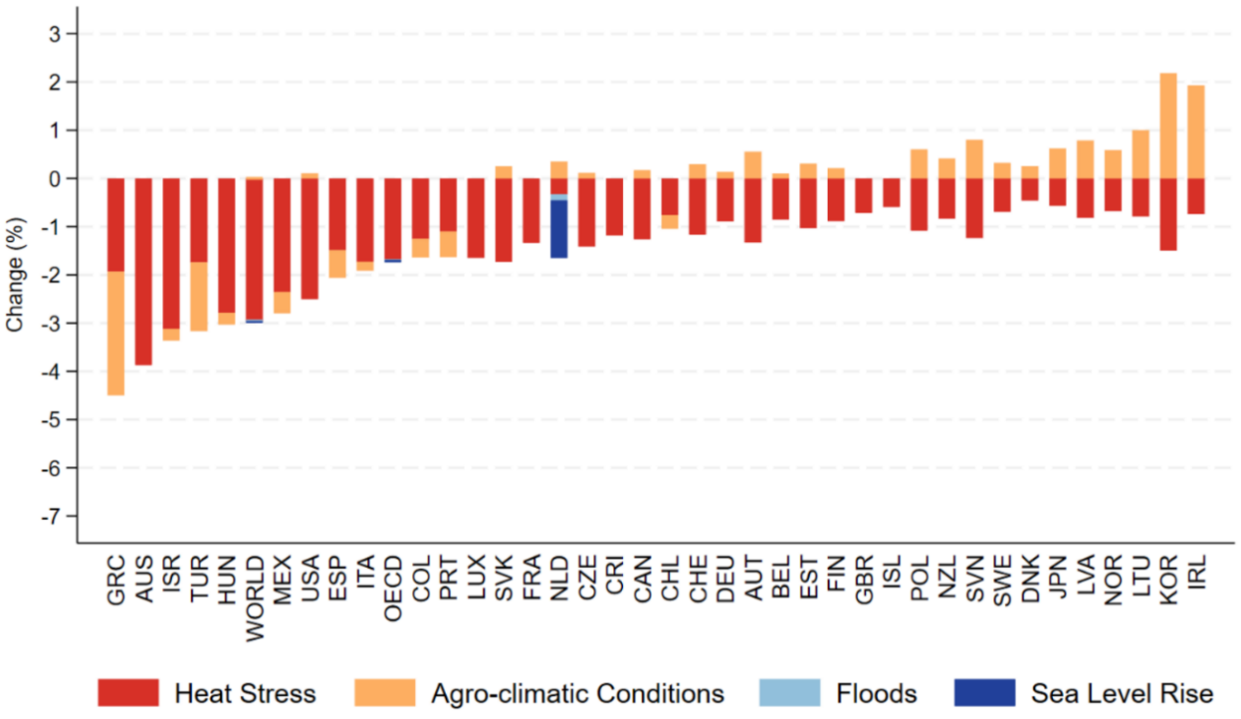
(b) Percentage change in GDP per capita in 2100



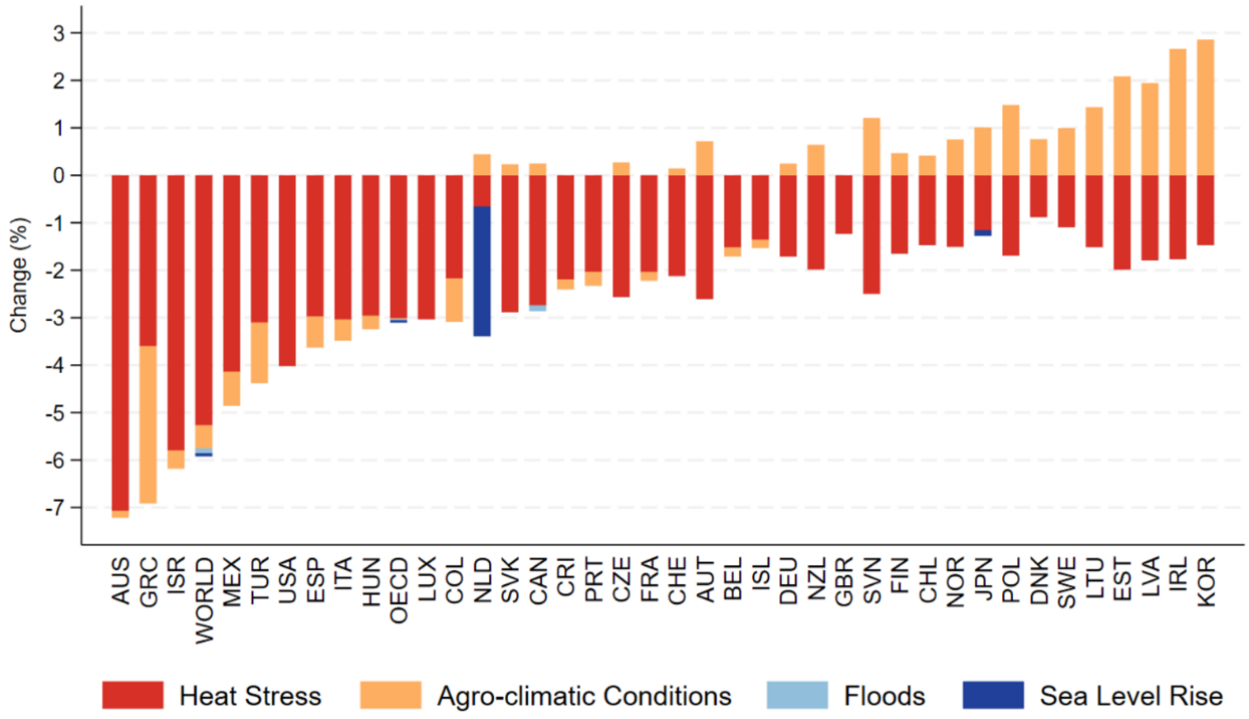
Source: Authors' calculations.
Notes: The figures show the model-implied loss in annual GDP per capita relative to a no-climate change scenario.

Figure A.6: Impact by channel in OECD countries under the current-policy scenario (SSP2-4.5)

(a) Percentage change in GDP per capita in 2050



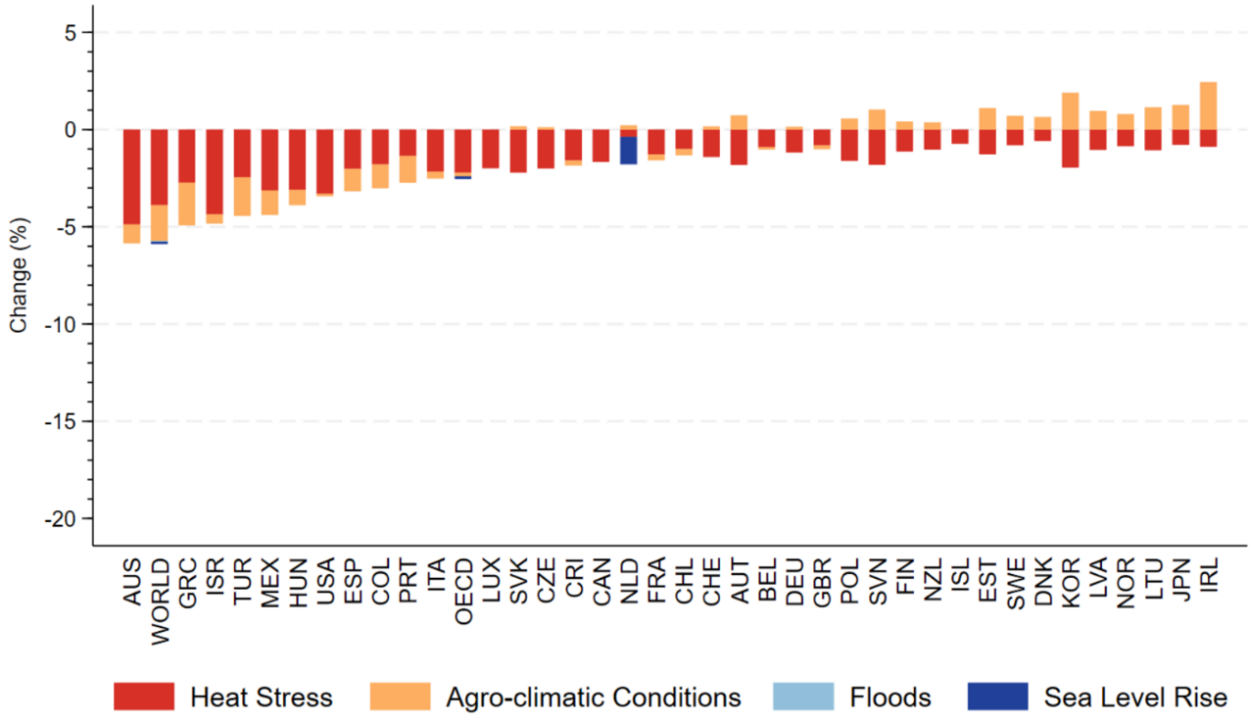
(b) Percentage change in GDP per capita in 2100



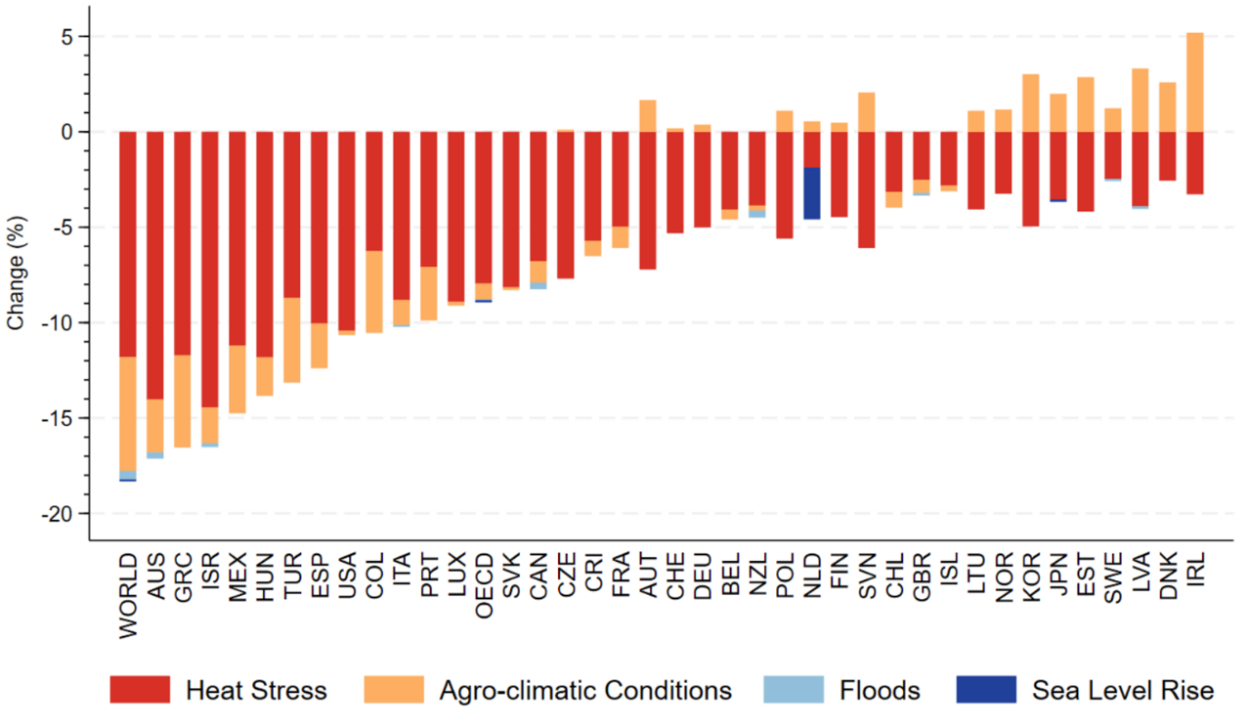
Source: Authors' own calculations.
Notes: The figure shows the model-implied loss in annual GDP per capita relative to a no-climate change scenario.

Figure A.7: Impact by channel in OECD countries under the high-emission scenario (SSP5-8.5)

(a) Percentage change in GDP per capita in 2050



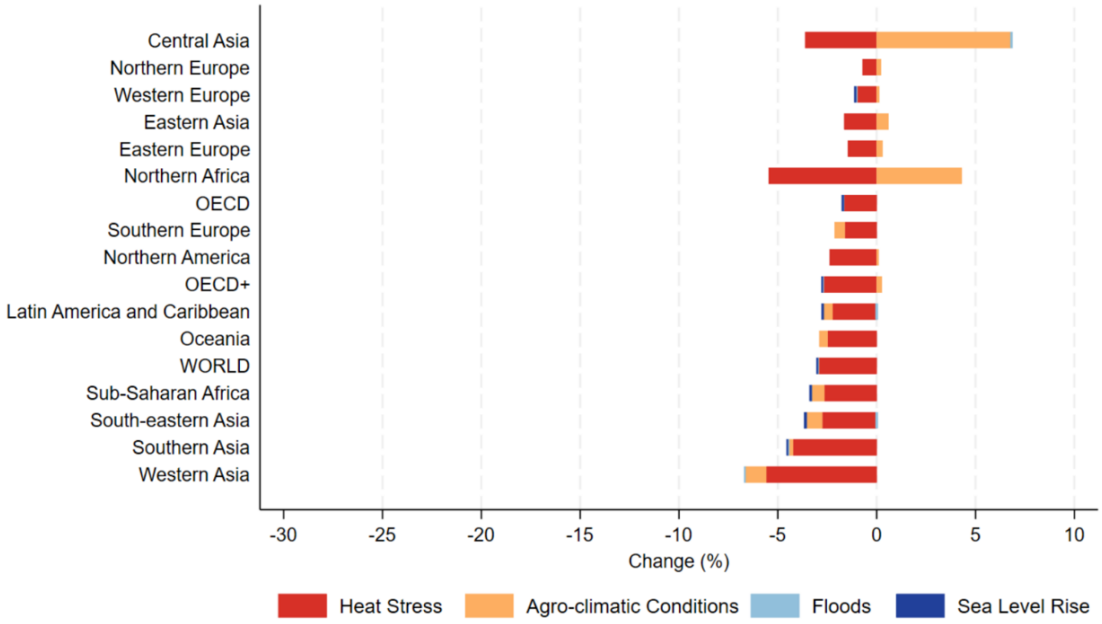
(b) Percentage change in GDP per capita in 2100



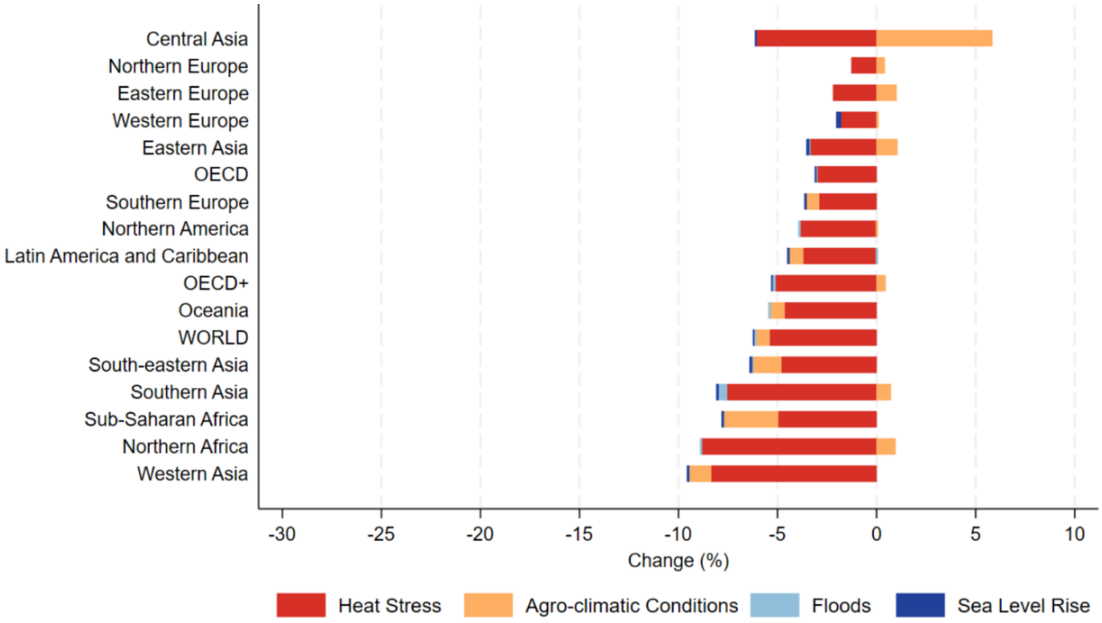
Source: Authors' own calculations.
Notes: The figure shows the model-implied loss in annual GDP per capita relative to a no-climate change scenario.

Figure A.8: Regional impact by channel under the current-policy scenario (SSP2-4.5)

(a) Percentage change in GDP per capita in 2050



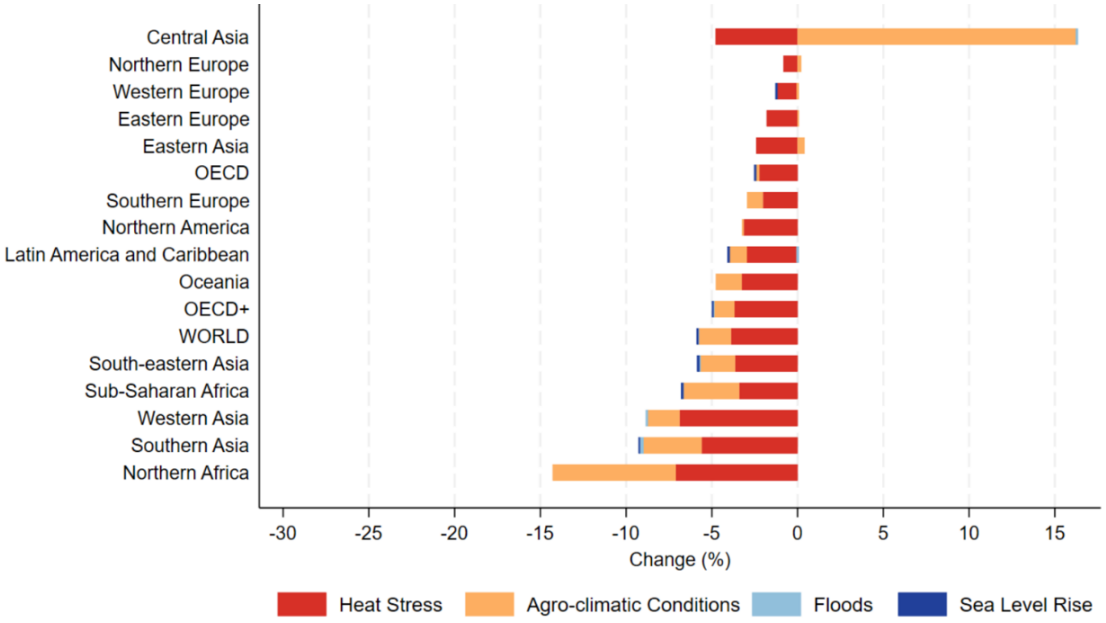
(b) Percentage change in GDP per capita in 2100



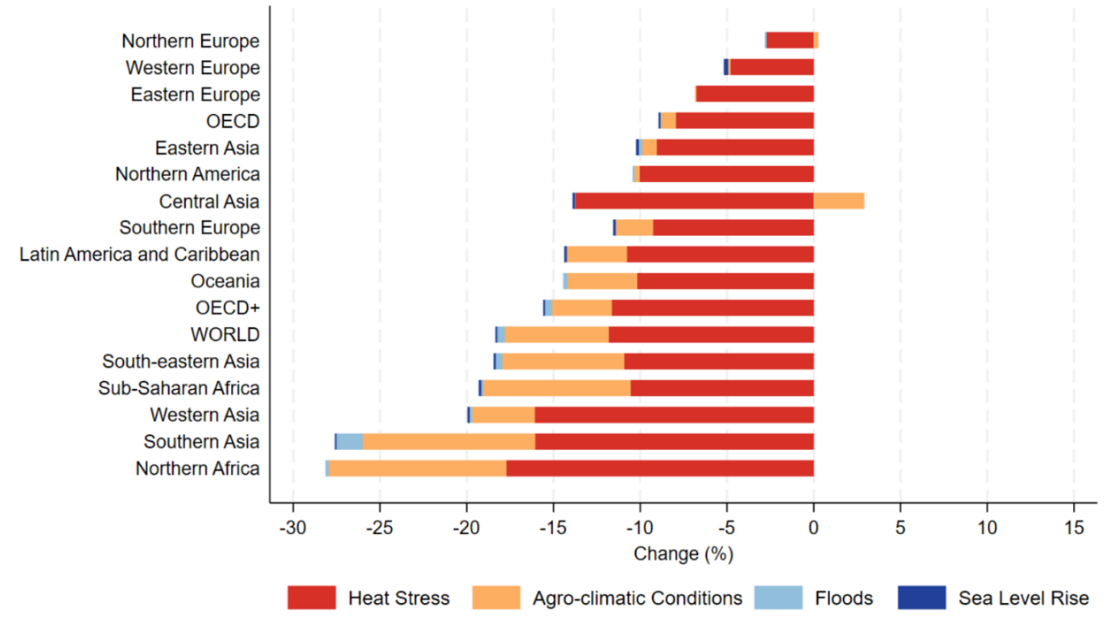
Source: Authors' own calculations.
Notes: The figures show the model-implied loss in annual GDP per capita relative to a no-climate change scenario. Regional GDP per capita losses are computed as a country population-weighted average.

Figure A.9: Regional impact by channel under the high-emission scenario (SSP5-8.5)

(a) Percentage change in GDP per capita in 2050



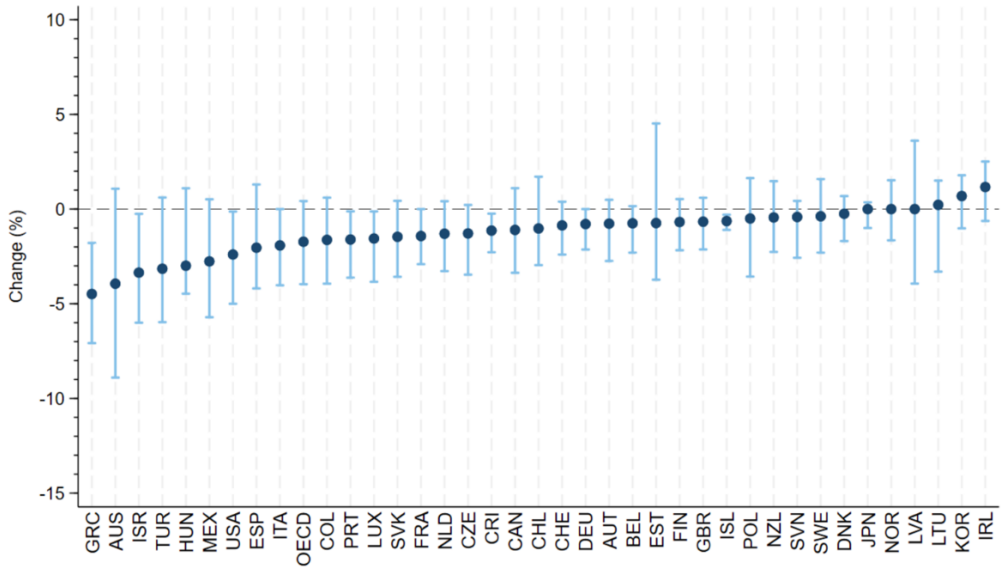
(b) Percentage change in GDP per capita in 2100



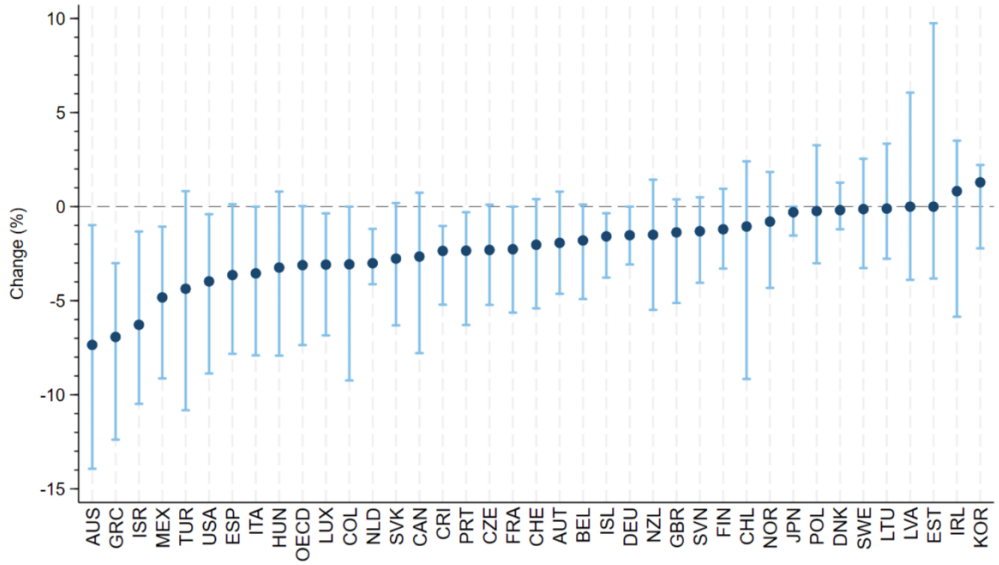
Source: Authors' own calculations.
Notes: The figures show the model-implied loss in annual GDP per capita relative to a no-climate change scenario. Regional GDP per capita losses are computed as a country population-weighted average.

Figure A.10: Impact in OECD countries under the current-policy scenario (SSP2-4.5)

(a) Percentage change in GDP per capita in 2050



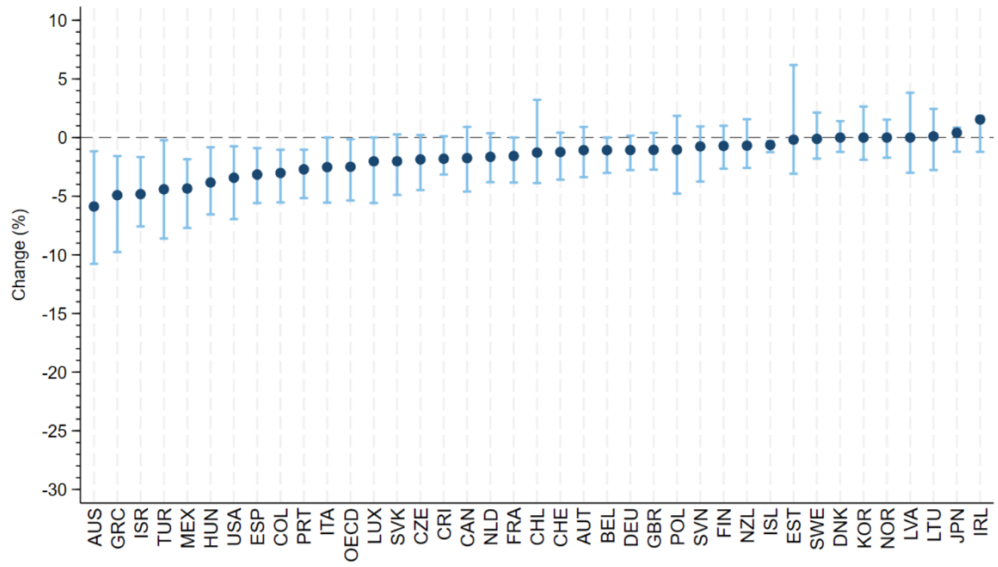
(b) Percentage change in GDP per capita in 2100



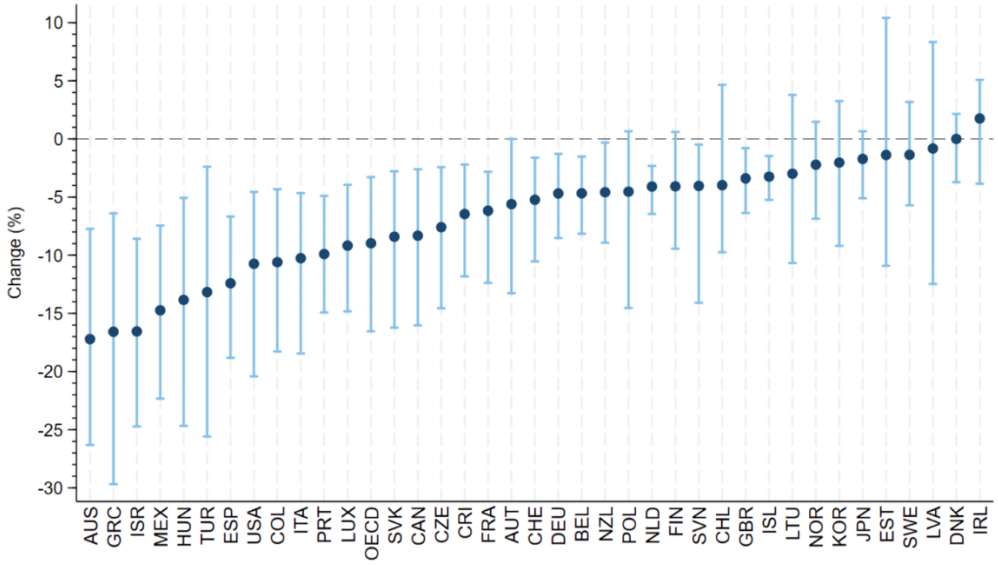
Source: Authors' pwn calculations.
Notes: The figure shows the model-implied loss in annual GDP per capita relative to a no-climate change scenario. The dots represent impact on GDP per capita based on ensemble median of climate projections, while the intervals represent a range of plausible impacts based on variation across climate model projections. The lower bound estimates are obtained by using 10th percentile projections for hot days together with the model (out of five) that yields the lowest GDP per capita losses in each country arising from changes in agro-climatic conditions and from flooding, and 5th percentile projections for sea level rise. Conversely, the upper bound estimates are obtained by using 90th percentile projections for hot days together with the model (out of five) that yields the highest GDP per capita losses in each country arising from changes in agro-climatic conditions and from flooding, and 95th percentile projections for sea level rise.

Figure A.11: Impact in OECD countries under the high-emission scenario (SSP5-8.5)

(a) Percentage change in GDP per capita in 2050



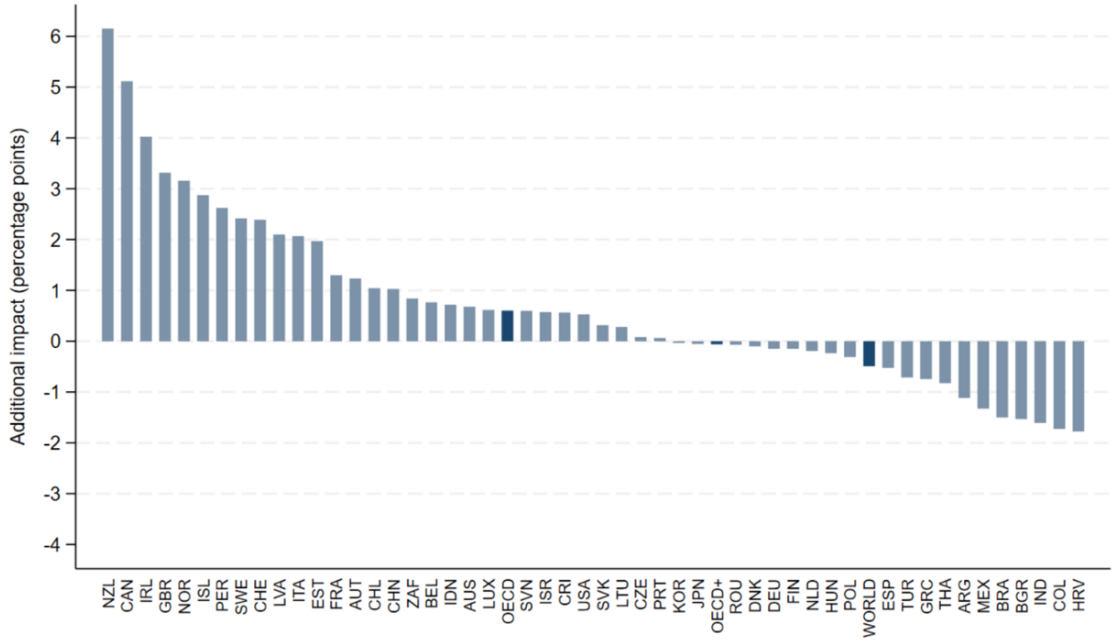
(b) Percentage change in GDP per capita in 2100



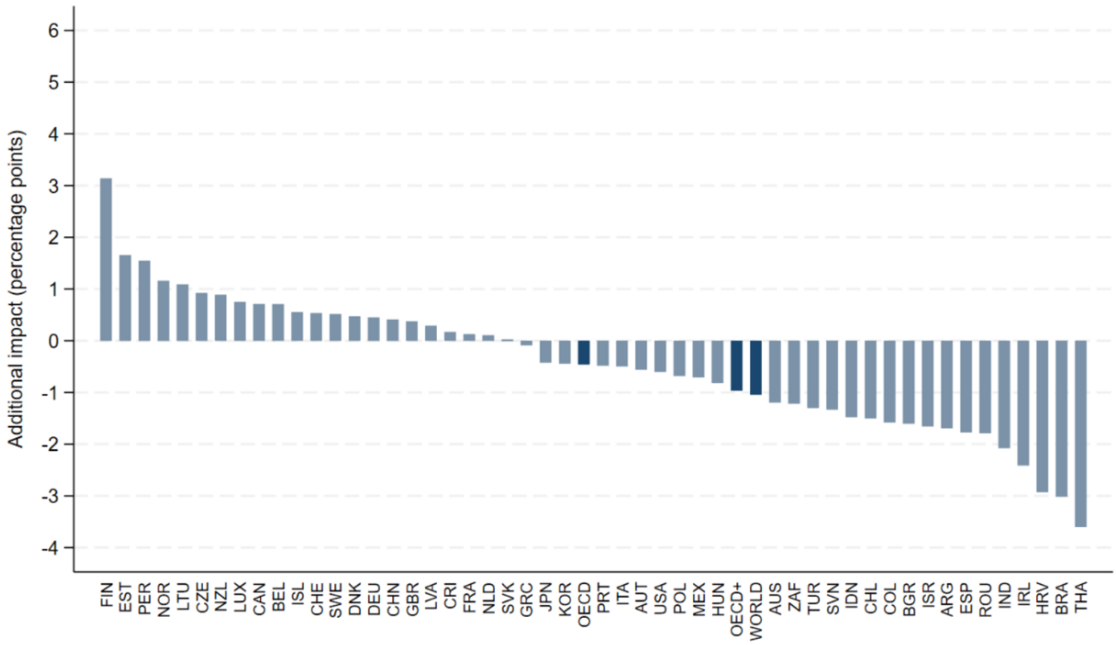
Source: Authors' own calculations.
Notes: The figure shows the model-implied loss in annual GDP per capita relative to a no-climate change scenario. The dots represent impact on GDP per capita based on ensemble median of climate projections, while the intervals represent a range of plausible impacts based on variation across climate model projections. The lower bound estimates are obtained by using 10th percentile projections for hot days together with the model (out of five) that yields the lowest GDP per capita losses in each country arising from changes in agro-climatic conditions and from flooding, and 5th percentile projections for sea level rise. Conversely, the upper bound estimates are obtained by using 90th percentile projections for hot days together with the model (out of five) that yields the highest GDP per capita losses in each country arising from changes in agro-climatic conditions and from flooding, and 95th percentile projections for sea level rise.

Figure A.12: Effect of ability to adjust to a changing climate on GDP per capita impacts across OECD+ countries in 2100 under the high-emission scenario (SSP5-8.5)

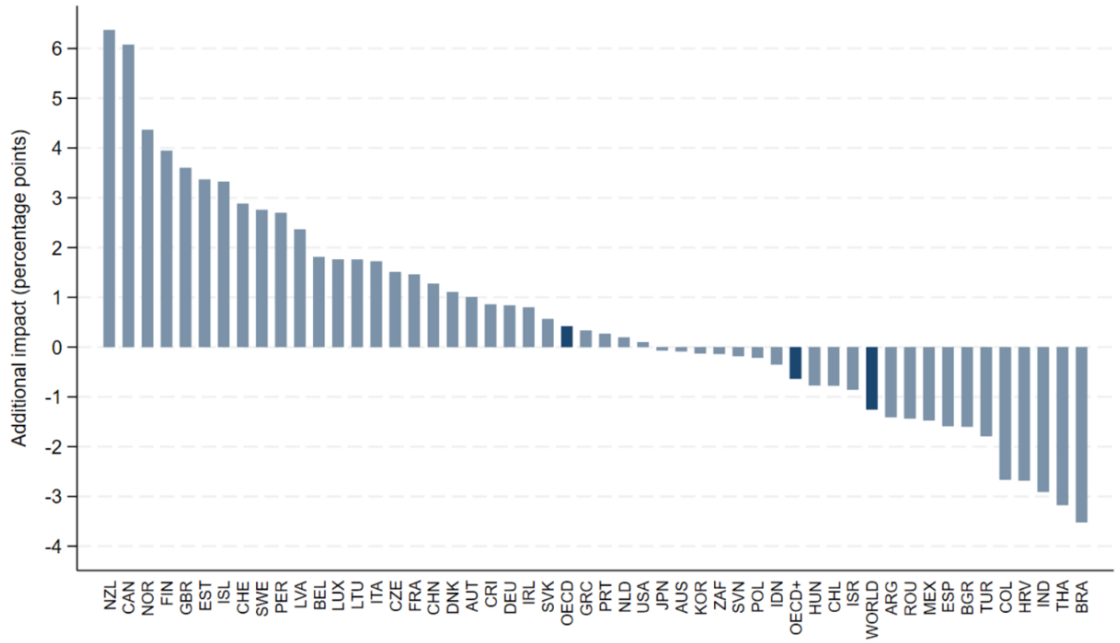
(a) Additional percentage point loss in GDP per capita due to adjustments in labour mobility



(b) Additional percentage point loss in GDP per capita due to adjustments in trade shares

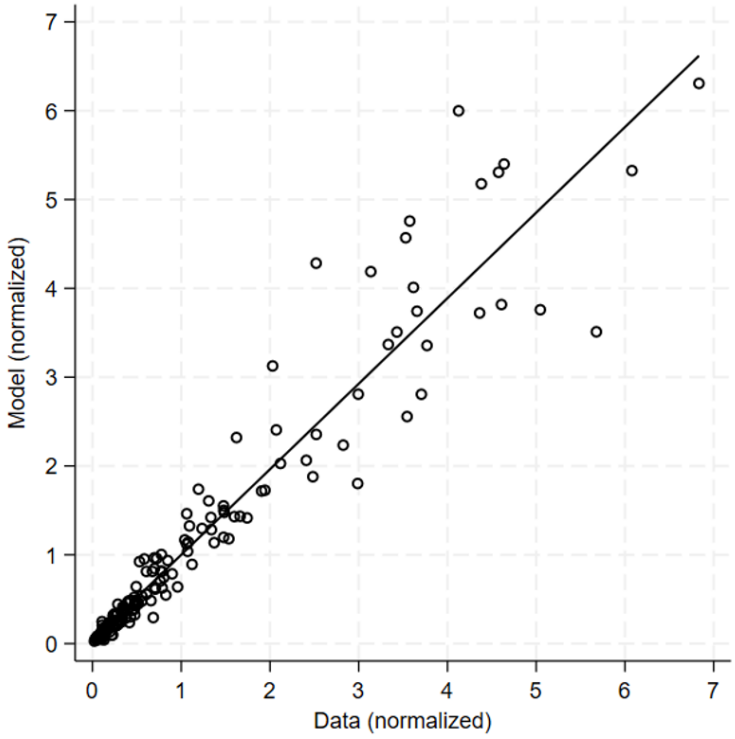


(c) Additional percentage point loss in GDP per capita due to adjustment in labour mobility and trade shares



Source: Authors' own calculations.
Notes: Comparison of scenarios with and without trade and migration adjustments.

Figure A.13: Country GDP per capita in 2011–2020: model vs data



Source: Authors' own calculations and World Bank data.
Notes: The figure plots GDP per capita levels implied by the baseline model calibration (using data for 2011–2020) against their empirical counterparts from World Bank data (GDP per capita, constant 2015 US$); for comparability, country-level values in both series are normalized by dividing by the cross-country average.

B. Further detail: flood firm-level analysis

B.1. Introduction

Floods are among the most damaging natural hazards, with wide-ranging effects on infrastructure, supply chains, and firm-level operations (IPCC, 2022; Felbermayr and Gröschl, 2014; Noy, 2009). Their economic relevance is expected to grow, as climate change is projected to increase both the frequency and intensity of extreme precipitation events (Masson-Delmotte, 2021). Understanding how floods affect firm performance, and the factors that affect this relationship, is therefore essential for informing climate adaptation policies and private-sector resilience strategies. Despite its importance, current estimates remain ambiguous, due partly to challenges of measuring flooding at disaggregated levels – particularly in cross-country settings – and varying methodological approaches (Botzen et al., 2019).

This section fills this gap by estimating the impact of flooding on firm-level outcomes across 17 European and Asian developed economies between 2000 and 2018. Using geographically detailed data on the location of major flooding events, we examine the static and dynamic impacts of flooding on determinants of firm value added, with a particular focus on the capital stock. This temporal lens is essential, as impacts often unfold gradually through infrastructure damage, credit constraints, or input market disruptions. High geographical disaggregation is equally important, as relying on aggregated regional indicators would mask substantial within-region heterogeneity and conflate the direct impact experienced by firms affected by flooding from those experiencing spillover effects in the surrounding area.

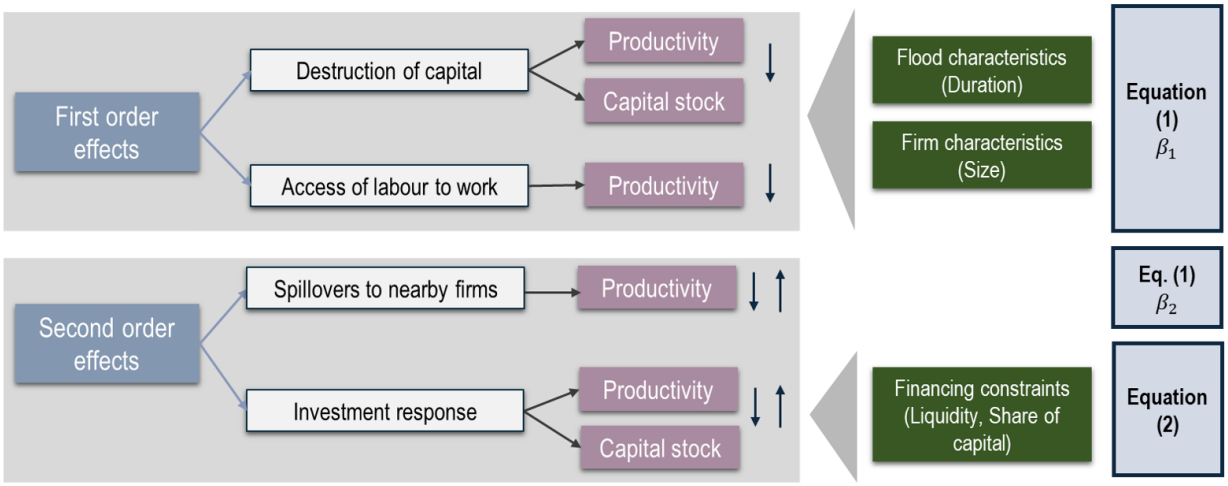
Flooding can affect firm-level outcomes through multiple channels, with distinct short- and medium-term effects (Figure B.1). The most immediate effects stem from the destruction of physical capital: direct physical damage to firm assets, including buildings, machinery, and inventory, can lead to immediate losses and increased costs for repairs or replacements (Kellenberg and Mobarak, 2011). Labour market disruptions, as employees experience displacement or are unable to commute due to damaged transport networks and public services, could further materialize as productivity losses, as employment remains fixed but working hours are decreased (Belasen and Polachek, 2008). These two channels jointly reduce effective inputs and translate into short-run declines in value added, even for firms that remain formally active after the event.

Beyond these direct impacts, floods generate a range of second-order indirect effects that propagate through the surrounding economic environment. Nearby firms that are not physically damaged may still experience disruptions through supply chains, customer flows, or shared infrastructure, leading to reductions in productivity even in the absence of asset losses (Barrot and Sauvagnat, 2016). Recent evidence suggests that such spillovers can account for a substantial share of the regional economic cost of extreme weather events (Costa and Hooley, 2025). A further mechanism operates through firms' investment responses. In the medium term, some firms may rebuild or upgrade capital while others may under-invest due to liquidity constraints thus hindering the recovery (Noy, 2009). These heterogeneous responses influence both productivity and capital stock in the

medium run, reinforcing the initial shock or facilitating recovery.

The magnitude and persistence of flood impacts depend critically on several conditioning factors. The duration of the event shapes the extent of physical destruction and the length of operational disruptions, amplifying the reduction in productivity and capital stock when damage is widespread or prolonged. Firms' fixed asset structure by asset type further mediates exposure: businesses with a higher share of tangible assets are more vulnerable to direct losses, while those relying more heavily on intangible capital may face comparatively smaller physical damages but still experience productivity disruptions. Insurance availability plays a central role for both channels, determining how quickly firms can replace damaged assets and resume operations. For firms indirectly affected, credit conditions and financing constraints shape their investment responses, influencing whether they can undertake repairs, upgrade capital, or instead postpone investment following the shock. These factors collectively determine the extent to which initial damage translates into temporary disruptions or triggers more persistent declines in production.

Figure B.1: Micro-level transmission channels



Source: Authors.

B.2. Methodology: data sources

Our analysis of the impact of flooding on firms relies on two main sources. Specifically, we use firm-level balance sheet data from Moody's Orbis dataset, and information on the location and duration of flood events from the Global Flood Database (GFD), produced by Tellman et al. (2021). We additionally use meteorological data from the ERA-5 global reanalysis dataset produced by the European Centre for Medium-Range Weather Forecasts and available through the Copernicus Climate Change Service.

Orbis combines information from regulatory and other sources to collect balance sheet data for listed and unlisted firms across manufacturing and services sectors in a wide range of economies. Currently, Orbis is the largest cross-country firm-level dataset available and accessible for economic

and financial research. To ensure international and inter-sectoral comparability, we implement the data cleaning and harmonisation procedures commonly used in OECD empirical studies, following Gal (2013) and Özcan et al. (2024). These include retaining harmonised unconsolidated accounts, deflating all nominal variables using country- and 2-digit industry-specific price indices, and removing observations displaying implausible ratios or excessive variation across years.

Capital input is proxied by the deflated value of fixed assets. Firm-level multifactor productivity (MFP) is estimated using the value-added–based GMM procedure of Wooldridge (2009). Labour input is proxied by the number of employees, and intermediate inputs (e.g. material costs) serve as instruments for unobserved firm-specific productivity shocks. Because parts of our identification strategy rely on within-firm variation, we further require firms to appear in the dataset for at least three consecutive years for the static analysis and at least six years for the dynamic analysis. Lastly, we eliminate countries that were not affected by any flood in our sample period. After the cleaning we are left with over 16.7 million firm-year observations for our static analysis and 6.7 million for the dynamic analysis.

Geocoding of firms is performed following the methodology in Costa et al. (2024). We assign firms to locations using geographic information parsed by Orbis from the headquarters address – geographical coordinates when available, or otherwise postcodes or municipality identifiers – combined with publicly available GIS datasets. Using this approach, we match 91.6% of eligible firms to a precise location. While headquarters locations may imperfectly reflect operational exposure for multi-plant firms, this limitation is likely modest in our dataset, as most firms are small and are less likely to operate across more than one plant.[15]

We combine these firm-level data with information on the location and duration of flood events from the Global Flood Database (GFD), produced by Tellman et al. (2021). The GFD is built using satellite imagery and remote-sensing techniques to systematically map the observed surface-water extent during 913 large flood events documented by the Dartmouth Flood Observatory (DFO) from 2000 to 2018, primarily drawing on optical and radar satellite data. It provides spatially explicit information on the geographic extent, timing and duration of major flood events around the world, allowing for a consistent global comparison of flood exposure across locations and over time. For a flood to be documented by the DFO it should as a minimum meet one of three criteria: significant damage to structures or agriculture; fatalities; and/or 1-2 decades-long reported interval since the last similar event. Satellite-based mapping of floods has the benefit of high precision but is not able to map certain floods for example due to cloud coverage, small or flash floods, or complex terrain.[16]

We retrieve all flood maps available in the GFD for the period 2000–2018 for the set of countries covered by the Orbis sample. This yields a total of 78 major flood events, each mapped at a very high spatial resolution—on the order of a few hundred metres per pixel—allowing us to identify

[15] 74% (89%) of firms in our sample employ fewer than 20 (50) workers, and 98% are SMEs.

[16] Additionally, the flood catalogue from DFO is built based primarily on news report, which means that potentially large floods underrepresented by the media may be absent from the database. This is less likely to be a concern across the developed economies studied in this analysis.

flooded areas with exceptional geographic precision. This level of detail is critical for distinguishing between firms that are directly exposed to flooding and those that are nearby but remain unaffected.

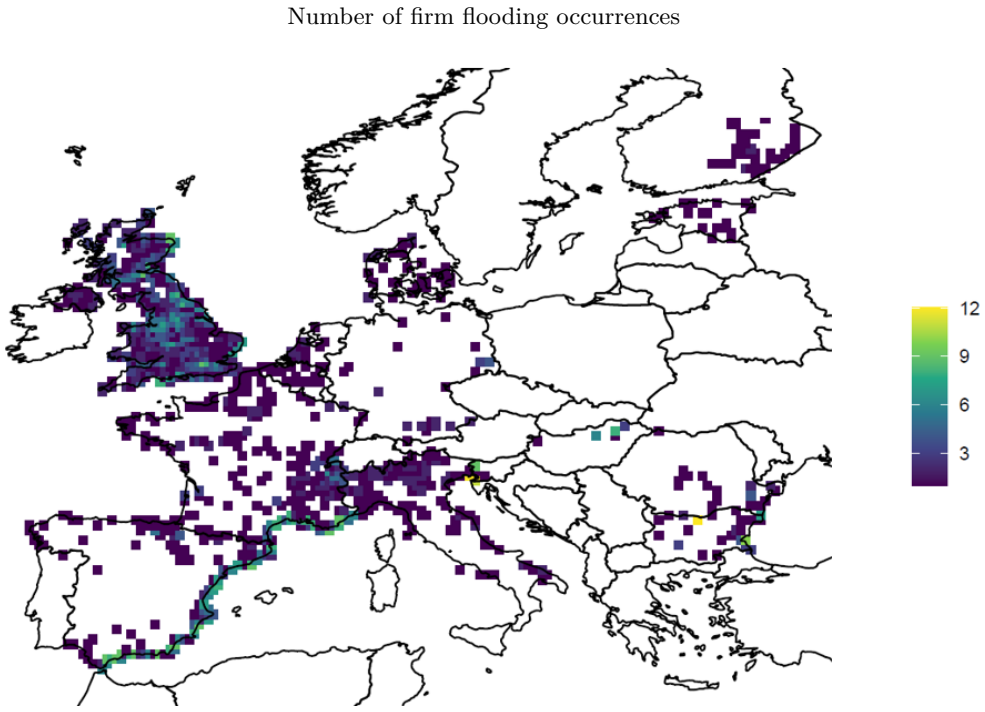
Using the geo-location of firms, we overlay the flood maps on the firm dataset to identify which firms were directly affected by each flood event, as well as the timing and duration of their exposure. This enables us to construct a detailed, event-based panel indicating for each firm whether, when and for how long it was flooded. To further support identification and account for potential spatial spillovers, we also compute the distance from each firm to the nearest flooded firm for each event. This allows us to define clean control groups and to analyse how the impacts of flooding propagate through space beyond the directly affected areas.

Figure B.2 illustrates the spatial distribution of these flood events across the location of firms in the Orbis sample over the sample period of 2000-2018. It reveals substantial spatial variation in the incidence of flooding events across Europe. Flood occurrences are most frequent in Western and Central Europe, with particularly high concentrations in northern Italy, southern Germany, eastern France, the Benelux region, and most of the United Kingdom. Several river basins—including the Rhine, Danube, and Po—stand out with clusters of locations experiencing more than a dozen events. Eastern Europe shows fewer high-frequency hotspots, but scattered areas in Poland, Hungary, and Romania still record multiple firm-level flood impacts. Large regions with no observed flooding (shown in white) reflect both the absence of events and areas where no firms in the Orbis sample are located. Overall, the map highlights how exposure to flooding is highly localized and often concentrated in low-lying or river-adjacent regions, underscoring the uneven distribution of climate-related hazards even within advanced economies.

Finally, we use the merging procedure described in Costa et al. (2024[7]) to assign firms to weather data, including yearly average temperature, precipitation, humidity, and number of warm days, as controls. Our final dataset covers over 2.5 million firms across 17 countries between 2000-2018.[17]

[17]The 17 countries included in the analysis are: Belgium, Bulgaria, Czechia, Germany, Denmark, Estonia, Finland, France, Hungary, Italy, Japan, Korea, Netherlands, Portugal, Romania, Spain, Sweden, and United Kingdom

Figure B.2: Spatial distribution of flooding events (2000-2018)



Source: Authors' own calculations based on information from the Global Flood Database (Dartmouth Flood Observatory) and Orbis.
Notes: Pixels represent 0.25° x 0.25° cells. All areas in white correspond to no observed flooding. The figure only shows flooding occurrences in the locations of firms in the Orbis sample. Flooding that may have occurred in locations where no firm from the Orbis sample is present is not included and therefore appears in white (i.e. zero occurrences).

B.3. Methodology: empirical strategy

We estimate the impact of flooding on firm performance by comparing firms directly exposed to floods with otherwise similar firms located more than 100 km away, while also separately accounting for spillovers to firms that are within these 100km but were unflooded through local supply chains, infrastructure and labour markets. Using panel data, we relate flood exposure to outcomes such as capital, productivity, value added and employment, controlling for firm characteristics and local weather conditions. To capture the persistence and dynamics of flood impacts, we complement this static analysis with a local projection estimates of the multi-year response of capital stocks following a flood, allowing effects to evolve flexibly over time. Identification relies on the assumption that, conditional on fixed effects and controls, the timing of floods is exogenous to firm-level outcomes. The full econometric specifications, variables and robustness checks are reported in Section B.5.

Our baseline empirical strategy estimates the static effect of flooding on firm outcomes by comparing firms that were inside a flooded area with a control group made of firms that were more than 100km away from a flooded area. Specifically, we estimate:

$$Y_{i(cs),t} = \beta_1 \,\text{Flooded}_{i(cs),t} + \beta_2 \,\text{Spillover}_{i(cs),t} + \beta_3 \,\mathbf{X}_{i(cs),t-1} + \beta_4 \,\mathbf{W}_{i(cs),t} + \delta_{st} + \delta_{ct} + \delta_{i(cs)} + \varepsilon_{i(cs),t} \quad (22)$$

where $Y_{i(cs),t}$ is the outcome variable of interest for firm i (of sector s and country c) in year t. This includes value added, capital stock, measured by the deflated value of fixed assets, multi-factor productivity, and number of employees, all logged.[18] The variable $Flooded_{i(cs),t}$ is an indicator equal to 1 if a firm is flooded in year t and remains equal to 1 in all subsequent years.[19] We treat the post-flood period as an absorbing treatment state because the economic consequences of a flood unfold over several years, even though the physical inundation is short-lived. Coding the treatment as active in all post-flood years therefore provides a standard way to capture these continuing effects within a post-treatment framework.

The variable $Spillover_{i(cs),t}$ is an indicator equal to 1 if firm i was not affected by a flood but was within 100 kilometers of a flood. This variable accounts for spillover effects operating through shared infrastructure, local supply chains, labour markets and demand conditions, which may affect nearby firms even in the absence of direct physical damage. The vector $\mathbf{X}_{i(cs),t-1}$ contains a set of lagged firm level controls, including an indicator of firm size based on the number of employees (3-10, 11-19, 20-49, 50-99, 100-249, 250+), age classes (young, from 0 to 5 years old firms mature, from 5 and 10 years; old for firms operating since more than 10 years), profitability, measured as the ratio of EBITDA over total assets, and a measure of capital intensity and liquidity, proxied by the share of fixed assets over total assets.[20] The vector $\mathbf{W}_{i(cs)t}$ includes a set of weather-related controls that are likely to affect how well individuals are able to work, averaged over the year: wind speed, precipitation and humidity, as well as the number of warm days as described in Costa et al. (2024).

The specification includes firm fixed effects $\delta_{i(cs)}$, which absorb all time-invariant firm characteristics, as well as sector-by-year fixed effects δ_{st} and country-by-year fixed effects δ_{ct}, which control for common shocks affecting firms in the same sector or country in a given year.[21] Standard errors are clustered at the firm level. The estimations are robust to clustering standard errors at the sector or region level. Identification relies on the assumption that, conditional on fixed effects and controls, the timing of floods is exogenous to firm-level outcomes. Firms located more than 100 kilometers away from any flood event serve as the control group, ensuring that they are unlikely to

[18] Firm-level multifactor productivity is estimated using the value-added–based GMM procedure of Wooldridge (2009).

[19] We restrict the analysis to the four years following each flood event. This window ensures that estimated effects remain plausibly attributable to the original shock, maintains a consistent comparison across events, and avoids the sample loss that would arise from imposing longer horizons given firms' uneven observation patterns. Focusing on a uniform four-year period therefore provides a stable sample while capturing the medium-run consequences of flooding. The results are similar when varying the number of years as well as to returning the flooding indicator to zero after four years. We further exclude firms that were affected by more than one flood in a year, which made up only 0.45% of all flooded firms.

[20] The controls vary with the dependent variable. Namely, regressions with labour productivity and value added include all controls; those with MFP exclude capital intensity, and those with employment exclude the size categories.

[21] For example, accounting for different growth trajectories of countries and development stages of different sectors.

be affected by either direct flooding or local spillovers.

To analyse the dynamic response of firm outcomes to flooding, in turn, we estimate impulse responses using a local projection approach (Jordà, 2005). This framework allows the effects of flooding to evolve flexibly over time without imposing restrictive dynamic assumptions. We focus on the dynamics of capital stocks due to its importance. Specifically, we estimate:

$$\begin{aligned}
&\text{CapitalStock}_{i(cs),t+k} - \text{CapitalStock}_{i(cs),t-1} = \\
&\quad = \beta_1 \, \text{Flooded}_{i(cs),t} + \beta_2 \, \text{Spillover}_{i(cs),t} + \sum_{h=1}^{k} \phi_h \, \text{Flooded}_{gc,t+h} \\
&\quad + \sum_{h=1}^{2} \sigma_h \, \text{Flooded}_{gc,t-h} + \sum_{h=1}^{k} \vartheta_h \, \text{Spillover}_{gc,t+h} \\
&\quad + \sum_{h=1}^{2} \tau_h \, \text{Spillover}_{gc,t-h} + \gamma \, Y_{i(cs),t-1} + \beta_3 \, \mathbf{X}_{i(cs),t-1} + \beta_4 \, \mathbf{W}_{i(cs),t} \\
&\quad + \delta_{cs} + \delta_{ct} + \delta_{i(cs)} + \varepsilon_{i(cs),t} \ , \quad \text{for} \quad k = 0, ..., 4
\end{aligned} \tag{23}$$

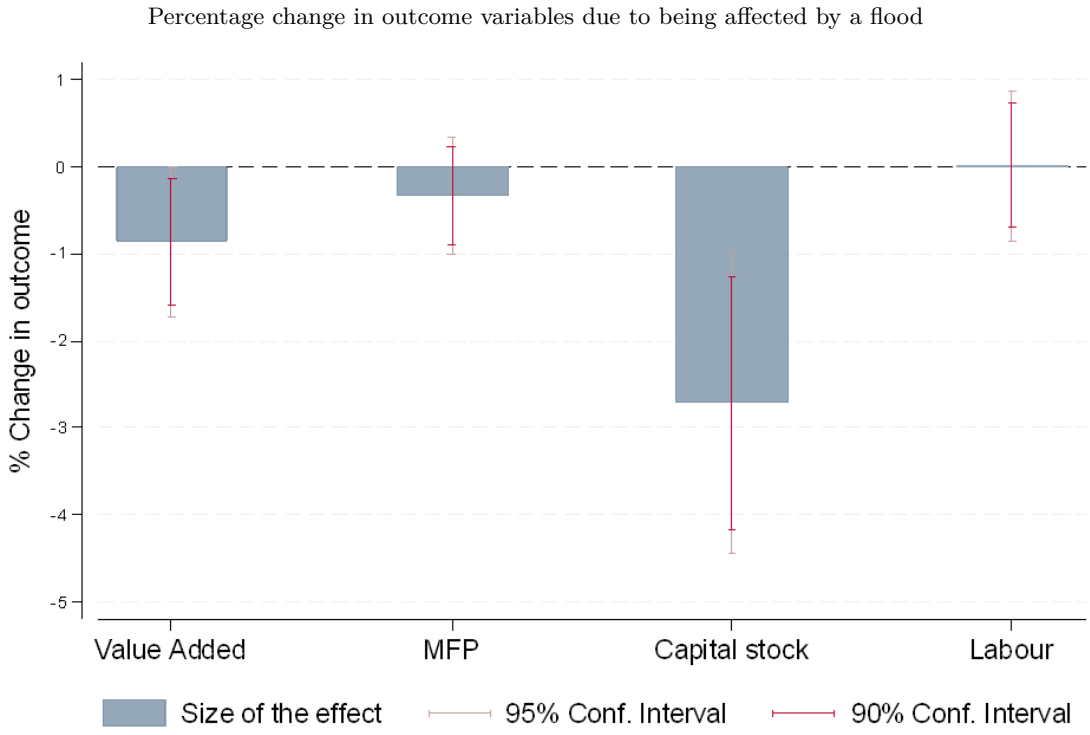
where $k = \{0, \ldots, 4\}$ denotes the horizon in years after the flood event. The dependent variable measures cumulative changes in the capital stock in each horizon relative to the pre-flood year $t-1$, allowing for a direct interpretation of coefficients as impulse responses. Leads and lags of both flood exposure and spillover indicators are included because impacts are persistent. The same control variables and fixed effect structure as in the static specification are included.

B.4. Results

17. Our results suggest that flooding impacts firm value added mainly through its effect on the capital stock. Specifically, being affected by a flood decreases a firm's capital stock by 2.7% on average in the four years after the flood. This is reflected in a decrease of firm value added. In contrast, estimated effects on multi-factor productivity are modest and statistically insignificant and labour appears to be unaffected.[22] Taken together, this suggests that floods mainly operate through balance-sheet and asset destruction channels rather than through sustained changes in production efficiency. These findings align with recent firm-level evidence showing that climate shocks often materialise through capital and scale effects rather than through immediate productivity losses (e.g. Pelli et al., 2023; Prieto and Noy, 2025 for New Zealand). Figure B.3 shows the static impacts of a flood on the four dependent variables.

[22]The impact on capital of 2.7% along with a resulting impact of 0.86% on value added, without changes in MFP or labour, implies a share of capital of around 0.32 assuming a Cobb-Douglas production function, which is in line with the literature.

Figure B.3: Floods affect firms mainly through their impact on capital stocks



Source: Authors' calculations based on Orbis, the Global Flood Database and Copernicus.
Notes: Bars represent estimated coefficients and vertical lines the respective 95% and 90% confidence intervals. They are obtained by estimating Equation 22 five times with each variable as the outcome: fixed assets, MFP, labour productivity, value added, and number of employees (all logged) multiplied by 100 to be interpreted as percentage changes. The full results are available in Table B.1.

Flooding also generates economically meaningful spillovers to firms that are not directly inundated. Figure B.4 compares the estimated coefficients for directly affected firms and for firms located within 100 kilometers of a flooded area. For capital stock, productivity, and value added, negative spillover effects are sizeable and statistically significant, with magnitudes between 38% and 68% of the direct effect.[23] These results are consistent with disruptions to shared infrastructure, local input-output linkages, financial system spillovers, and changes in demand conditions, and echo evidence from the production-network literature documenting how localised shocks propagate through supply chains (e.g. Barrot and Sauvagnat, 2016).[24] Ignoring such spillovers would therefore lead to a substantial underestimation of the economic costs of flooding.

Finally, the impacts of flooding are highly heterogeneous, depending both on the severity of the hazard and on firm characteristics that shape resilience. Firms affected by floods lasting longer than the sample median experience substantially larger capital losses, with average declines of 3.3%, compared to losses of 2.2% for firms affected for shorter durations. Losses to value added are only

[23] The positive estimated spillover for labour signals a possible reallocation effect, with close but unaffected firms growing as a result of a flood.

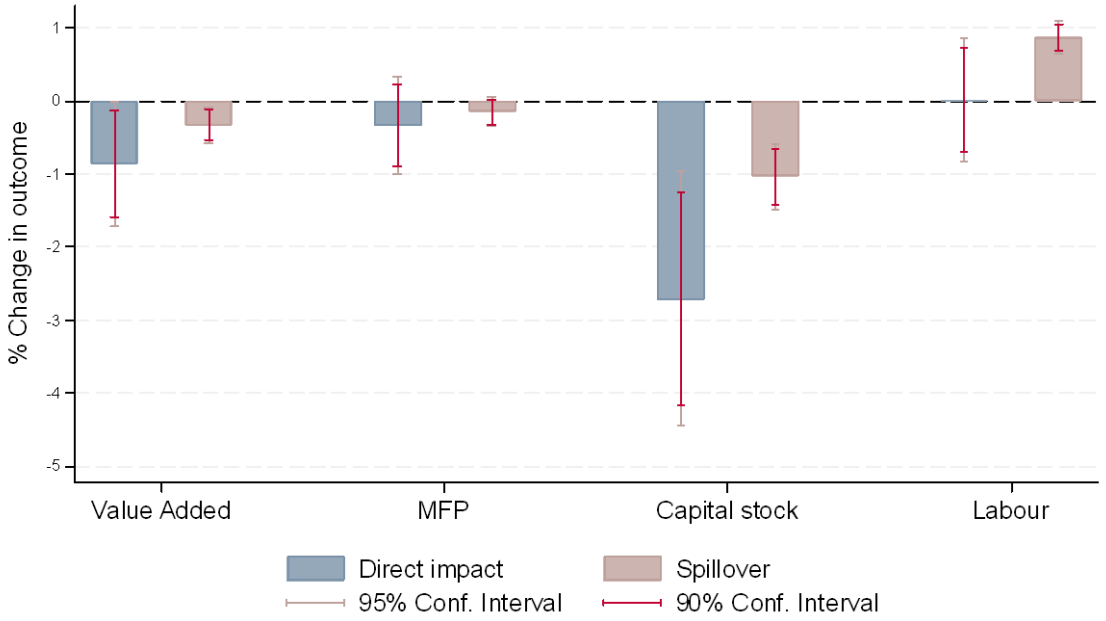
[24] Financial system spillovers can go well beyond the local area. However, evidence shows that firms, particularly SMEs, tend to obtain credit at the local level (Guiso et al., 2004).

significant for longer flooding episodes, indicating that short-lived inundations primarily damage capital stocks, while longer disruptions have broader operational impacts (Figure B.7).

Firm size also plays a key role in shaping vulnerability. Smaller firms are affected the most, with micro firms (those with fewer than 10 employees) experiencing losses to capital stock of almost 5% due to a flooding event, while impacts on large firms (those with more than 250 employees) are not statistically significant and can even be positive (Figure B.8). This pattern is consistent with smaller firms facing tighter financial constraints, more limited insurance coverage and lower capacity to absorb and smooth large, sudden shocks to physical capital, and large firms being able to reconstruct better.

Figure B.4: Spillovers are substantial

Percentage change in outcome variable due to being affected by or being close to a flood

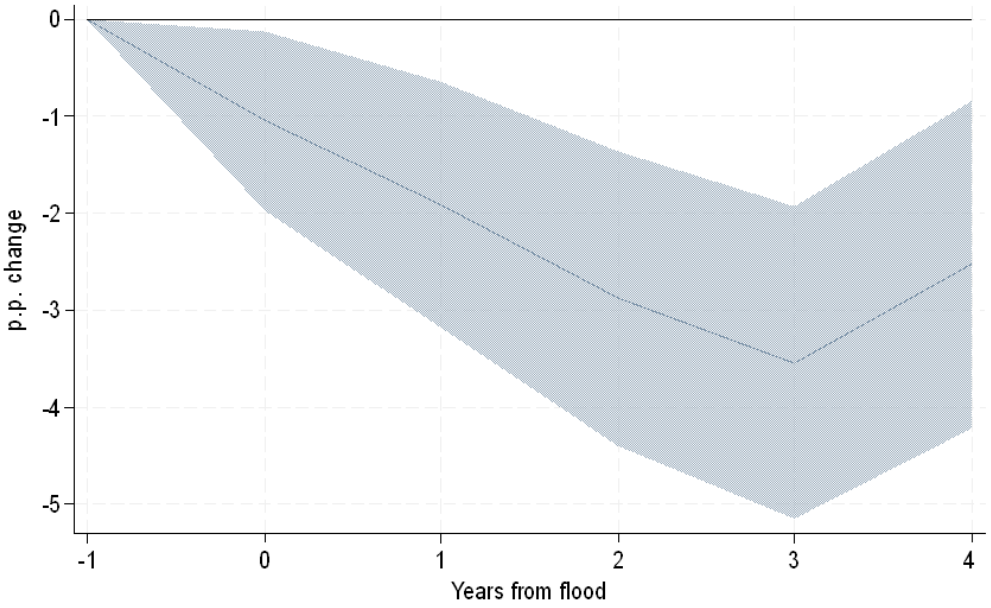


Source: Authors' calculations based on Orbis, the Global Flood Database, and Copernicus.
Notes: Bars represent estimated coefficients and vertical lines the respective 95% and 90% confidence intervals. They are obtained by estimating Equation (1) five times with each variable as the outcome: fixed assets, MFP, labour productivity, value added, and number of employees (all logged), and correspond to β_1 and β_2 multiplied by 100. The full results are available in Table B.1.

Turning to the dynamic estimates based on local projections, we find that capital accumulation declines sharply in the year of the flood and continues to deteriorate over subsequent years, with the largest negative effect observed around three years after the event (Figure B.5). While there are signs of partial recovery thereafter, capital stocks do not fully revert to their pre-flood trajectory within the four-year horizon considered. This pattern indicates that floods lead to capital stock write offs and that rebuilding capital is a slow process, consistent with frictions in financing, insurance payouts or reconstruction capacity (Noy, 2009).

Figure B.5: Floods have a lasting impact on the capital stock

Impact of one flooding event on the growth rate of capital stock



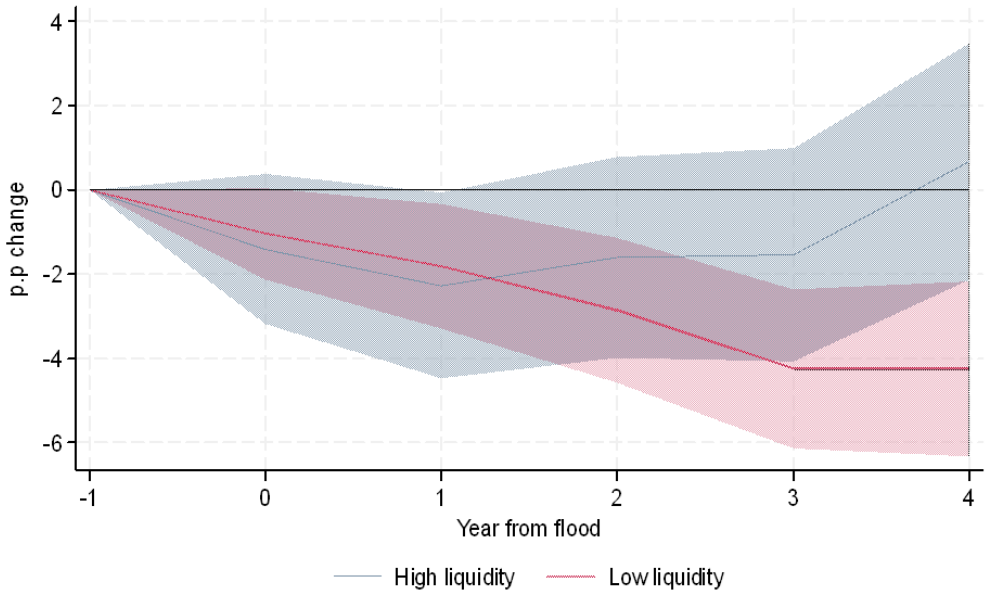
Source: Authors' calculations based on Orbis, the Global Flood Database, and Copernicus.
Notes: The line represents the estimated coefficients at each year relative to the flooding event and the shaded areas 90% confidence intervals. These coefficients are obtained by estimating Equation (23). Figure B.4 depicts also the spillover effect.

Recovery dynamics differ markedly across firms depending on their financial conditions. Figure B.6 splits firms by their pre-flood liquidity, proxied by the share of fixed assets in total assets. While the immediate impact is similar, firms with lower liquidity experience more persistent declines in capital stocks following a flood, while those with higher liquidity show a faster recovery path. This heterogeneity suggests that financial conditions play a role in shaping post-disaster adjustment, amplifying the long-term economic consequences of flooding. These findings are in line with earlier evidence that limited access to finance can slow post-disaster reconstruction and prolong output losses (Felbermayr and Gröschl, 2014).

Taken together, the results highlight three key features of flood-related economic damage at the firm level. First, floods primarily affect firms through capital destruction rather than through immediate declines in productivity. Second, indirect spillovers to nearby firms are large and pervasive, underscoring the importance of accounting for spatial linkages. Third, recovery is slow and uneven across firms, with financially constrained firms facing significantly greater and more persistent losses. These empirical findings provide a strong motivation for incorporating capital dynamics and spatial spillovers into macroeconomic assessments of climate change, as is done in the modelling framework presented in Section 5.

Figure B.6: Liquidity constraints hamper recovery

Impact of one flooding event on the growth rate of capital stock by fixed capital intensity in assets

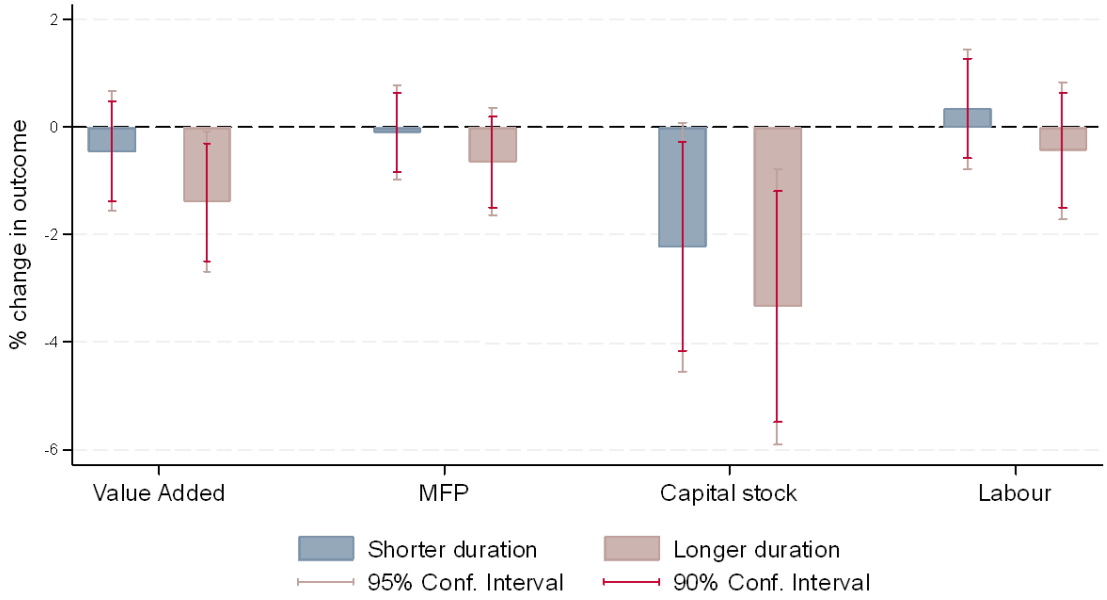


Source: Authors' calculations based on Orbis, the Global Flood Database, and Copernicus.
Notes: The line represents the estimated coefficients at each year relative to the flooding event and the shaded areas 90% confidence intervals. These coefficients are obtained by estimating Equation (23) interacting $Flood_{i(cs),t}$ with a dummy variable equal to 1 if the firm was above the sample median in its share of fixed assets in total assets (low liquidity) in the year before the flood.

B.5. Further results: Figures and tables

Figure B.7: Flooding impacts vary by duration of flooding

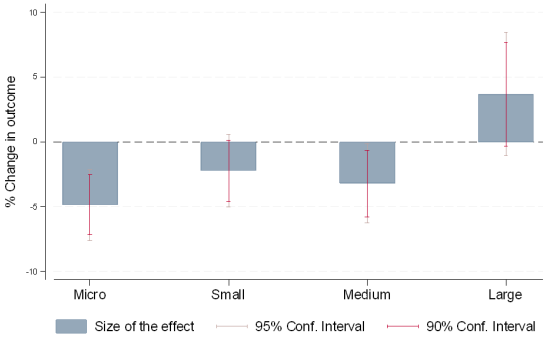
Change in outcomes due to flooding episodes of shorter and longer duration



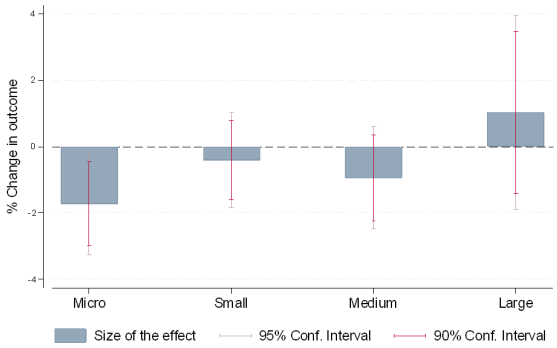
Source: Authors' calculations based on Orbis, the Global Flood Database, and Copernicus.
Notes: Bars represent estimated coefficients and vertical lines the respective 95% confidence intervals. They are obtained by estimating Equation (22) five times with each variable as the outcome: fixed assets, MFP, labour productivity, value added, and number of employees (all logged) interacted with the duration dummy.

Figure B.8: Flooding impacts vary by firm size

(a) Capital Stock



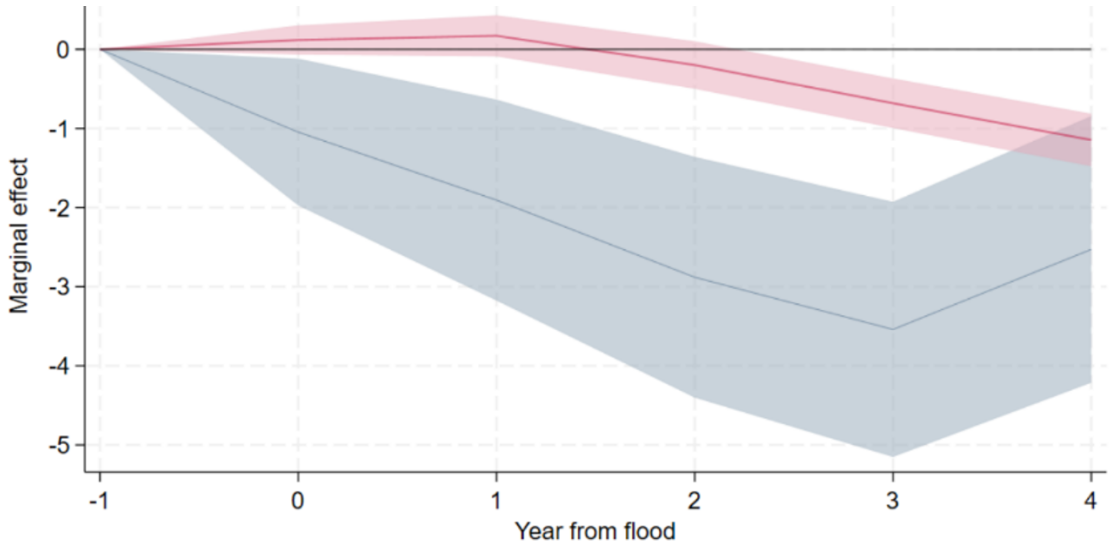
(b) Value Added



Note: Bars represent estimated coefficients and vertical lines the respective 95% confidence intervals. They are obtained by estimating Equation (22) with the flood variable interacted with a size dummy. Micro firms are those with up to 10 employees, small between 11 and 50 employees, medium between 51 and 250 employees, and large firms are those with more than 250 employees. The dependent variables are real fixed assets (Panel A) and real value added (Panel B).
Source: Authors' calculations based on Orbis, the Global Flood Database and Copernicus.

Figure B.9: Delayed spillover effects on neighbouring firms

Impact of flooding on capital stock: direct and spillover effects



Source: Authors' calculations based on Orbis, the Global Flood Database, and Copernicus.
Notes: The line represents the estimated coefficients at each year relative to the flooding event and the shaded areas 90% confidence intervals. These coefficients are obtained by estimating Equation (23) and correspond to the direct and spillover coefficients.

Table B.1: Baseline results

Impact of one flood event on firm outcomes (Equation 22)

	(1)	(2)	(3)	(4)	(5)
Firm Outcome	MFP	Labour Productivity	Capital Stock	Value Added	Labour
$Flooded_{i(cs),t}$	-0.00335	-0.00530	-0.02709***	-0.00860*	0.00008
	(-1.0)	(-1.5)	(-3.1)	(-2.0)	(0.0)
$Spillover_{i(cs),t}$	-0.00154	-0.00363***	-0.01042***	-0.00334***	0.00869***
	(-1.5)	(-3.5)	(-4.6)	(-2.6)	(7.8)
Controls	Firm-level controls + weather				
Fixed effects	Firm + Country-Sector + Sector-Year + Country-Year				
Observations	16,760,590	16,947,346	16,760,590	16,947,346	17,020,000
R-squared	0.85658	0.82669	0.92086	0.93354	0.93596

Sources: Authors' calculations based on Orbis, the Global Flood Database, and Copernicus.
Notes: The coefficients are from estimating Equation (22) five times independently with each firm outcome as the dependent variable. The coefficients can be interpreted as percentage changes by multiplying by 100. Firm controls include size, age, profitability, and capital intensity, as defined in Section B.3. Columns (2) and (3) added include all controls; column (1) excludes capital intensity, and column (5) excludes the size categories. Weather controls include yearly averages of humidity, precipitation, and wind speed, as well as number of warm days for all regressions. Significance Level: * 15%,* *10%, ***5%. T-statistics in parentheses; standard errors clustered at the firm level.

C. Further detail: impact of heat stress on firm productivity

We use and build on estimates of the impact of heat stress on labour productivity from Costa et al. (2024) to calibrate the size of climate damages. Costa et al. (2024) use firm-level data from Orbis (Moody's), providing detailed information on output, input usage, firm characteristics, and the geographic location of over 2.7 million firms across 23 advanced economies from 2000 to 2021. To capture climatic conditions, it uses ERA-5 reanalysis data containing high-resolution daily temperature and other weather variables at approximately 28 x 28 km resolution near the equator. With these two datasets, one can examine the relationship between firm-level outcomes and localized climatic variations with high spatial and temporal precision. To measure the impact of heat stress, we follow their paper in defining hot days as the number of annual days in which the maximum daily temperature falls within a given temperature bin, allowing us to assess the effects of varying temperature exposures on firm performance.

C.1. Regression specification

To account for the heterogeneous impact of heat stress, we employ a regression specification that accommodates varying levels of heat stress and local average temperature as a mediating factor. This approach enables us to capture differential vulnerabilities across sectors while also considering the broader climatic context in which firms operate, whereby the same level of heat may have a smaller or larger impact. The impact of heat stress has been found to vary depending on whether a location has a predominantly cold or warm climate, as different adaptation systems and infrastructures are in place to manage temperature extremes (Costa et al., 2024). Hotter countries are likely to be better prepared for high temperatures, whereas firms in colder regions may face greater disruptions due to a lack of pre-existing heat adaptation measures. We estimate the following regression using the full sample in the paper:

$$Z_{int}^{j} = \sum_{b=1}^{B} \left(\beta^{b} + \sum_{h=1}^{H} \delta_{h} \, \text{AvgTemp}_{n}^{h} \right) \text{HotDays}_{nt}^{b} + \gamma_{1} \, \mathbf{X}_{it} + \gamma_{2} \, \mathbf{W}_{nt} + \theta_{i} + \lambda_{c(n)t} + \varepsilon_{int}^{j} \qquad (3)$$

where i denotes firm, j denotes sector, n denotes location, $c(n)$ denotes the country to which location n belongs and t denotes year. The variables above are defined as follows:

- Z_{int}^{j}: firm-level productivity measured as multi-factor productivity. This is estimated using the generalized method of moments value added-based procedure from Wooldridge (2009[43]). This procedure relies on a system of moment conditions where firm-level inputs serve as proxies for productivity shocks. The estimated residual from the production function represents TFP, which captures variations in output not explained by firm inputs. The deflated value

of fixed assets is used as a proxy for the capital input, the number of employees as a proxy for the labour input, and intermediate inputs as an instrument for unobserved firm-specific productivity shocks.

- AvgTemp_n^h: dummy for whether average annual maximum daily temperature in 2000–2021 in location n falls within band $h \in \{1, \ldots, H\}$
- HotDays_{nt}^b: number of hot days where daily maximum temperature falls within band $b \in \{1, \ldots, B\}$
- $\mathbf{X}_{it}$: time-varying firm characteristics including firm size, age, and average profitability
- $\mathbf{W}_{nt}$: yearly averages of weather variables, namely wind speed, moisture, and precipitation
- θ_i: firm fixed effect controlling for all time-invariant firm characteristics
- $\lambda_{c(n)t}$: country-year fixed effects controlling for common time-trends in each country

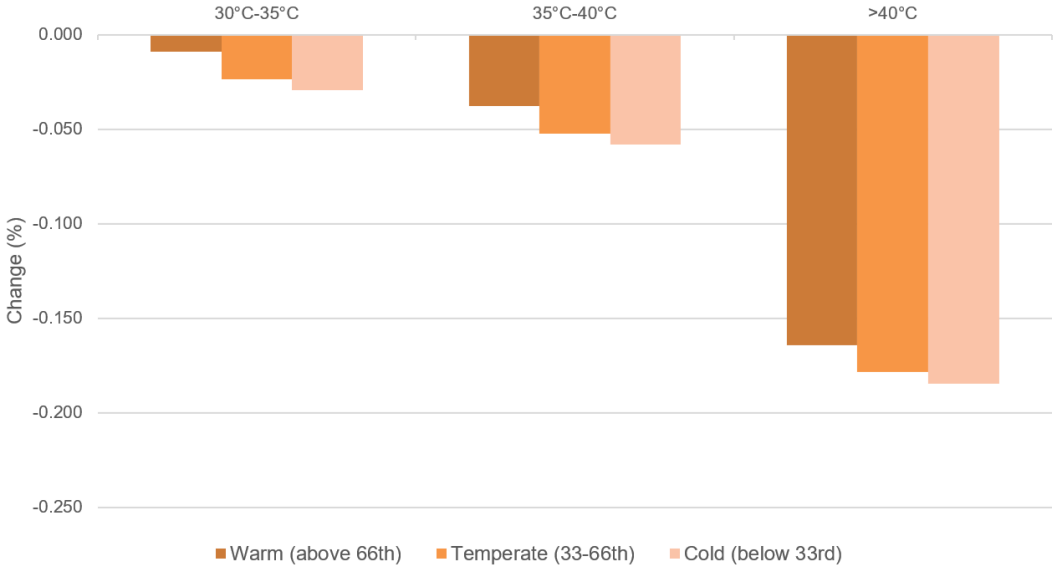
We parameterize average temperature bins $h \in \{1, \ldots, H\}$ by categorizing locations based on their average maximum daily temperature percentiles: below the 33rd (cold), between and including the 33rd and 66th (temperate), and above the 66th (warm). In turn, hot day bins $b \in \{1, \ldots, B\}$ are parameterized by separating each day into those whose maximum temperature was between 30°C and 35°C, between 35°C and 40°C, and above 40°C. Standard errors are clustered at the firm-year level.

C.2. Results

Figure C.1 shows the impacts of an additional hot day in each sector, which are based on the estimated coefficients from Equation 3. All estimates should be interpreted as the level of firm productivity relative to a day when the temperature is lower than 30°C, which is the temperature bin we set as the baseline.

Figure C.1: Impact of an additional hot day on firm productivity

Percent change in annual TFP by temperature bin and climate type



Source: Authors' own calculations based on Costa et al. (2024) and Climate Change Knowledge Portal (World Bank).
Notes: The figure shows the impact of an additional day for locations on log multi-factor productivity. The values are either derived from the estimated coefficients in Equation (3). The legend denotes the percentile interval of average annual maximum daily temperature.

D. Further detail: projections of future flood damages

D.1. Flood Protection Standards

A necessary first step in projecting future flood risk is to characterise the baseline probability of flooding. Historical flood exposure reflects not only natural hydrological conditions, but also the level of protection provided by existing flood defences, such as levees, dikes and coastal barriers. Understanding the relationship between natural flood hazard and protection standards is therefore essential for assessing how the frequency of flooding may evolve under future climate scenarios.

Baseline protection levels for riverine flooding are obtained from the FLOPROS (Flood Protection Standards) database, developed by Scussolini et al. (2016) as part of a joint effort by researchers at IVM (Vrije Universiteit Amsterdam), the World Bank, and other partners. FLOPROS provides spatially explicit estimates of existing flood protection standards across the globe, expressed in terms of return periods (e.g. a 1-in-50-year or 1-in-100-year level of protection). These values represent the capacity of local flood defences and are compiled using a combination of national reports, engineering assessments, model-derived simulations and proxy indicators such as income levels and urbanisation. Protection values for coastal flooding are obtained from Tiggeloven et al. (2020) . Both FLOPROS and the dataset from Tiggeloven et al. (2020) are available at a sub-national resolution, allowing one to account for variation in protection standards within countries.

D.2. Climate-Driven Hazard Projections

To translate these protection standards into measures of flood risk under future climatic conditions, we combine them with riverine and coastal flood hazard maps produced under the Aqueduct Floods framework by the World Resources Institute (WRI). These maps provide spatial estimates of flood depth for a range of return periods (from 1-in-2 to 1-in-1000-year events), at a very high spatial resolution of 30 arc-seconds - roughly 1 x 1 km at the equator in the years 2030, 2050, and 2080 under RCP4.5 and RCP8.5. The projections are based on downscaled climate model outputs combined with hydrological and hydraulic modelling, allowing them to capture changes in precipitation patterns, river discharge and storm-surge dynamics. Separate sets of maps are available for riverine flooding and coastal flooding.

Using these data, we assess how the frequency of flooding is expected to change under the assumption that current flood protection standards remain constant over time. Specifically, for each location, we compare projected flood depths to the historical protection threshold implied by the local FLOPROS return period. If the projected flood depth exceeds the historical protection level more frequently in the future, this implies an increase in the probability of overtopping or failure, and therefore a higher frequency of damaging flood events. This approach allows us to isolate the effect of changing climatic conditions on flood risk, holding the existing level protection infrastructure constant. This approach allows us to isolate the effect of changing climatic conditions on flood risk, holding the existing level of protection infrastructure constant.

To assess economic relevance, we combine the geographic extent of flood-prone areas with spatial

population data provided by the Gridded Population of the World, Version 4 (GPWv4) dataset. This allows us to compute, for each location, the share of the population residing in areas subject to flooding under baseline protection standards. We do this by first identifying the pixels in which the projected flood depth exceeds zero in a 1-in-100-year flood and then computing the share of total population in each GPW grid cell residing in flood-exposed land.

Figure D.1: Effect of climate change on coastal flood frequency in 2080 relative to 1980

Percent change in the annual frequency of coastal flooding under RCP8.5 (ensemble mean)



Source: Scussolini et al. (2016), World Resources Institute (Aqueduct), and authors' own calculations.
Note: The map reports values at the resolution of a 0.25° × 0.25° grid cell (approximately 25 km at the equator). Values greater than 50% and less than -50% are windsorized at 50% and -50%, respectively. The projections assume flood protection standards remain the same as in the baseline period (i.e. 1980).

For coastal flooding, the WRI projections incorporate both changes in storm surge behaviour and the effects of rising mean sea levels, which increase the baseline water level on which storm surges are superimposed. In areas where the annual probability of coastal flooding reaches 50 percent - effectively implying a permanent or near-permanent inundation - the hazard is no longer characterised as intermittent flooding. In such cases, we treat the impact as a separate and distinct risk, captured under sea level rise rather than episodic coastal flooding. The treatment of sea-level rise as a standalone hazard is done separately. For all other cases, we treat coastal flooding similarly to riverine flooding. Figure D.1 shows projected changes in the frequency of coastal flooding in such cases.

D.3. Baseline Exposure and Population Overlay

Flood risk does not affect all locations equally. Large parts of the world's population and economic activity lie outside flood-prone areas, while others are highly exposed to recurrent riverine or coastal flooding. Before assessing the potential economic consequences of future flood events, it

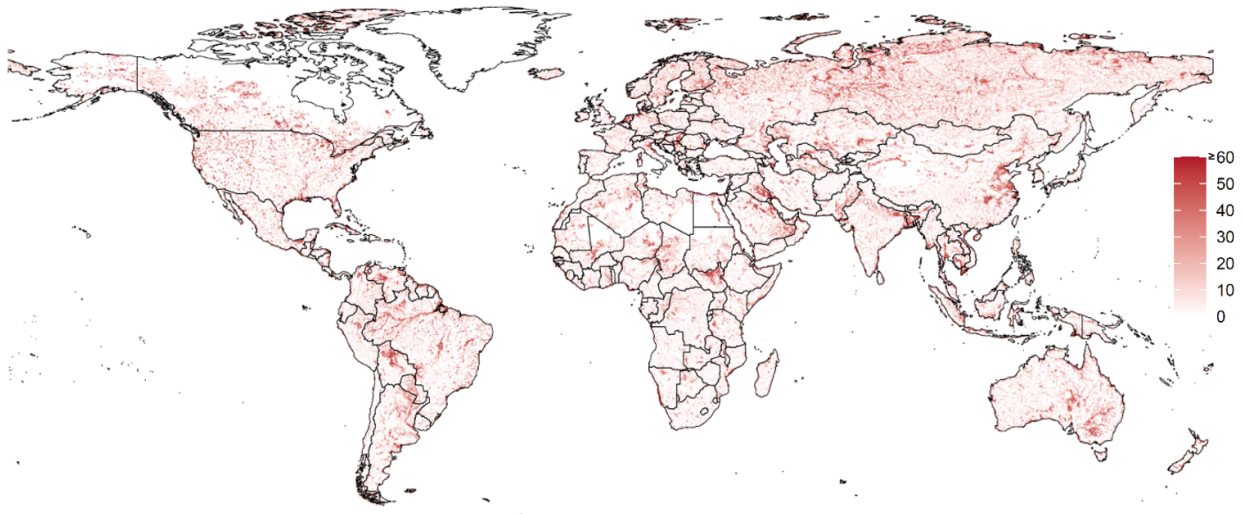
is therefore important to establish the underlying extent and spatial distribution of exposure. In this context, exposure is defined as the presence of people, assets and economic activity in areas that are subject to inundation, conditional on a given hazard threshold.

To measure the extent of exposure, we first take historical 1-in-100-year flood hazard maps for both riverine and coastal flooding. For each grid cell, we identify whether the projected flood depth exceeds zero. All locations for which the estimated flood depth is strictly positive are classified as flood-exposed under the historical baseline, irrespective of the precise depth or recurrence probability beyond this threshold. This binary classification allows us to establish the geographic extent of areas that are potentially subject to flooding under current climatic and protection conditions, and to treat all such locations as equally exposed in the baseline.

To translate this geographic extent into a measure of economic exposure, we overlay the flood hazard maps with high-resolution population data from the Gridded Population of the World, Version 4 (GPWv4) dataset, produced by the Center for International Earth Science Information Network (CIESIN) in collaboration with the National Aeronautics and Space Administration (NASA). GPWv4 provides gridded estimates of population counts and densities at the same spatial resolution of 30 arc-seconds as the flood hazard maps, offering a globally consistent depiction of the geographic distribution of population. We use population as a proxy for overall economic exposure, recognising that this abstracts from potential differences in asset intensity and infrastructure density across locations. By combining the flood exposure mask with the GPWv4 population grid, we compute, for each sub-national region, the share of the population residing in flood-exposed areas.

Figure D.2: Population exposed to riverine flooding

Percentage of population exposed to a 1-in-100-year riverine flood



Source: World Resources Institute (Aqueduct), Gridded Population of the World (GPW v4.11), and authors' own calculations.
Note: The map reports values at the resolution of a 0.25° × 0.25° grid cell (approximately 25 km at the equator). Values greater than 60% are windsorized at 60%.

Figure D.2 maps the share of the population exposed to a 1-in-100-year riverine flood across the globe, revealing substantial spatial variation. High exposure is concentrated in densely populated river basins, including parts of Central and Eastern Europe, northern Italy, the Rhine and Danube basins, regions along major river systems in the United States and, most notably, the Netherlands. In several of these locations, a sizeable share of the population resides within the historical 100-year floodplain, reflecting the long-standing co-location of economic activity and settlement patterns with river networks. In contrast, large parts of OECD countries characterised by limited river networks or lower population density, display lower exposure. The map highlights where baseline hydrological risk intersects with population density, offering a clearer sense of the human footprint in flood-prone areas. The figure captures potential exposure, not expected damage: many regions with high exposure may face low damages if they have significant protective infrastructure, while those with low exposure may still face substantial impacts if protective capacity is limited and/or flooding is frequent.

E. Model description, equilibrium, calibration, and counterfactuals

E.1. Equilibrium conditions

Here, we provide a list of equations that fully characterizes the economy's equilibrium. We add a time subscript to emphasize the equilibrium sequence aspect of the model's equilibrium path.

Cost of input bundle

$$x_{nt}^j = \mu_n^j \left(w_{nt}^\lambda r_{nt}^\eta Q_{nt}^{1-\lambda-\eta} \right)^{\beta^j} \prod_{k=1}^{J} (P_{nt}^k)^{\gamma^{jk}}, \quad \text{where } \beta^j + \sum_{k=1}^{J} \gamma^{jk} = 1 \tag{24}$$

Sectoral goods price index

$$P_{nt}^j = \Gamma(\xi_n^j)^{\frac{1}{1-\theta^j}} \left(\prod_{i=1}^{N} (x_{it}^j \tau_{nit}^j)^{-\theta_j} (A_{it}^j)^{\theta_j} \right)^{-1/\theta_j} \tag{25}$$

Final goods price index

$$P_{nt} = \prod_{j=1}^{J} (P_{nt}^j)^{\alpha^j}, \quad \text{where } \sum_{j=1}^{J} \alpha^j = 1 \tag{26}$$

Optimal trade shares

$$\pi_{nit}^j = \frac{A_{it}^{\theta j} (x_{nt}^j \tau_{ni}^j)^{-\theta^j}}{\sum_{l=1}^{N} A_{mt}^{\theta j} (x_{mt}^j \tau_{nm}^j)^{-\theta^j}} \tag{27}$$

Optimal migration shares

$$\lambda_{nit} = \frac{B_{nt} (\kappa_{ni} P_{nt}^\alpha Q_{nt}^{1-\alpha})^{-\varepsilon} w_{nt}^{-\varepsilon}}{\sum_{m=1}^{N} B_{mt} (\kappa_{mi} P_{mt}^\alpha Q_{mt}^{1-\alpha})^{-\varepsilon} w_{mt}^{-\varepsilon}} \tag{28}$$

Law of motion of capital

$$K_{nt+1} = \beta \, r_{nt} \, K_{nt} \tag{29}$$

Population distribution

$$L_{nt} = \sum_{i=1}^{N} \lambda_{nit} L_{i,t-1} \tag{30}$$

Goods market clearing

$$X_{nt}^j = \sum_{j=1}^{J} \gamma_n^{kj} \sum_{i=1}^{N} \pi_{int}^j X_{it}^k + \alpha^j w_{it} L_{it} \tag{31}$$

Labour market clearing

$$w_{nt}L_{nt} = \sum_{j=1}^{J}\sum_{i=1}^{N}(\lambda\beta_n^j\pi_{int}^j X_{nt}^j) \tag{32}$$

Capital market clearing

$$r_{nt}K_{nt} = \sum_{j=1}^{J}\sum_{i=1}^{N}(\eta\beta_{nt}^j\pi_{int}^j X_{nt}^j) \tag{33}$$

Real estate market clearing

$$Q_{nt} = T_{nt}^{-(1-\mu)}\left(\left(\frac{r_{nt}}{\mu}\right)^{\mu}\left((1-\alpha)w_{nt}L_{nt} + \sum_{j=1}^{J}\frac{w_{nt}L_{nt}^j}{\beta^j(1-\lambda-\eta)}\right)\right)^{1-\mu}, \tag{34}$$

where μ_n^j and ξ_n^j are constants and $\Gamma(\cdot)$ is the gamma function.

E.2. Calibration of baseline model

E.2.1 Data sources

The model calibration relies on multiple sources of data, which we describe below and summarise in Table E.2:

- **OECD Regional Data:** we obtain information on gross value added, population, and employment for all 38 OECD countries at the region- and sector-region-level for the period 2000-2023 from a series of OECD datasets.[25] Whenever sectoral data are absent at the regional level, we apply the region average and whenever that is not available, we apply the national average.

- **Database of Sub-national Economic Output (DOSE v2):** for OECD accession countries and OECD key partners, we use GDP and employment figures from the MCC–PIK Database of Sub-national Economic Output (DOSE v2), produced by researchers at the Mercator Research Institute on Global Commons and Climate Change (MCC) and the Potsdam Institute for Climate Impact Research (PIK), and available at the Admin-1 level following the GADM regional boundaries. DOSE provides harmonized estimates of economic activity for approximately 1,660 of first-level administrative regions across 83 countries from 1953 to 2020. Because DOSE reports GDP and employment only at an aggregated sectoral level - agriculture, manufacturing, and services - our calibration for these countries follows this three-sector breakdown.

- **World Bank Development Indicators:** for all countries outside the sub-national datasets described above, we measure economic activity at the national level using sectoral indicators

[25] These are: Gross value added by main economic activity – Regions (OECD Regions and Cities); Employment by main economic activity – Regions (OECD Regions and Cities); Gross domestic product - Regions (OECD Regions and Cities); Annual GDP and components (OECD National Accounts).

from the World Bank's World Development Indicators (WDI). Specifically, we collect GDP and employment data for the three broad sectors reported consistently across countries - agriculture, manufacturing, and services. These indicators provide internationally comparable measures constructed using national statistical offices and harmonized by the World Bank. Because WDI sectoral accounts are available for nearly all countries and extend over several decades, they offer the most reliable and comprehensive source of country-level economic structure for regions where subnational information is unavailable. This allows us to maintain a consistent three-sector decomposition across the entire dataset.

- **OECD Input-output Tables:** provides country-level tables that record inter-industry transactions, capturing how goods and services flow between sectors within and across economies from 1995 until 2020. It includes, for each sector, the value of purchases of goods and services from all sectors (including itself) to be used as inputs in production, and the value of final consumption by households, gross output, and value-added. We use data from 2011-2020 to compute shares of value-added, material input expenditure shares, and consumption expenditure for each sector at the country-level.

- **OECD International Migration Data:** we use data from the OECD International Migration Database to measure annual bilateral migration flows between OECD member countries for the period 2000–2023. The OECD dataset is based on harmonized national population registers, residence permit records, and labour-force surveys, providing the highest-quality and most comparable cross-country information on migration movements within the OECD. It reports inflows by country of origin and, for many destinations, outflows as well, enabling the construction of consistent bilateral flow matrices at an annual frequency. Because the OECD systematically standardizes definitions of migrants, migration events, and residence changes, these data offer a reliable foundation for analysing international mobility patterns within the OECD bloc.

- **OECD Internal Mobility Data:** to measure mobility within countries, we use OECD data on internal residential movements, which record the share of a region's population that relocates to another region within the same country.[26] These indicators are available annually for 2000–2021 and are constructed from harmonized national population registers and administrative records, ensuring comparability across OECD member states. The dataset captures moves across TL2 regions, which allows us to quantify the extent of within-country reallocation.

- **United Nations Department of Economic and Social Affairs:** to extend migration coverage beyond OECD member countries, we complement the OECD International Migration Database with five-year bilateral migration flow estimates from Abel and Cohen (2019[23]), which are constructed using the United Nations Department of Economic and Social Affairs

[26]Source: Population mobility within the country – Regions (OECD Regions and Cities).

(UN DESA) migrant stock data. UN DESA provides globally harmonized estimates of international migrant stocks for virtually all countries, reported at five-year intervals and available consistently from 1990 onward (with historical stock data extending back to 1960). Abel and Cohen (2019[23]) apply demographic accounting and statistical smoothing methods to convert these stock figures into bilateral migration flows, producing a global dataset of inferred flows where direct statistics are unavailable.

- **ITPD-E International Trade Data:** The International Trade and Production Database for Estimation (ITPD-E), provided by the United States International Trade Commission, contains information on international annual bilateral trade flows in 2000-2019 across 265 countries disaggregated by 170 industries. We aggregate all trade flows into the 11 sectors included in the model calibration for OECD countries, and also for the 3 broader sectors of agriculture, manufacturing, and services.

We combine the information from these data sources with parameter values taken from the literature to calibrate the model parameters and unobserved exogenous variables, as summarized in Table E.3. Local sectoral TFPs, local amenities, and trade and migration cost functions are estimated through 'model inversion', as is common in the quantitative spatial literature. Below, we provide a detailed treatment of the 'model inversion' procedure.

Table E.2: Data sources used in the model calibration

Category	Variable	Sources
Regional Economy	Population Wages Sectoral employment shares	OECD Regional Data, Database of Sub-national Economic Output (DOSE), World Development Indicators (World Bank)
Production Function	Share of value-added Purchases of intermediate inputs	OECD Input-output Tables
Consumption	Final consumption shares	OECD Input-output Tables
Trade	Bilateral trade flows by sector Country bilateral characteristics	International Trade and Production Database for Estimation (ITPD-E, International Trade Commission)
Migration	International migration flows Within-country mobility	OECD Migration Database, DESA (United Nations), OECD Regions and Cities
SSP Projections	Population	International Institute for Applied Systems Analysis (IIASA)

Notes: The table shows the different sources of data used for calibrating the baseline model.

E.2.2 Trade costs

The cost of trading between any two locations i and n is defined as

$$\tau_{in}^{j} = (\text{dist}_{in})^{\rho^j} \phi_{\sigma(i),\sigma(n)} \ , \tag{35}$$

where the cross-border trade cost of moving goods from country $\sigma(i)$ to country $\sigma(n)$ is equal to 1 if $i = n$, i.e. the cost of moving goods within a country is entirely determined by the distance-decay function $(\text{dist}_{in})^{\rho^j}$. We first discuss how we calibrate cross-border trade costs $\phi_{\sigma(i),\sigma(n)}$ and then how we estimate distance-decay parameters ρ^j.

Cross-border trade costs

I estimate the matrix of bilateral trade costs for all country pairs and sectors following the method proposed by Head and Ries (2001[24]). In this approach, trade costs are inferred solely from observed bilateral import shares and do not rely on any other model variables. This has the advantage of avoiding more computationally demanding calibration procedures - such as simulated method of moments - that are sometimes used in the literature. The idea is to recover the level of bilateral trade costs that is consistent with the observed pattern of trade flows implied by the model.

Assume that bilateral trade costs are symmetric, that is, $\tau_{in}^{j} = \tau_{ni}^{j}$ for any countries i and n in sector j. Then, evaluate optimal trade shares at the country-pair level as

$$\pi_{\sigma(n),\sigma(i)t}^{j} = \frac{A_{\sigma(i)t}^{\theta} (x_{\sigma(n)t}^{j} \tau_{\sigma(n),\sigma(i)}^{j})^{-\theta}}{\sum_{l=1}^{N} A_{\sigma(m)t}^{\theta} (x_{\sigma(m)t}^{j} \tau_{\sigma(n),\sigma(m)}^{j})^{-\theta}} \ . \tag{36}$$

One can the show that the following relationship holds:

$$\frac{\pi_{\sigma(i),\sigma(n)}^{j}}{\pi_{\sigma(n),\sigma(i)}^{j}} \frac{\pi_{\sigma(i),\sigma(i)}^{j}}{\pi_{\sigma(n),\sigma(n)}^{j}} = (\phi_{\sigma(i),\sigma(n)})^{-2\theta} \ . \tag{37}$$

This expression makes it possible to recover τ_{in}^{j} using only country-to-country bilateral import shares, which we observe using data from ITPD-E, and the dispersion parameter θ. Intuitively, the more two countries import from each other relative to how much they source domestically, the lower their bilateral trade costs must be. The ratio on the left-hand side is constructed so that any productivity differences between the two countries cancel out, leaving only trade-cost terms.

Distance-decay parameters

We estimate a gravity equation of trade to estimate how trade flows decay with distance. Based on equation (27) and our definition of trade costs above, we can define the empirical relationship between trade flows X_{ni}^{j} and bilateral distance dist_{ni}

$$\log(X_{ni}^{j}) = \rho^j \theta \log(\text{dist}_{ni}) + \theta \log(\phi_{\sigma(i),\sigma(n)}) + \varepsilon_{ni}^{j} \ . \tag{38}$$

Since we do not have information on trade flows within countries, we can only estimate equation (38)

at the level of country pairs. Defining the coefficient $\gamma^j = \rho^j \theta$ and using the estimated cross-border factors $\phi_{\sigma(i),\sigma(n)}$ from above, one can estimate equation (38) through OLS using country-to-country trade flows data from the ITPD-E and retrieve the estimated value of the distance-decay parameter as $\hat{\rho}^j = \hat{\gamma}^j / \theta$.

E.2.3 Prices

Now, we show how sectoral prices can be retrieved based on data on the distribution of demand and supply across space and knowledge on iceberg trade costs, which are estimated as above. We begin by noting that imports of goods from i to n are given by

$$X_{ni}^j = \frac{(p_{ii}^j \tau_{ni}^j)^{-\theta}}{(P_n^j)^{-\theta}} X_n^j \ . \tag{39}$$

In addition, total sales Y_n^j from origin n can be obtained by summing exports across all destinations so that we obtain the relationship

$$Y_n^j = \sum_i X_{in}^j = (p_{nn}^j)^{-\theta} \sum_i \left(\left(\frac{\tau_{in}^j}{P_i^j} \right)^{-\theta} X_i^j \right) \ . \tag{40}$$

Substituting this equation into (39) yields the gravity equation

$$X_{in}^j = \frac{Y_n^j X_i^j}{X^j} \left(\frac{\tau_{in}^j}{\Pi_n^j P_i^j} \right)^{-\theta} \tag{41}$$

and where the price index Π_n^j is given by

$$\Pi_n^j \equiv \left(\sum_m \left(\frac{\tau_{mn}^j}{P_m^j} \right)^{-\theta} \frac{X_m^j}{X^j} \right)^{-1/\theta} \ , \tag{42}$$

with X^j denoting nation-wide expenditures on industry j. Equation (41) shows that trade flows follow a gravity structure. Imports from source n are decreasing in transportation costs τ_{ni}^j of moving goods from n to i, increasing in the size of origin Y_n^j and destination X_i^j, and decreasing in the degree of origin and destination multilateral resistance (Anderson and van Wincoop, 2003), as captured by the price indexes Π_n^j and P_i^j, respectively.

Table E.3: Calibrated model parameters

Parameter or variable	Description	Source or matched moment
Borrowed from literature		
$\theta = 6$	Productivity dispersion	Eaton and Kortum (2002[14])
$\varepsilon = 4.5$	Location preference dispersion	Morten and Oliveira (2024[26])
$\zeta = 1.75$	Elasticity of housing supply	Saiz (2010[27])
$\lambda = 0.67$	Share of labour in value added	Standard
$\eta = 0.19$	Share of capital in value-added	Greenwood et al. (1997[28])
$\alpha = 0.3$	Share of final goods in consumption	Standard
$\delta = 0.025$	Depreciation rate of capital	Standard
Calibrated from data		
$\{L_{0n}\}_{n=1}^{N}$	Initial population	OECD Regional Data, DOSE, PWT
$\{\beta_n^j\}_{n=1,j=1}^{N,J}$	Value added shares	OECD Input-output Tables
$\{\gamma_n^{jk}\}_{n=1,j=1,k=1}^{N,J,J}$	Material input shares	OECD Input-output Tables
$\{\alpha_n^j\}_{n=1,j=1}^{N,J}$	Final consumption shares	OECD Input-output Tables
$\{\rho^j\}_{j=1}^{J}$	Trade distance-decay rate	Estimated from trade gravity equation using international trade data. Source: ITPD-E, DGD
φ	Migration distance-decay rate	Estimated from migration gravity equation. Source: OECD bilateral migration flows
Calibrated via model inversion		
$\{\Phi_{\sigma(i),\sigma(n)}\}_{i=1,n=1}^{N,N}$	Country-to-country trade costs	Match international bilateral trade flows using method in Head and Ries (2001). Source: ITPD-E
$\{\Psi_{\sigma(i),\sigma(n)}\}_{i=1,n=1}^{N,N}$	Country-to-country migration costs	Match bilateral international migration flows data. Source: OECD Migration Source, DESA (UN)
$\{\eta_n\}_{n=1}^{N}$	Cost of internal mobility	Match within-country population mobility, Source: OECD Regions and Cities
$\{P_n^j\}_{n=1,i=1}^{N,J}$	Sectoral prices	Match spatial distribution of sectoral spending and income using method in Anderson and van Wincoop (2003[25]). Source: OECD regional data
$\{A_n^j\}_{n=1,j=1}^{N,J}$	Sectoral Productivities	Match spatial distribution of population, wages, and sectoral prices Source: OECD regional data
$\{B_n\}_{n=1}^{N}$	Amenities	Match population shares. Source: OECD regional data

Notes: The calibration is performed for $N = 927$ regions and $J = 11$ sectors. OECD member countries are divided into TL2 subnational regions, OECD accession countries and key partners are divided into Admin-1 regions following the Global Administrative Areas (GADM) classification, and we use the entire country's territory for all other countries.

Moreover, by adding up imports across all origins, and combining this with the gravity equation (41) we obtain expenditures

$$X_i^j = \sum_n \frac{Y_n^j X_i^j}{X^j} \left(\frac{\tau_{in}^j}{\Pi_n^j P_i^j} \right)^{-\theta} , \tag{43}$$

which, solving for prices P_i^j, yields

$$P_i^j = \left(\sum_m \left(\frac{\tau_{im}^j}{\Pi_m^j} \right)^{-\theta} \frac{Y_m^j}{Y^j} \right)^{-1/\theta} , \tag{44}$$

where we have that, due to market clearing, that $X^j = Y^j \equiv \sum_i Y_i$. Prices P_i^j can then be recovered by solving equations (42) and (44) jointly.

E.2.4 Productivities

Sectoral productivities are calibrated based on the goods market equilibrium condition (31). When combined with the assumption of a Cobb-Douglas production function in intermediate goods production, it may be written as

$$\frac{w_{it} L_{nt}^j}{\lambda \beta_n^j} = \sum_{j=1}^{J} \gamma_n^{kj} \sum_{i=1}^{N} \frac{A_{nt}^{\theta j} (x_{mt}^j \tau_{in}^j)^{-\theta^j}}{(P_{it}^j)^{-\theta j}} \frac{w_{it} L_{nt}^k}{\lambda \beta_n^k} + \alpha^j w_{it} L_{it} , \tag{45}$$

where x_{nt}^j is given by equation (24).

Then, upon knowledge of prices $\{P_{nt}^j, w_{nt}, Q_{nt}, r_{nt}\}_{t=1}^T$ and allocations $\{L_{nt}^j, L_{nt}\}_{t=1}^T$, given parameters $\{\beta^j, \gamma^{jk}, \tau_{ni}^j\}$, one can solve for productivities $\{A_{nt}^j\}_{t=1}^T$ for all $j = 1, \ldots, J$ and $n = 1, \ldots, N$. This is feasible since we have data for wages $\{w_{nt}\}_{t=1}^T$ and labour allocations $\{L_{nt}^j, L_{nt}\}_{t=1}^T$; sectoral prices $\{P_{nt}^j\}_{t=1}^T$ and building prices $\{Q_{nt}\}_{t=1}^T$ are estimated as above, and because the steady-state rental rate of capital is equal to $r_n = 1/\beta - (1 - \delta)$.

E.2.5 Amenities and migration costs

We jointly calibrate amenities B_n and migration costs κ_{in} by simultaneously matching relevant equilibrium conditions. Recall that bilateral migration costs are defined as

$$\kappa_{in} = e^{-\eta_n \mathbf{1}\{i=n\}} (\text{dist}_{in})^{\phi} \psi_{\sigma(i),\sigma(n)} , \tag{46}$$

where the cross-border cost of moving people from country $\sigma(i)$ to country $\sigma(n)$ $\psi_{\sigma(i),\sigma(n)}$ is equal to 1 if $i = n$. This means that the cost of moving people within a country depends only on the combination of the distance-decay function $(\text{dist}_{in})^{\phi}$ and the within-country mobility factor $e^{-\eta_n \mathbf{1}\{i=n\}}$, which controls the likelihood of a household moving out of its current location, all else equal. Below we show how we estimate each of these terms.

Distance-decay parameter

Following again the same procedure used for trade costs, we estimate the distance-decay pa-

rameter ϕ by estimating the migration gravity equation

$$\log(\lambda_{in}) = \phi\varepsilon \log(\text{dist}_{ni}) + \varepsilon \log(\psi_{\sigma(i),\sigma(n)}) + u^j_{ni} \ . \tag{47}$$

Cross-border migration costs

We estimate cross-border migration costs $\psi_{\sigma(i),\sigma(n)}$ similarly to the method used for estimating cross-border trade costs $\phi_{\sigma(i),\sigma(n)}$, shown above. More specifically, we consider the optimal migration share condition (28) at the country-pair level and manipulate it to yield

$$\frac{\lambda_{\sigma(i),\sigma(n)}}{\lambda_{\sigma(n),\sigma(i)}} \frac{\lambda_{\sigma(i),\sigma(i)}}{\lambda_{\sigma(n),\sigma(n)}} = (\psi_{\sigma(i),\sigma(n)})^{-2\varepsilon} \ . \tag{48}$$

With information on country-to-country migration flows obtained from UN DESA and Abel and Cohen (2019), one can then back out cross-border costs $\psi_{\sigma(i),\sigma(n)}$.

Within-country mobility factor and local amenities

After having obtained cross-border costs $\psi_{\sigma(i),\sigma(n)}$ and parameter ϕ, we solve for the within-country mobility factors η_n and local amenities B_n through a nested loop algorithm. In the inner loop, we solve for η_n based on a given value of B_n; in the outer loop, we find the value B_n while satisfying the conditions of the inner loop is, such that $\eta_n = \eta_n(B_n)$. We begin by guessing a value of amenities $B_n = B_{n0}$.

Inner loop: Combining the optimal migration shares (28) and the definition of migration costs in (46), we can write the share of households living in n who move to i as

$$\lambda_{in} = \frac{B_{nt}(e^{-\eta_n \mathbf{1}\{i=n\}}(\text{dist}_{in})^{\phi}\psi_{\sigma(i),\sigma(n)}P_{nt}^{\alpha}Q_{nt}^{1-\alpha})^{-\varepsilon}w_{nt}^{-\varepsilon}}{\sum_{m=1}^{N} B_{mt}(e^{-\eta_m \mathbf{1}\{i=n\}}(\text{dist}_{im})^{\phi}\psi_{\sigma(m),\sigma(n)}P_{mt}^{\alpha}Q_{mt}^{1-\alpha})^{-\varepsilon}w_{mt}^{-\varepsilon}} \ . \tag{49}$$

We then make a guess for $\eta_n = \eta_{n0}$ for all $n = 1, \ldots, N$ and compute the implied share of households in a country c that chooses to move to another location within the same country, $\tilde{\lambda}_c$, which is given by

$$\tilde{\lambda}_c = \sum_{i:\sigma(i)=c} \frac{L_i}{\sum_{i:\sigma(i)=c} L_i} \lambda_{in} \ . \tag{50}$$

We check the implied value $\tilde{\lambda}_c$ and compare it against its empirical counterpart, which is derived from OECD data on the share of people within each country that moves to another region of the same country. We adjust our guess for η_n and iterate until convergence.

Outer loop: Having found $\eta_n = \eta_n(B_0)$, we now search for the value of amenities B^* that matches observed changes in population while also satisfying the inner loop solution $\eta_n = \eta_n(B^*)$. To do so, we begin by noting that combining the population law of motion (30), optimal migration shares

(28) and the definition of migration costs yields

$$L_{nt} = \sum_{i=1}^{N} \frac{B_{nt}(e^{-\eta_n(B^*)\mathbf{1}\{i=n\}}(\text{dist}_{in})^{\phi}\psi_{\sigma(i),\sigma(n)}P_{nt}^{\alpha}Q_{nt}^{1-\alpha})^{-\varepsilon}w_{nt}^{-\varepsilon}}{\sum_{m=1}^{N} B_{mt}(e^{-\eta_m(B^*)\mathbf{1}\{i=n\}}(\text{dist}_{im})^{\phi}\psi_{\sigma(m),\sigma(n)}P_{mt}^{\alpha}Q_{mt}^{1-\alpha})^{-\varepsilon}w_{mt}^{-\varepsilon}} L_{i,t-1} \tag{51}$$

Given information on current and past population, consumption prices and rental rates, as well as the parameters of the migration cost function, one can solve equation (51) through a fixed-point algorithm. We compare the values of current population L_{nt} implied by (51) with those observed in the data, update our guess for B_n and update until convergence.

E.2.6 Steady state

We calibrate the baseline model so that all locations are in steady state, i.e. $K_{nt} = K_{n,t-1}$ for all $n = 1, \ldots, N$. We make a guess for capital, take all estimated (and externally calibrated) parameters and solve the model forward, each time updating the capital stock following the law of motion (29) until a steady state is reached in all $n = 1, \ldots, N$.

E.3. Impact of flooding on capital

E.3.1 Impact on depreciation rate

Here we provide additional detail on how we calibrate flood-related damages using the firm-level estimates from Section 3.1. We focus on baseline specification (22), reported in Figure B.3, which implies that a firm's capital stock is on average 2.7 percent lower in the four years following a flood. To translate this into a model-consistent parameter, we calibrate the increase in the capital depreciation rate so that the model's impulse response of capital to a flooding shock matches this observed 2.7 percent decline relative to the no-flood baseline.

Let the depreciation rate of capital in a location hit by a flood be given by $\delta_{nt} = \delta + \Delta$, where δ is the baseline depreciation rate, equal to 0.025 in the calibrated model, and Δ is the flood-induced increase. We obtain Δ using an iterative search procedure. Starting from an initial guess $\Delta = \Delta_0$. Then, we simulate a one-off flooding event in each location $n = 1, \ldots, N$ such that $\delta_{nt} = \delta + \Delta$ in period $t = 0$ and $\delta_{nt} = \delta$ in periods $t = \{1, 2, 3, 4\}$. For each guess, we compute the average deviation of capital from its no-flood baseline across all locations, compare it with the empirical target of a 2.7 percent decline, update Δ and iterate until convergence.

E.3.2 Continent resilience factors

Since our damage estimates rely primarily on data from European countries, we allow the impacts of flooding to differ across continents. To do so, we draw on the depth-damage functions provided by Huizinga et al. (2017), who develop a global, harmonised set of flood-damage curves for residential, commercial, and industrial assets. Their study combines several studies and data sources to estimate how damage varies with inundation depth across world regions while accounting

for building types, construction costs, asset values, and flood vulnerability to. These depth-damage functions give us a scalable way to adjust the magnitude of capital losses outside Europe, ensuring that our calibration reflects regional differences in exposure and structural vulnerability.

We combine these depth–damage functions with flood hazard maps from the World Resources Institute (WRI), which report expected inundation depths for different return periods. Using the damage function for commercial buildings, we compute in each location the share of assets damaged at flood depths of $\{0, 0.5, 1, 1.5, 2, 3, 4, 5, 6\}$ meters for Europe, North America, Central and South America, Asia, and Oceania, and use the global average curve for Africa. We then weight these damage shares by the probability of each flood intensity category and average the resulting values across locations within each continent.

Taking the ratio of each continent's average to that of Europe yields a continent-specific multiplier that captures how much more—or less—damage a flood of a given depth is expected to cause relative to Europe. We apply this multiplier to our estimated value of Δ to scale the flood-induced increase in capital depreciation rates across regions accordingly. The values of the multiplier are 2.13 for North America, 3.51 for Central and South America, 2.12 for Asia, 1.43 for Africa, and 1.37 for Oceania.

E.4. Counterfactual simulations

In this section, we describe how we implement the counterfactual simulations shown in Sections 5.2 and 5.3. The first set of counterfactual exercises - those examining the role of economic linkages in transmitting shocks - requires a full recalibration of the model, as the counterfactual economy differs structurally from the baseline climate-change scenario. By contrast, the second set of exercises - those assessing the role of adjustment mechanisms - relies on the same baseline calibration but alters the equilibrium conditions to reflect a world in which trade and migration shares are effectively "frozen". We discuss each set of exercises in turn below.

E.4.1 The role of economic linkages in transmitting climate shocks

We implement the no-spatial linkages model counterfactual by imposing trade costs are equal to infinity for all locations, i.e. $\tau_{in} = \infty$ for all $i \neq n$ while keeping $\tau_{ii} = 1$ for all i, and similarly for migration costs, i.e. $\kappa_{in} = \infty$ for all $i \neq n$ while keeping $\kappa_{ii} = 1$ for all i. As trade and migration costs cannot in practice be set to infinity, we set them a value so large (1000) that trade and migration flows become negligible. For the no-input-output linkages model counterfactuals, we simply impose that the share of value added β^j in all locations and sectors is the same and equal to one, effectively removing all inter-sectoral purchases of material inputs. For both model counterfactuals, we re-calibrate the model following the same procedure as above while imposing these conditions and re-simulate the climate change scenario simulation for 2025-2100.

E.4.2 The role of adjustment: how trade and labour mobility shape the distribution of global losses

In the no-trade-adjustment counterfactual, we retain the baseline calibration and compute the equilibrium by solving equations (24)-(34) while introducing a trade-cost adjustment factor ff^j_{nit} for every origin–destination pair and simulation period. These factors are chosen so that the sequence of bilateral import shares $\{\pi^j_{nit}\}_{t=1}^T$ in the climate-change simulation exactly replicates the baseline path without climate shocks. In practice, this amounts to modifying the pricing and import-share equations to include ff^j_{nit}:

$$P^j_{nt} = \Gamma(\xi^j_n)^{(1/(1-\theta^j))} \left(\prod_{i=1}^{N} (ff^j_{nit} x^j_{it} \tau^j_{nit})^{-\theta_j} (A^j_{it})^{\theta_j} \right)^{-1/\theta_j} \tag{52}$$

$$\pi^j_{nit} = \frac{A^{(\theta^j)}_{it} (x^j_{nt} ff^j_{nit} \tau^j_{ni})^{(-\theta^j)}}{\sum_{l=1}^{N} A^{(\theta^j)}_{mt} (x^j_{mt} ff^j_{nit} \tau^j_{nm})^{(-\theta^j)}} \tag{53}$$

The adjustment factors ff^j_{nit} are obtained through an iterative search procedure: starting from an initial guess, we update their values until the bilateral import shares implied by the climate-shock simulation coincide with those generated by the model along the no-climate-change baseline.

For the no-labour adjustment counterfactual, we modify the optimal migration share condition (28) by directly imposing that equilibrium shares match those under the baseline path, defined as $\bar{\lambda}_{nit}$. In other words, we replace equation (28) with $\lambda_{nit} = \bar{\lambda}_{nit}$, effectively preventing migration shares from deviating from the no-climate change baseline path. To also prevent labour from moving across sectors within locations we need to introduce sector-specific wages and impose fixed sectoral-labor shares $\left(\overline{\frac{L^j_{nt}}{L_n}}\right)$ matching those in the baseline path. We drop equation (32) and replace with the following two equations:

$$w^j_n = \frac{(\lambda \beta^j) R^j_n}{\left(\overline{\frac{L^j_{nt}}{L_n}}\right) L_n} \tag{52}$$

$$w_n = \sum_{j=1}^{J} \left(\overline{\frac{L^j_{nt}}{L_n}}\right) w^j_n \ , \tag{53}$$

where the first expression is implied by the assumption of a Cobb-Douglas production function for intermediate goods whereby firms spend a fixed share of total revenues $\lambda\beta^j$ on hiring labour. Revenues R^j_n can be obtained as the sum of sales across all destinations as $R^j_n = \sum_{i=1}^{N} \pi^j_{in} R^j_i$. The second equality characterizes the average local wage, defined as the employment-weighted average across all sectors.

For the final counterfactual where we impose both no-trade and no-labour adjustments, we combine all the conditions above. This forces trade shares, migration patterns, and sectoral labour shares to remain the same as in the baseline path.

F. Further results on quantitative analysis: Impact on population

Before examining the specific role of migration in the model's transmission mechanisms, it is useful to describe how population patterns evolve endogenously under the business-as-usual climate scenario. Figures F.1 and **??** show the model-implied change in population by 2050 and 2100 that results from households' optimal locational choices in response to the distribution of climate damages. These results should be interpreted as the population outcome given the modelled climate impacts, not a causal assessment of migration's contribution to GDP losses. This is done in the following subsections through targeted counterfactual simulations.

By mid-century (2050), the high-emission scenario induces modest but noticeable shifts in population across regions. As shown in Figures F.2a and F.4a, Northern Africa, Western Asia, Southern Asia, and Sub-Saharan Africa record early losses, where climate damages reduce local productive capacity, prompting households to relocate to regions relatively less affected by climate. These departures from climate-vulnerable regions contribute directly to population gains observed elsewhere, such as Northern Europe, Central Asia, Southern Europe, and North America, which all register positive inflows by mid-century, typically in the range of 1–6 percent. These migration flows include not only cross-border migration but also significant shifts within countries. In many countries, such as Spain, internal movements from hotter southern provinces toward cooler northern regions constitute an important share of the overall migration response, highlighting that migratory responses occur not only internationally but also domestically.

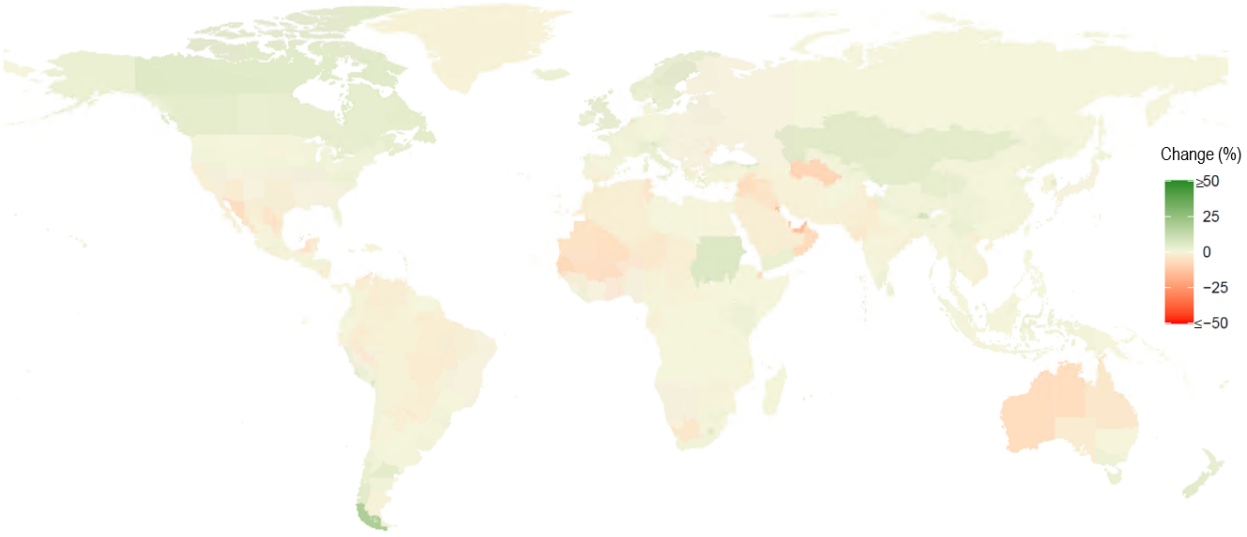
By 2100, these redistributive forces intensify substantially, with sharp contrasts emerging between population-losing and population-gaining regions. Figures F.2b and F.4b shows large declines in Northern Africa (-11 percent), Western Asia (-8 percent), Southern Asia (-7 percent), and Sub-Saharan Africa (-7 percent), consistent with the severe GDP losses concentrated in these regions. The map in Figure 18 highlights particularly pronounced outflows from the Sahel, the Horn of Africa, and parts of South Asia - areas facing some of the largest economic damages at the hands of climate hazards. These outflows, in turn, fuel sizable population gains in cooler, less climate-affected regions. Northern Europe (+20 percent), Central Asia (+10 percent), North America (+8 percent), and Oceania (+8 percent) become major net recipients of migrants by 2100. Among OECD countries, the map reveals strong inflows into Canada, Nordic countries, and northern parts of the United States, while internal migration continues to reshape national population distributions. This includes, for instance, movement toward cooler northern areas of Spain, Portugal, and Mexico. The OECD as a whole experiences population gains, but with substantial variation. Northern Europe and North America emerge as clear destinations for climate-driven migration, while Southern Europe sees only modest inflows owing to higher local damages. Oceania and parts of Eastern Asia also register increases, whereas some OECD+ economies in warmer climates face mild declines.

Overall, the figures show that climate change not only reduces economic output but also significantly reshape global and domestic population patterns, as people move away from intensifying climate risks and towards less affected locations. These movements arise endogenously in the

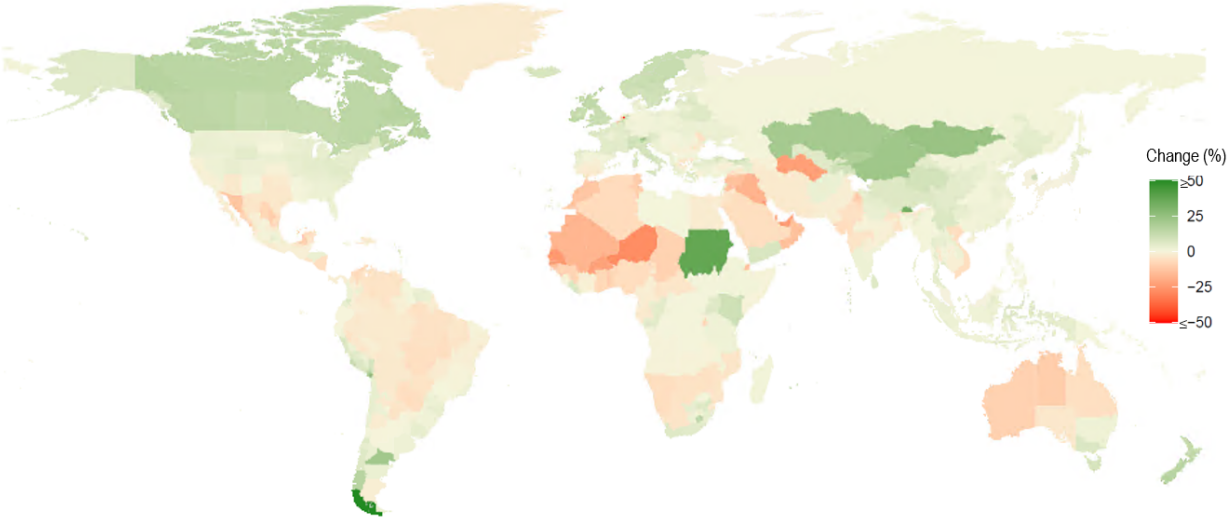
model and interact with economic outcomes in important ways. In the next subsection, we directly quantify the role of migration - and other adjustment mechanisms - by simulating counterfactual scenarios in which these margins are shut down.

Figure F.1: Change in population due to climate change under the current-policy scenario (SSP2-4.5)

(a) Percentage change in population in 2050



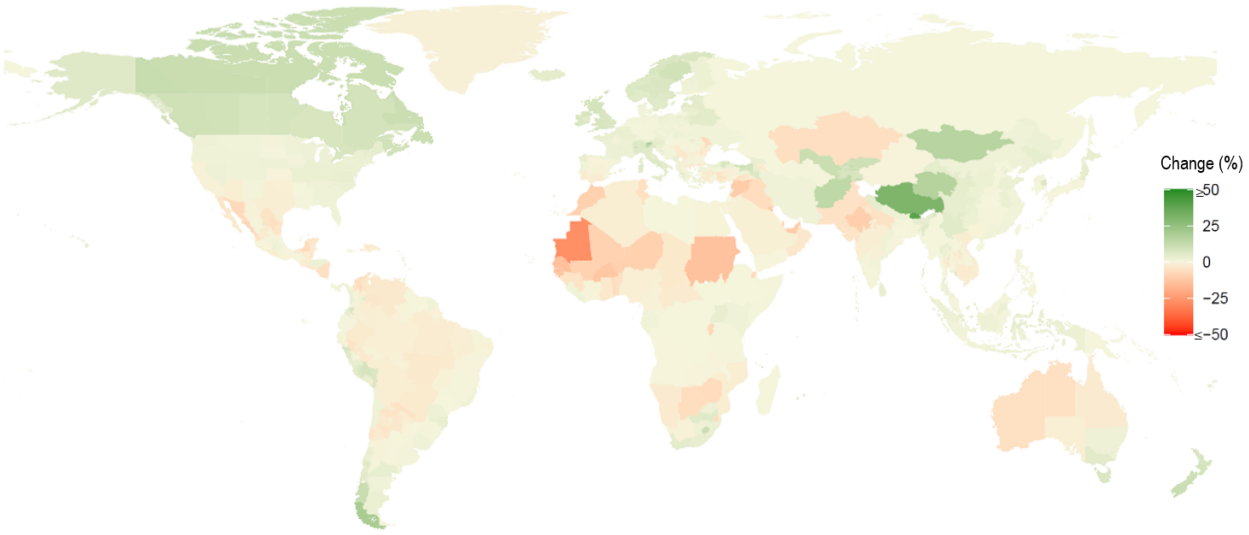
(b) Percentage change in population in 2100



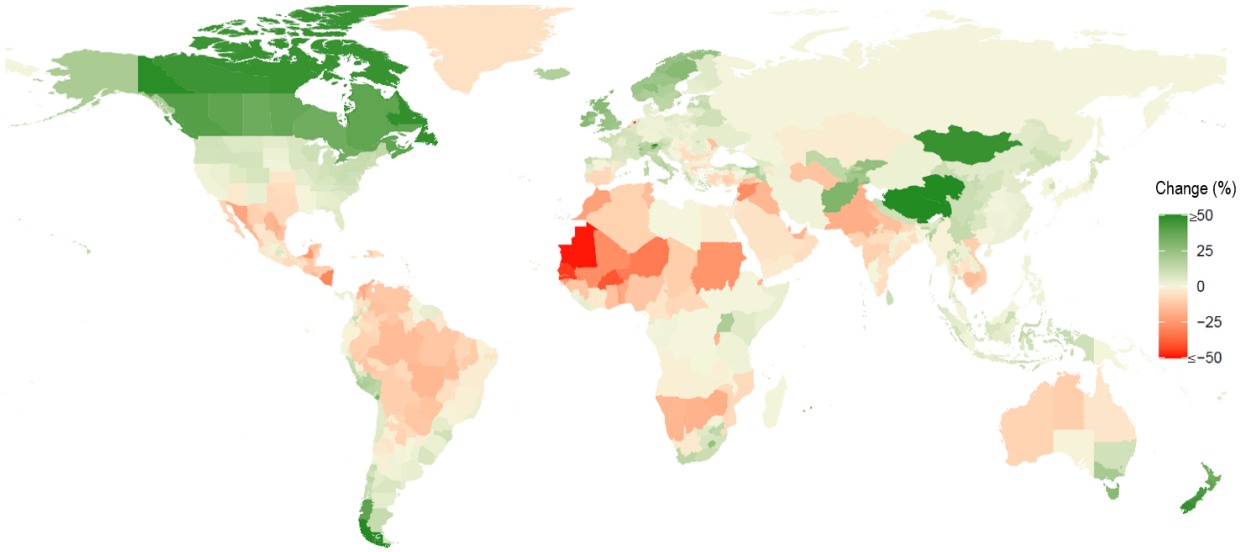
Source: Authors' own calculations.
Note: The figure shows the model-implied percent change in population relative to a no-climate change scenario. All values below -50 and above 50 are windsorized at -50 and 50, respectively.

Figure F.2: Change in population due to climate change under the high-emission scenario (SSP5-8.5)

(a) Percentage change in population in 2050



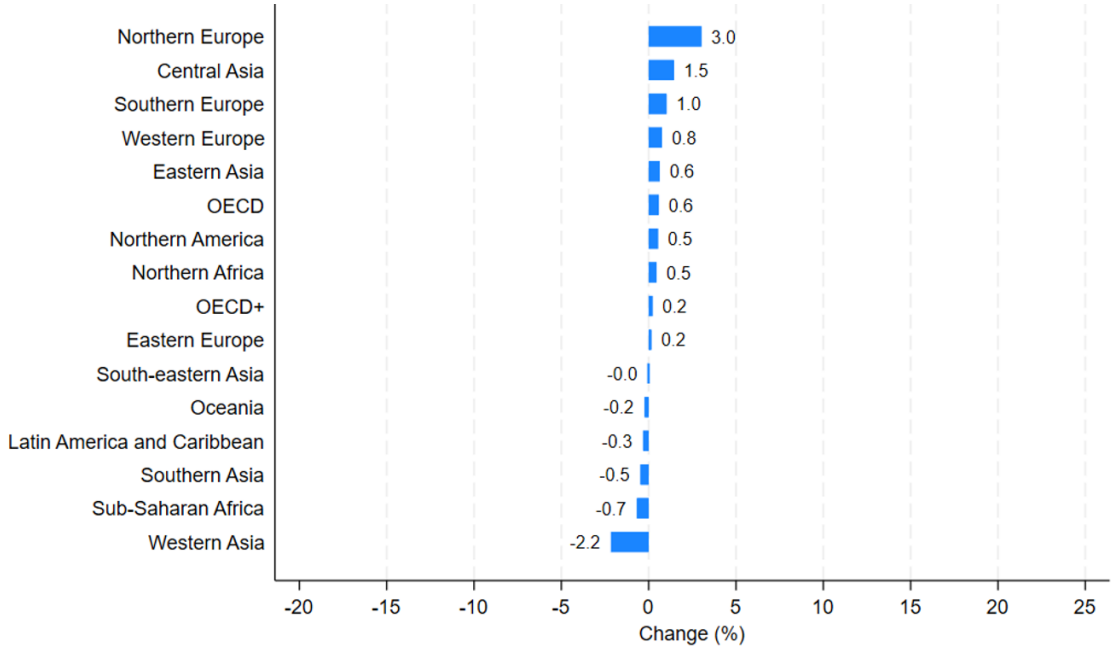
(b) Percentage change in population in 2100



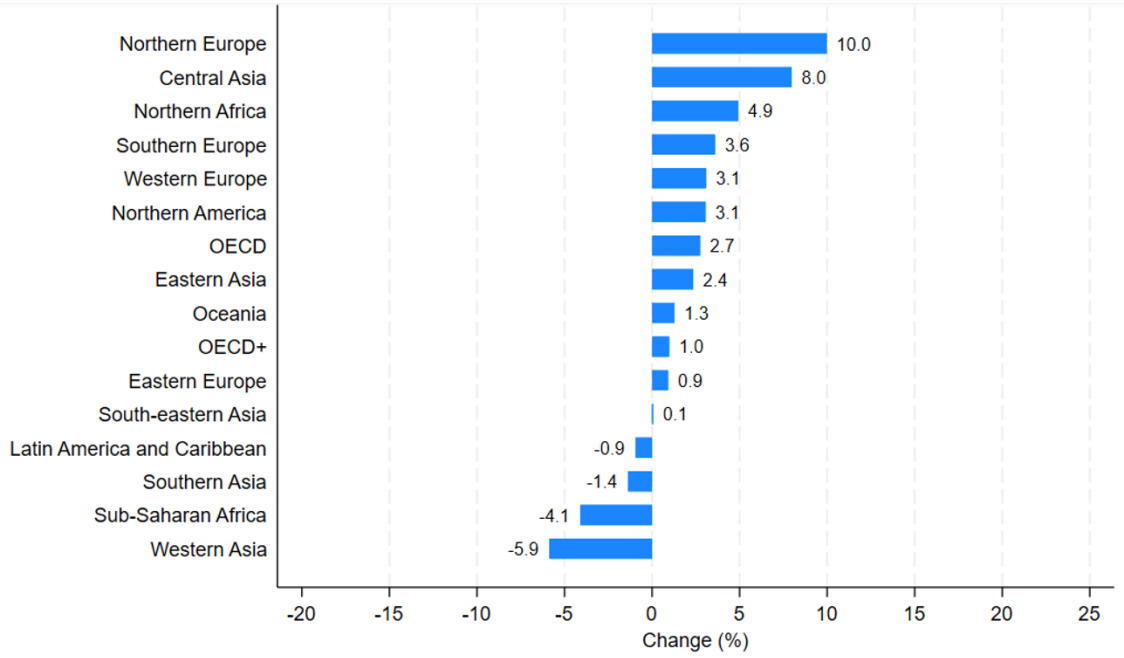
Source: Authors' own calculations.
Note: The figure shows the model-implied percent change in population relative to a no-climate change scenario. All values below -50 and above 50 are windsorized at -50 and 50, respectively.

Figure F.3: Regional population changes under the current-policy scenario (SSP2-4.5)

(a) Percentage change in population in 2050



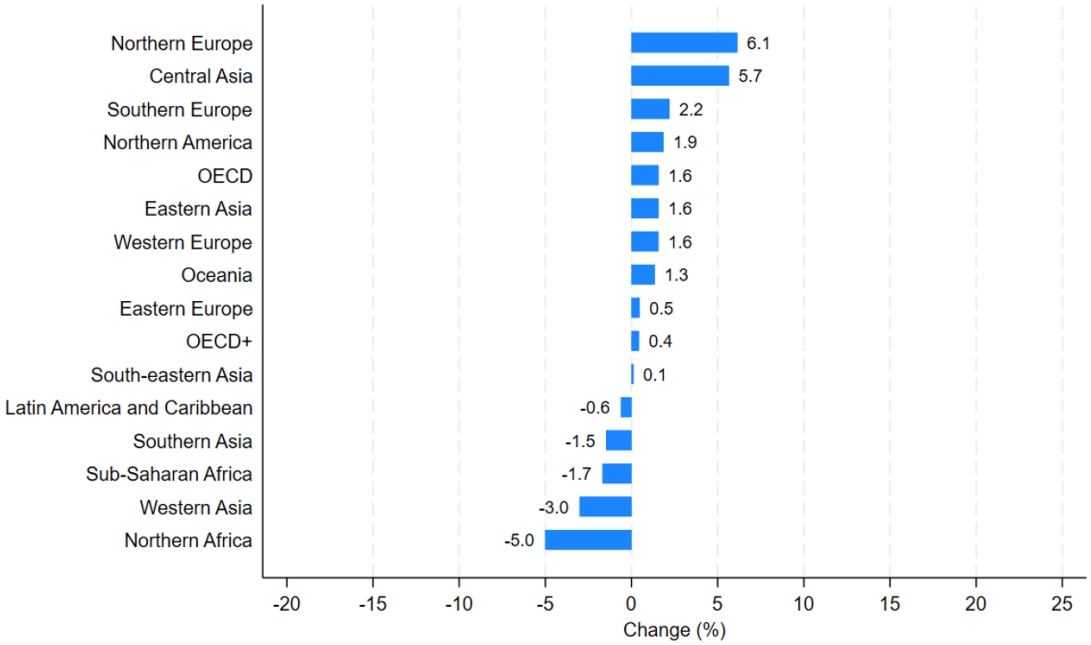
(b) Percentage change in population in 2100



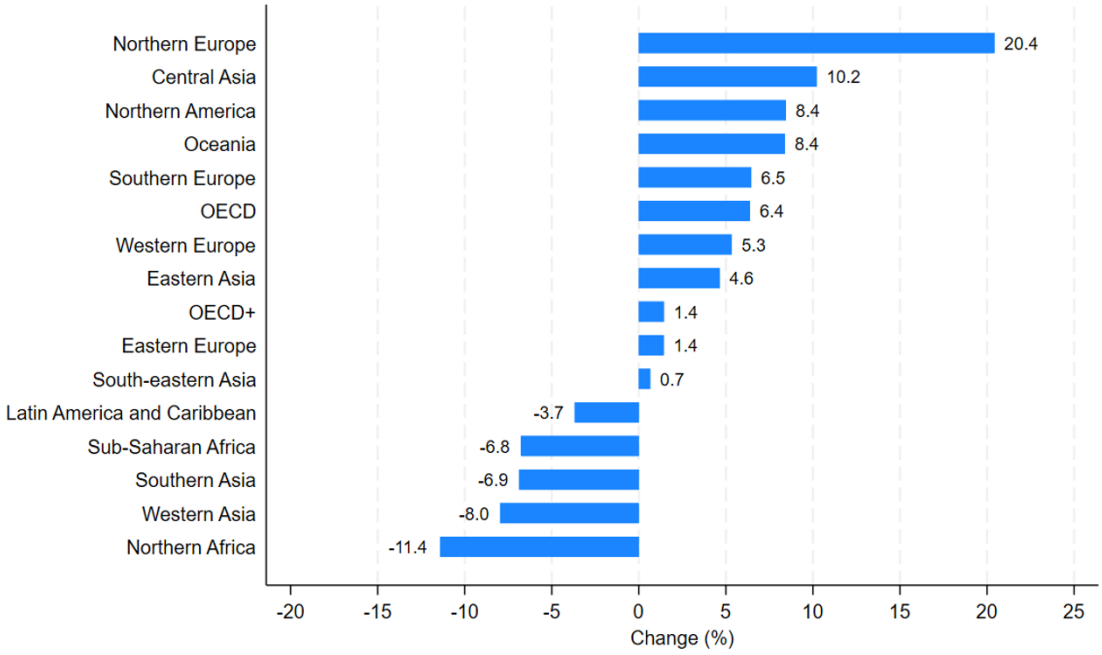
Note: The figure shows the model-implied change in population relative to a no-climate change scenario. Regional population changes are computed as a country population-weighted average.
Source: Authors' calculations.

Figure F.4: Regional population changes under the high-emission scenario (SSP5-8.5)

(a) Percentage change in population in 2050



(b) Percentage change in population in 2100



Note: The figure shows the model-implied change in population relative to a no-climate change scenario. Regional population changes are computed as a country population-weighted average.
Source: Authors' calculations.